

THEORETICAL INVESTIGATION OF
CONJUGATE CONDENSATION HEAT TRANSFER
INSIDE VERTICAL TUBES

A THESIS SUBMITTED TO
THE GRADUATE SCHOOL OF NATURAL AND APPLIED SCIENCES
OF
MIDDLE EAST TECHNICAL UNIVERSITY

BY

SERHAT KÖSE

IN PARTIAL FULFILLMENT OF THE REQUIREMENTS
FOR
THE DEGREE OF DOCTOR OF PHILOSOPHY
IN
THE DEPARTMENT OF MECHANICAL ENGINEERING

SEPTEMBER 2010

Approval of the thesis:

**THEORETICAL INVESTIGATION OF CONJUGATE CONDENSATION
HEAT TRANSFER INSIDE VERTICAL TUBES**

submitted by **SERHAT KÖSE** in partial fulfillment of the requirements for the degree of **Doctor of Philosophy in Department of Mechanical Engineering, Middle East Technical University** by,

Prof. Dr. Canan Özgen
Dean, Graduate School of **Natural and Applied Sciences**

Prof. Dr. Suha Oral
Head of Department, **Mechanical Engineering**

Prof. Dr. A. Orhan Yeşin
Supervisor, **Mechanical Engineering Dept., METU**

Examining Committee Members:

Prof. Dr. Faruk Arınç
Mechanical Engineering Dept., METU

Prof. Dr. A. Orhan Yeşin
Mechanical Engineering Dept., METU

Prof. Dr. Mecit Sivrioğlu
Mechanical Engineering Dept., Gazi University

Assoc. Prof. Dr. Cemil Yamalı
Mechanical Engineering Dept., METU

Assist. Prof. Dr. Almıla Güvenç Yazıcıoğlu
Mechanical Engineering Dept., METU

Date:

I hereby declare that all information in this document has been obtained and presented in accordance with academic rules and ethical conduct. I also declare that, as required by these rules and conduct, I have fully cited and referenced all material and results that are not original to this work.

Name, Last name: **Serhat KÖSE**

Signature :

ABSTRACT

THEORETICAL INVESTIGATION OF CONJUGATE CONDENSATION HEAT TRANSFER INSIDE VERTICAL TUBES

Köse, Serhat

Ph.D., Department of Mechanical Engineering

Supervisor: Prof. Dr. A. Orhan Yeşin

September 2010, 165 pages

Based on the well-known theoretical studies related to the film condensation inside vertical tubes, a known temperature distribution is prescribed as boundary condition at the inner surface of the tube wall. But, in reality, there is a thermal interaction between the condensate fluid and conduction through the wall where the temperature variation along the inner surface of the tube wall is unknown and this unknown temperature profile should be determined by taking account of this interaction. In other words, the heat conduction equation for the tube wall and the energy equation for the condensate fluid flow should be coupled and solved simultaneously. Therefore, this type of problem is named “conjugate condensation heat transfer problem”.

Subject to the conjugate condensation heat transfer problem in the industrial applications, there are two different fluid flows separated by a tube where the vapor flowing inside the tube condensates whereas the other one is heated and it flows externally in the counter current direction in the annular passages.

Because of its fundamental and practical importance, in this doctoral thesis, the studies are focused on the analytical and numerical investigation of conjugate heat transfer due to the steam condensation inside vertical tubes which is cooled externally by a fluid flowing in the counter current direction. The unknown wall temperatures of the condenser tube, condensate liquid layer inside the tube and the turbulent coolant flow outside the tube are coupled. A computer code, named ZEC, containing condensation conjugate heat transfer model is developed in FORTRAN 90 Language. This code and the models it contains are assessed against the various experimental databases.

The predictions of the code ZEC are found to reasonably agree with the experimental results over a wide range of conditions. Therefore, this developed code, ZEC, may be used for the preliminary design of in-tube condensers and for the performance evaluation of such condensers in operation.

Keywords: Condensation, Conjugate heat transfer, Vertical tube

ÖZ

DÜŞEY TÜPLERDE EŞLENİK YOĞUŞMALI ISI AKTARIMININ KURAMSAL ANALİZİ

Köse, Serhat

Doktora, Makina Mühendisliği Bölümü

Tez Yöneticisi: Prof. Dr. A. Orhan Yeşin

Eylül 2010, 165 sayfa

Düşey tüpler içerisinde film yoğuşması ile ilgili kuramsal çalışmalarda, sınır koşulu olarak tüp duvarının iç yüzeyinde bilinen bir sıcaklık dağılımı kabul edilir. Oysa, gerçekte, tüp duvarındaki ısı iletimi ile tüp içinde yoğuşan akışkan arasında ısı bir etkileşim vardır ve tüp boyunca iç yüzey sıcaklık dağılımı önceden sınır koşulu olarak bilinmez. Bilinmeyen sıcaklık profili ise bu ısı etkileşim göz önüne alınarak belirlenmelidir. Diğer bir deyişle, tüp duvarındaki ısı iletim eşitliği ile yoğuşan akışkanın enerji eşitliği birlikte düşünülerek bağlaşıp hale getirilmelidir. Bu nedenle, bu problem “eşlenik yoğuşmalı ısı aktarımı” olarak adlandırılmıştır.

Eşlenik yoğuşmalı ısı aktarımına bağlı olarak endüstriyel uygulamalarda, bir tüp ile birbirinden ayrılmış iki farklı akış vardır. Tüp içinden akan buhar yoğuşurken, tüp dışındaki akışkan ters yönde akarak ısınır.

Temel uygulamalardaki ve pratikteki önemi nedeniyle, bu doktora çalışmasında, dış yüzey duvarından soğutulan düşey bir tüp içerisinden akan su

ZEC programı ile geniş bir aralığı içeren deneysel sonuçların karşılaştırmaları yapıldığında, bu karşılaştırmalar neticesinde sonuçların tatminkar bir biçimde örtüştüğü görülmüştür. Bu nedenle, geliştirilmiş olan ZEC programı, tüp içi yoğuşturucuların öncül tasarımlarında kullanılabileceği gibi halen çalışmakta olan tüp içi yoğuşturucuların işlevlerini yerine getirme değerlendirmeleri için de kullanılması söz konusudur.

vii

To the memory of my father

To my family

ACKNOWLEDGMENTS

The author would like to express his deepest gratitude to his major Professor, A. Orhan Yeşin, for his support, guidance and supervision. It's the author's honor to perform this research and to explore the advanced field of engineering under his guidance. The author extends further gratitude to his advisory committee members, distinguished Assoc. Professor Cemil Yamalı and Professor Mecit Sivrioğlu for their valuable suggestions and comments. The author also sends his heartfelt prayers to his former advisory committee member; deceased Professor Ercan Ataer.

The author would like to thanks his colleagues; Dr. Ali Tanrıkut, Dr. İhsan Kılıç at Turkish Atomic Energy Authority and Dr. Şule Ergün at Nuclear Engineering Department of Hacettepe University, both present and past, for their helps and friendship.

Finally, the author would like to his sincere thanks and deep love to his wife Zehra, his son Kaan Erdem and his daughter Bilge Çiğdem. Their existence itself as well as their love deserves to be appreciated.

TABLE OF CONTENTS

ABSTRACT	iv
ÖZ.....	vi
ACKNOWLEDGMENTS.....	ix
TABLE OF CONTENTS	x
LIST OF TABLES	xiii
LIST OF FIGURES.....	xiv
NOMENCLATURE.....	xxi
CHAPTERS	
1. INTRODUCTION.....	1
2. SCOPE OF THE STUDY	7
2.1 Definition of the problem.....	7
2.2 Thesis objective and outline.....	7
3. LITERATURE SURVEY	11
3.1. Conjugate heat transfer at solid-fluid interfaces	11
3.2. Film-wise condensation.....	19
3.3. Heat transfer in the annular channels	20
3.4. Concluding comments.....	24
4. IN-TUBE CONDENSATION MODEL	25
4.1 Physical description of the problem	25
4.2 Formulation	27
4.2.1 Liquid layer	28
4.2.2 Vapor side	35
4.2.3 Energy balance	37
4.3 Solution procedure	39
4.4 Results and discussions	42

5. HEAT TRANSFER IN THE ANNULAR FLOW	55
5.1 Formulation	56
5.2 Velocity profile for the turbulent flow in an annulus.....	59
5.2.1 Shear stress distribution	60
5.2.2 Fluctuating velocity distribution	66
5.2.3 Numerical evaluation	70
5.3 Temperature profile in an annular flow.....	75
5.3.1 Heat transfer model	76
5.3.2 Solution procedure	80
5.4 Results and discussions	81
6. CONJUGATE CONDENSATION HEAT TRANSFER.....	86
6.1 Coupling of two different fluid flows separated by a solid wall.....	87
6.2 Solution procedure	92
6.3 Numerical results and discussions.....	96
6.3.1 Comparison of numerical calculations with UCB experiments.....	97
6.3.2 Comparison of numerical calculations with NASA experiments ...	108
6.3.3 Comparison of numerical calculations with METU experiments...	111
6.3.4 Concluding comments.....	114
7. EFFECTS OF PARAMETERS ON THE CONDENSATION.....	115
7.1 The effect of steam inlet pressure	115
7.2 The effect of steam inlet mass flow rate	118
7.3 The effect of cooling water inlet temperature	120
7.4 The effect of cooling water inlet mass flow rate.....	123
8. CONCLUSIONS.....	128
8.1 General comments.....	128
8.2 Recommendations for future work.....	130
REFERENCES.....	131
A. OH-MODEL FOR IN-TUBE CONDENSATION.....	148
B. NUMERICAL ACCURACY FOR IN-TUBE CONDENSATION MODEL	155
C. THERMODYNAMIC PROPERTIES OF WATER	157

D. EFFECT OF AXIAL HEAT CONDUCTION INSIDE THE CONDENSER	
TUBE WALL	163
VITA	165

LIST OF TABLES

TABLES

Table 4.1 Comparison of the parameters for the pure steam experiments.....	44
Table 4.2 Simulated runs and conditions at the tube inlet for UCB tests	45
Table 4.3 Simulated runs and conditions at the tube inlet for NASA tests.....	45
Table 4.4 Simulated runs and conditions at the tube inlet for METU tests	45
Table 5.1 Inlet conditions and parameters for Kang's experiments [Kang (2001)].....	83
Table 6.1 Inlet conditions for UCB tests.....	97
Table 6.2 Inlet boundary conditions for NASA tests	109
Table 6.3 Inlet boundary conditions for METU tests.....	112
Table C.1 Error percentages of thermodynamic properties of saturated water vapor estimated by polynomial functions	161
Table C.2 Error percentages of thermodynamic properties of liquid water estimated by polynomial functions	162

LIST OF FIGURES

FIGURES

Figure 1.1 The containment cooling of AP1000 during the accident	5
Figure 1.2 Arrangement of isolation condenser in the pool	6
Figure 2.1 Schematic representation of the physical model.....	8
Figure 4.1 Film-wise condensation in a vertical cylindrical tube	26
Figure 4.2 Force balance in the condensate liquid layer	29
Figure 4.3 Typical vapor volume element, used to apply the momentum conservation	36
Figure 4.4 Flowchart of the calculation procedure	41
Figure 4.5 Condenser wall temperatures measured in UCB experiments.....	46
Figure 4.6 Liquid film thickness comparison for UCB Run 6.1-2.....	47
Figure 4.7 Liquid film thickness comparison for UCB Run 1.4-1.....	47
Figure 4.8 Liquid film thickness comparison for UCB Run 1.2-4R1	47
Figure 4.9 Liquid film thickness comparison for UCB Run 1.1-1.....	47
Figure 4.10 Comparison of condensation HTC for UCB Run 6.1-2.....	49
Figure 4.11 Comparison of condensation HTC for UCB Run 1.4-1.....	49
Figure 4.12 Comparison of condensation HTC for UCB Run 1.2-4R1	49
Figure 4.13 Comparison of condensation HTC for UCB Run 1.1-1.....	49
Figure 4.14 Calculated and experimental heat fluxes for UCB Run 6.1-2	50
Figure 4.15 Calculated and experimental heat fluxes for UCB Run 1.4-1	50
Figure 4.16 Calculated and experimental heat fluxes for UCB Run 1.2-4R1.....	50
Figure 4.17 Calculated and experimental heat fluxes for UCB Run 1.1-1	50
Figure 4.18 Comparison of condensation HTC for NASA Run 6	52
Figure 4.19 Comparison of condensation HTC for NASA Run 14	52
Figure 4.20 Comparison of condensation HTC for NASA Run 10	52

Figure 4.21 Comparison of condensation HTC for NASA Run 4	52
Figure 4.22 Liquid film Reynolds number comparison for METU Run 1.3.1	53
Figure 4.23 Liquid film Reynolds number comparison for METU Run 1.4.1	53
Figure 4.24 Liquid film Reynolds number comparison for METU Run 1.5.1	53
Figure 4.25 Liquid film Reynolds number comparison for METU Run 1.6.1	53
Figure 4.23 Comparison of heat fluxes for METU Run 1.3.1	54
Figure 4.25 Comparison of heat fluxes for METU Run 1.4.1	54
Figure 4.27 Comparison of heat fluxes for METU Run 1.5.1	54
Figure 4.29 Comparison of heat fluxes for METU Run 1.6.1	54
Figure 5.1 The annular flow and heat transfer inside the jacket tube	57
Figure 5.2 Schematic representation of velocity, turbulent shear stress, total shear stress and the force balance in an annulus.....	61
Figure 5.3 Computed radial variation of the non-dimensional fluctuating velocities in an annulus	71
Figure 5.4 Predicted velocity profiles for different flow and aspect ratios.....	73
Figure 5.5 Measured and calculated velocity profiles [Kuzay (1973)].....	74
Figure 5.6 Measured and calculated velocity profiles [Ball (1972)].....	74
Figure 5.7 Schematic representation of thermal energy balance in the annulus..	77
Figure 5.8 Flow chart of the temperature distribution calculation in the annulus	82
Figure 5.9 Comparison of measured and calculated velocity profiles [Kang (2001)].....	84
Figure 5.10 Comparison of measured and calculated velocity profiles [Kang (2001)].....	84
Figure 5.11 Comparison of measured and calculated velocity profiles [Kang (2001)].....	84
Figure 5.12 Comparison of measured and calculated temperature profiles for experiment 2 [Kang (2001)].....	84
Figure 5.13 Comparison of measured and calculated temperature profiles for experiment 3 [Kang (2001)].....	85
Figure 5.14 Comparison of measured and calculated temperature profiles for experiment 5 [Kang (2001)].....	85

Figure 5.15 Comparison of measured and calculated temperature profiles for experiment 6 [Kang (2001)]	85
Figure 5.16 Comparison of measured and calculated temperature profiles for experiment 8 [Kang (2001)]	85
Figure 6.1 Schematic representation of the coupling procedure	88
Figure 6.2 Flow chart of the whole calculational procedure	95
Figure 6.3 Thermal conductivity variation of SS304	96
Figure 6.4 Mean temperature variation of coolant inside the jacket for Run 6.1-2	99
Figure 6.5 Mean temperature variation of coolant inside the jacket for Run 1.4-1	99
Figure 6.6 Mean temperature variation of coolant inside the jacket for Run 1.3-2	100
Figure 6.7 Mean temperature variation of coolant inside the jacket for Run 1.2-4R1	100
Figure 6.8 Mean temperature variation of coolant inside the jacket for Run 1.2-1	100
Figure 6.9 Mean temperature variation of coolant inside the jacket for Run 1.1-1	100
Figure 6.10 Outer surface temperature variation of the condenser tube wall for Run 6.1-2	101
Figure 6.11 Outer surface temperature variation of the condenser tube wall for Run 1.4-1	101
Figure 6.12 Outer surface temperature variation of the condenser tube wall for Run 1.3-2	101
Figure 6.13 Outer surface temperature variation of the condenser tube wall for Run 1.2-4R1	101
Figure 6.14 Outer surface temperature variation of the condenser tube wall for Run 1.2-1	102
Figure 6.15 Outer surface temperature variation of the condenser tube wall for Run 1.1-1	102

Figure 6.16 Inner surface temperature variation of the condenser tube wall for Run 6.1-2.....	102
Figure 6.17 Inner surface temperature variation of the condenser tube wall for Run 1.4-1	102
Figure 6.18 Inner surface temperature variation of the condenser tube wall for Run 1.3-2.....	103
Figure 6.19 Inner surface temperature variation of the condenser tube wall for Run 1.2-4R1	103
Figure 6.20 Inner surface temperature variation of the condenser tube wall for Run 1.2-1	103
Figure 6.21 Inner surface temperature variation of the condenser tube wall for Run 1.1-1	103
Figure 6.22 Vapor Reynolds number variation for Run 6.1-2	104
Figure 6.23 Vapor Reynolds number variation for Run 1.4-1	104
Figure 6.24 Vapor Reynolds number variation for Run 1.3-2	104
Figure 6.25 Vapor Reynolds number variation for Run 1.2-4R1.....	104
Figure 6.26 Vapor Reynolds number variation for Run 1.2-1	105
Figure 6.27 Vapor Reynolds number variation for Run 1.1-1	105
Figure 6.28 Condensate liquid film thickness comparison for Run 6.1-2.....	105
Figure 6.29 Condensate liquid film thickness comparison for Run 1.4-1.....	105
Figure 6.30 Condensate liquid film thickness comparison for Run 1.3-2.....	106
Figure 6.31 Condensate liquid film thickness comparison for Run 1.2-4R1	106
Figure 6.32 Condensate liquid film thickness comparison for Run 1.2-1.....	106
Figure 6.33 Condensate liquid film thickness comparison for Run 1.1-1.....	106
Figure 6.34 Local condensation heat transfer coefficients for Run 6.1-2	107
Figure 6.35 Local condensation heat transfer coefficients for Run 1.4-1	107
Figure 6.36 Local condensation heat transfer coefficients for Run 1.3-2	107
Figure 6.37 Local condensation heat transfer coefficients for Run 1.2-4R1	107
Figure 6.38 Local condensation heat transfer coefficients for Run 1.2-1	108
Figure 6.39 Local condensation heat transfer coefficients for Run 1.1-1	108

Figure 6.40 Mean temperature variation of coolant inside the jacket for Run 6	109
Figure 6.41 Mean temperature variation of coolant inside the jacket for Run 10	109
Figure 6.42 Inner surface temperature variation of the condenser tube wall for Run 6	110
Figure 6.43 Inner surface temperature variation of the condenser tube wall for Run 10	110
Figure 6.44 Local condensation heat transfer coefficients for Run 6	111
Figure 6.45 Local condensation heat transfer coefficients for Run 10	111
Figure 6.46 Mean temperature variation of coolant inside the jacket for Run 1.3.1	112
Figure 6.47 Mean temperature variation of coolant inside the jacket for Run 1.4.1	112
Figure 6.48 Inner surface temperature variation of the condenser tube wall for Run 1.3.1	113
Figure 6.49 Inner surface temperature variation of the condenser tube wall for Run 1.4.1	113
Figure 6.50 Local condensation heat transfer coefficients for Run 1.3.1	114
Figure 6.51 Local condensation heat transfer coefficients for Run 1.4.1	114
Figure 7.1 Variation of temperature difference between the steam and inner surface of condenser tube wall along the condenser tube	116
Figure 7.2 Local liquid film Reynolds number variation along the condenser tube	117
Figure 7.3 Local liquid film thickness variation along the condenser tube	117
Figure 7.4 Local condensation heat transfer coefficient and liquid film Nusselt number variation along the condenser tube for different steam inlet pressures. 117	
Figure 7.5 Local liquid film Reynolds number variation along the condenser tube	119
Figure 7.6 Local liquid film thickness variation along the condenser tube	119

Figure 7.7 Local condensation heat transfer coefficient and liquid film Nusselt number variation along the condenser tube.....	119
Figure 7.8 Variation of cooling water mean temperature inside the jacket annulus for different coolant inlet temperatures	121
Figure 7.9 Variation of the outer surface temperature of the condenser tube wall for different coolant inlet temperatures	121
Figure 7.10 Variation of the inner surface temperature of the condenser tube wall for different coolant inlet temperatures	121
Figure 7.11 Local liquid film Reynolds number variation along the condenser tube for different coolant inlet temperatures	121
Figure 7.12 Local liquid film thickness variation along the condenser tube for different coolant inlet temperatures.....	122
Figure 7.13 Local condensation heat transfer coefficient and liquid film Nusselt number variation along the condenser tube.....	123
Figure 7.14 Variation of local heat transfer coefficient and local Nusselt number inside the jacket for different coolant inlet mass flow rates.....	124
Figure 7.15 Temperature difference between outer surface of the condenser tube wall and the mean temperature of the cooling water	125
Figure 7.16 Condenser tube outer surface temperature variation for different coolant inlet mass flow rates	125
Figure 7.17 Condenser tube inner surface temperature variation for different coolant inlet mass flow rates	125
Figure 7.18 Local liquid film Reynolds number variation along the condenser tube for different coolant inlet mass flow rates.....	125
Figure 7.19 Local liquid film thickness variation along the condenser tube for different coolant inlet mass flow rates	126
Figure 7.20 Local condensation heat transfer coefficient and Nusselt number variation along the condenser tube for different coolant inlet mass flow rates...	127
Figure A.1 Physical model of the in-tube condensation used by OH-model.....	149
Figure B.1 P Calculated local Γ values for different number of nodes	156

Figure D.1 Local radial heat transfer rate from the outer surface of the condenser tube wall	164
Figure D.2 Local axial heat transfer rate along the condenser tube	164

NOMENCLATURE

Latin Symbols:

A	Area (m^2)
c_p	Specific heat at constant pressure (KJ/kg.K)
D	Diameter (m)
g	Gravitational constant (m/s^2)
G	Mass flux (kg/s.m^2)
h	Convective heat transfer coefficient ($\text{W/m}^2.\text{K}$)
h_{fg}	Latent heat of vaporization (J/kg)
k	Thermal conductivity (W/m.K)
L	Length of the tube (m)
\dot{m}	Mass flow rate (kg/s)
Nu	Nusselt number (hD/k)
p	Pressure, (N/m^2)
P	Perimeter (m)
Pr	Prandtl number ($\mu c_p/k$)
R	Radius (m)
r	Radial location in cylindrical geometry
Re	Reynolds number
q	Heat transfer rate (W)
q''	Heat flux (W/m^2)
T	Temperature (K or $^{\circ}\text{C}$)
u	Velocity component in z-direction (m/s)
\bar{u}	Local time-mean velocity in z-direction (m/s)
x	Independent variable
y	Wall coordinate or dependent variable

z Axial location in cylindrical geometry

Greek symbols:

δ Condensate liquid or boundary layer thickness (m)
 Γ Condensate mass flow rate per unit length (kg/m.s)
 α Thermal diffusivity, $k/\rho c$ (m²/s)
 μ Dynamic viscosity (kg/m.s)
 ρ Density (kg/m³)
 τ Shear stress (N/m²)
 Δ Difference
 ε Convergence criteria

Subscripts:

cl Centerline
 $cond$ Condensate liquid
 cal Calculated
 cw Cooling water
 eff effective
 exp experimental
 $film$ Film
 G Gas, steam
 H Hydraulic
 I Interface
 i Inner surface of the condenser tube or inner region of the annulus
 $in, inlet$ Inlet
 iw Inner surface of the annular passage (Outer surface of the condenser tube wall)
 j Jacket side (annular tube)
 L Liquid
 m Mean

<i>max</i>	Maximum
<i>o</i>	Outer region of the annulus
<i>ow</i>	Outer surface of the annular passage (Inner surface of the jacket tube)
σ	zero shear stress (N/m ²)
<i>sat</i>	Saturation
<i>tot</i>	total
<i>tur</i>	Turbulent
<i>v, vap</i>	Vapor
<i>w</i>	Wall of the condenser tube

Superscripts:

+, *	Dimensionless quantities
<i>n</i>	Iteration index for condensation calculations
<i>l</i>	Iteration index for conjugate heat transfer calculations
-	Mean

Abbreviations:

AP1000	Advanced Passive 1000 MW _e Pressurized Reactor
HTC	Heat Transfer Coefficient
IC	Isolation Condenser
LOCA	Loss of Coolant Accident
METU	Middle East Technical University
NASA	National Aeronautics and Space Administration
PCCS	Passive Containment Cooling System
SBWR	Simplified Boiling Water Reactor
UCB	University of California Berkeley

CHAPTER 1

INTRODUCTION

Conjugate heat transfer is a term used to describe the heat transfer between two different media such as fluid-solid or fluid-fluid where the interface boundary conditions between them are unknown. Conjugate heat transfer occurs when heat transfer in one medium is coupled with the heat transfer in the other. In common industrial applications, the fluid-solid problems are encountered and the flow properties affect the heat transfer and surface temperature in the solid region. Therefore, the governing energy equations for solid and fluid regions are solved simultaneously.

Typically, the unknown parameter is the interface temperature, which can be determined from some knowledge of the heat source. Ever since Perelman (1961) suggested the expression “conjugate heat transfer”, numerous studies have been devoted to this problem. The interest in the conjugate heat transfer problem stems not only from the fundamental nature of the problem, but also largely from the fact that the problem has a wide range of applications in the nuclear reactors, desalination units, cooling of electronic components etc. The conjugate heat transfer problems are encountered in many engineering applications mainly in the following two forms:

a. Heating/cooling of a fluid by a solid body

This form refers to a heat transfer process involving an interaction of heat conduction within a solid body with either of the free, forced, and mixed convection from its surface to a fluid (or to its surface from a fluid) flowing past over it. Thus, a realistic analysis of conjugate heat transfer problems requires the coupling of the conduction problem in the solid with the convection problem in the fluid by satisfying the conditions of continuity in temperature and heat flux at the solid–fluid interface. There are many engineering applications wherein this analysis becomes essential. One of the most common examples is a heat exchanger in which the heat conduction in the tube wall is greatly influenced by the convection in the surrounding fluid. Another important example of conjugate heat transfer problem can be found in fins [Barletta (2007), Mobedi (2006)]. The conduction within the fin and convection in the fluid surrounding it must be simultaneously analyzed to obtain design information precisely.

The conjugate heat transfer analysis finds yet another very important application in the fuel element of nuclear reactors. [Ramis (2007), Jahangeer (2007), Jilani(2002)]. Knowledge of the temperature distribution in the fuel element is needed in order to predict its performance, in particular the highest fuel element temperature and the rate of heat removal. This necessitates a detailed conjugate heat transfer analysis of the heat generating fuel element cooled by forced fluid flow. Conventional heat transfer analysis pertaining to applications of similar nature is based on the assumptions of a uniform surface temperature or uniform heat flux, both of which actually may vary over the solid surface.

Another application of conjugate heat transfer analysis is encountered in the electronic components, in which it is essential to maintain the temperature within the prescribed limits. Therefore, there are numerous conjugate heat transfer studies in the literature, in order to calculate the surface temperatures and to

analyze how it is affected by heat flux variations of the solid surface, depending on different inlet fluid flow conditions [Mathews (2006), Bautista (2006), etc].

In most of the theoretical analyses related to the heating/cooling of a fluid by a solid body which can be found even in the heat transfer textbooks, the temperature distribution along the solid surface is obtained based on the average heat transfer coefficient. However, the accurate temperature distribution at the solid surface can only be calculated by using problem specific local heat transfer coefficients instead of the average heat transfer coefficients obtained from empirical correlations. From another point of view, the calculation of local heat transfer coefficients directly depends on the determination of both the local fluid temperatures and local solid surface temperatures. Therefore, the conjugate solution where the heat conduction equation for the solid body and the energy equation for the fluid flow are coupled should be considered to provide more realistic results for these types of problems [Mobedi (2006)].

b. Two different fluid flows separated by a solid wall

There are common engineering applications for the coupling of two different fluid flows separated by a solid wall where one of them is cooled/heated whereas the other one is heated/cooled. An example for this type of application is the double-pipe heat exchangers. A specific application is the design of the multi-effect distillation plant for seawater desalination, financed by European Union [EasyMED-project (2007)]. The objective is to develop a prototype plant which is easy to operate and which is efficient in use of energy. The basic elements of the plant are vertical plates. On one side of a plate, seawater flows as a falling film and evaporates, whereas on the other side, the plate is heated by condensing vapor. Evaporating and condensing fluid flows at both sides of the plate are laminar [Raach (2005)], Raach (2007)].

In the nuclear technology, there are several engineering applications wherein the conjugate heat transfer becomes essential. The residual heat removal system of the pressurized power reactors (PWR) having once-through type of steam generators can be given as an example. System behavior during an accident initiated by the loss of residual heat removal system after reactor shutdown is greatly affected by the heat transfer mechanisms between the primary (tube) side and the secondary (shell) side of the steam generator, where the dominant mode of heat transfer in the tube is film-wise condensation. Many experimental research studies regarding countercurrent flow for the performance of the once-through type of steam generators during the accident were performed [Tanrıkut (2005), Seul (1999), etc].

Another example of this type of the problem is found in the containment design of some advanced pressurized power reactors (PWR) such as AP1000 [IAEA-TECDOC-872 (2001)]. This design utilizes a unique system to maintain the containment pressure and temperature within design limits. Figure 1.1 shows a schematic of the reactor containment. In the event of a postulated accident where high pressure cooling water escapes into the containment, the pressure and temperature will increase as water flashes to steam. The steam will in turn start to condense on the steel containment vessel surface which is initially at ambient temperature. This results in an increase in the surface temperature of the steel wall. The heating of the steel containment wall causes air flow from outside, due to buoyancy forces, to be drawn in through an air baffle between the concrete containment and the steel inner wall (not present in current reactors). This temperature difference along the wall leads to the condensation of steam inside the containment and sets up an air circulation in the countercurrent direction at the outside of the containment wall.

Another example is encountered in the design of one of the safety system of the simplified boiling water reactor (SBWR). One of the major innovations of the SBWR is the passive containment cooling system (PCCS) capable of

sustaining containment cooling for 72 hours (long term cooling). This passive cooling system relies upon condensation efficiency to remove steam from the containment atmosphere. Typical example of in- tube condensation of steam is the isolation condenser (IC) of the PCCS that has a function of a passive heat exchanger. After a typical loss of coolant accident, steam from the reactor containment/ pressure vessel may flow to the IC where it condenses moving downward inside, externally cooled vertical tubes located in a pool (Figure 1.2). This increases the containment's capability to withstand the loads expected in case of a hypothetical severe accident [Sato (2007), IAEA-TECDOC-1149 (1998)].

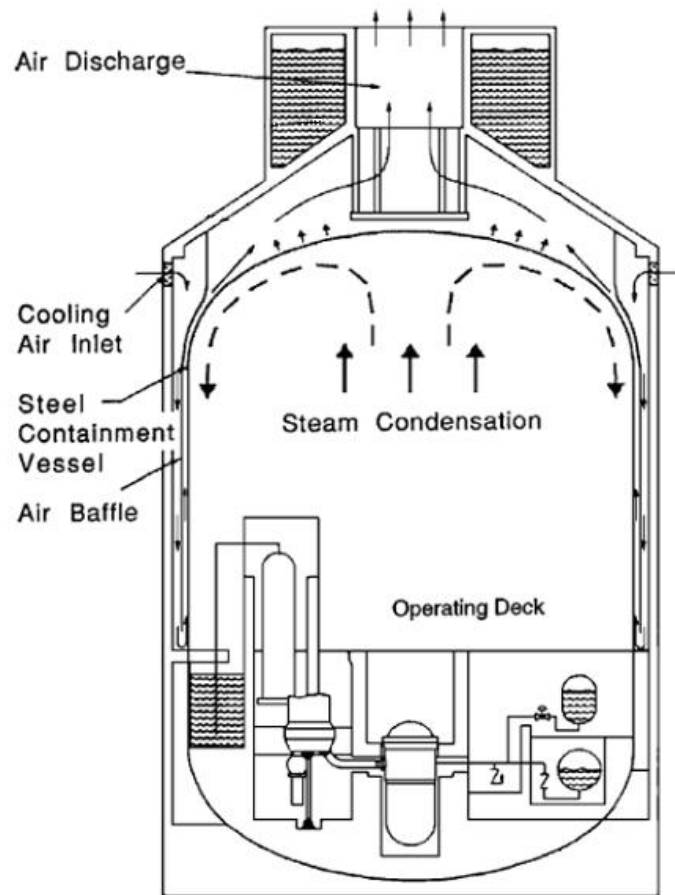


Figure 1.1 The containment cooling of AP1000 during the accident

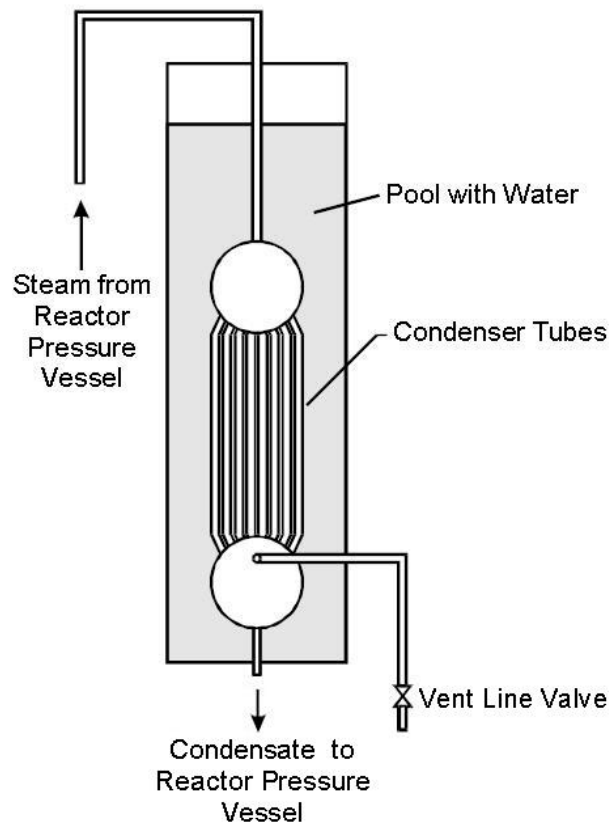


Figure 1.2 Arrangement of isolation condenser in the pool

CHAPTER 2

SCOPE OF THE STUDY

2.1 Definition of the problem

The thermal boundary layer formation over a wall surface is strongly influenced by the wall thermal conditions. These thermal conditions are either prescribed as wall temperature or wall heat flux. There is a third boundary condition where the interaction between the fluid convection and conduction through the wall is considered. In the third boundary condition, the temperature variation along the wall surface is generally unknown and the unknown temperature profile is determined by taking account of this interaction, i.e., coupling of the heat conduction equation for the wall, continuity, momentum and energy equations for the fluid flow. If there is a condensation process at one side of the wall, this condensation phenomenon is also involved into this interaction. Therefore, this type of problem is named “*conjugate condensation heat transfer problem*”.

2.2 Thesis objective and outline

In this study, the conjugate-condensation problem will be investigated in two concentric tubes. Figure 2.1 shows the system considered in the analysis. As the steam condenses downwards inside the condenser tube, the heat is transferred from the condenser tube by the cooling water flowing upwards in the jacket tube. The figure also shows the development of condensate liquid film layer inside the tube and thermal boundary layer in the coolant flow outside of the tube.

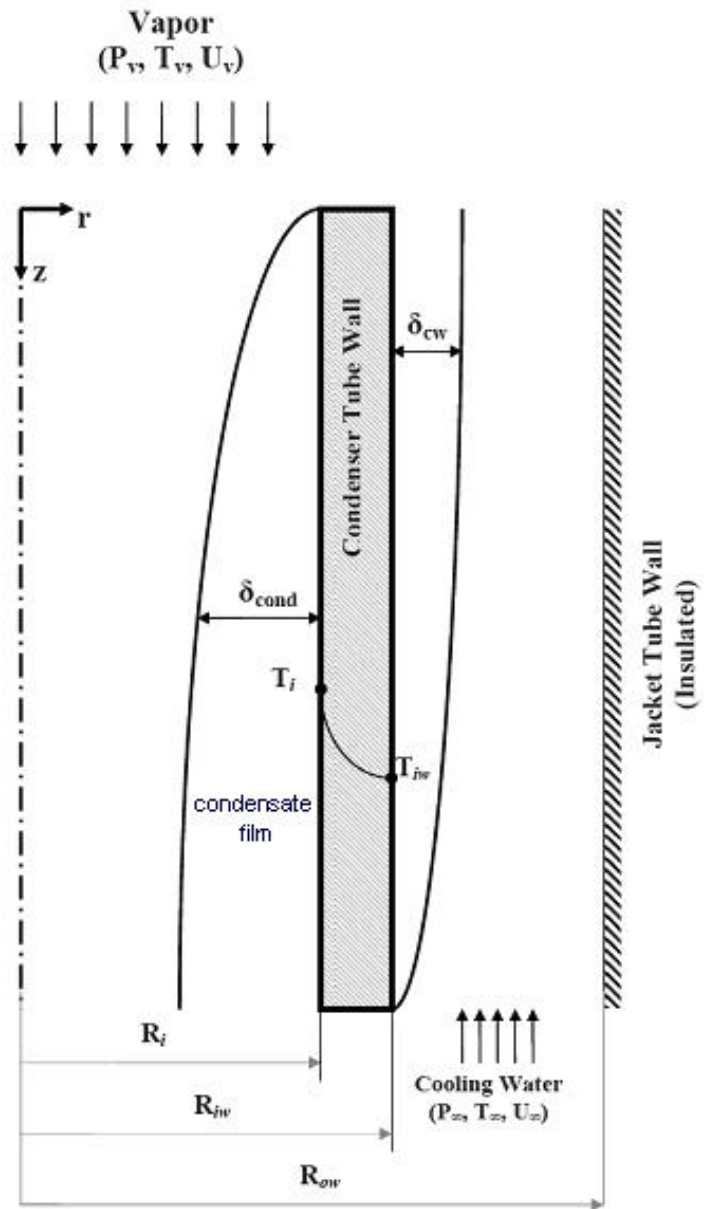


Figure 2.1 Schematic representation of the physical model

Due to unknown wall temperature of the condenser tube, formation of condensate liquid layer inside the tube and development of the thermal boundary layer in the cooling water flow are affected by the other's local conditions (Figure 2.1). Therefore, film-wise condensation, heat conduction through the condenser tube wall and heat removal from the outer surface of the condenser tube by cooling water flow should be coupled and solved simultaneously.

For the solution of the conjugate condensation heat transfer problem inside the vertical tubes, the following boundary conditions and assumptions are considered:

- a) The vapor and cooling water flows at both sides of the condenser tube wall are steady.
- b) Hydrodynamically fully developed flows are established for the vapor and cooling water entering the tube and annulus respectively.
- c) Inlet thermo-physical conditions of the vapor and cooling water are both known. The vapor entering the tube is saturated.
- d) The vapor and cooling water flows are turbulent, whereas the condensate film flow inside the tube is laminar.
- e) Only film-wise condensation occurs inside the condenser tube; mist formation and wavy effects are disregarded.
- f) The jacket tube wall is insulated.
- g) The interfacial shear stresses acting on the condensate film and the vapor are not equal due to the condensation process inside the tube.
- h) Heat is transferred from the condensate to cooling water thorough the condenser tube wall only in radial direction.
- i) Dimensions of the condenser tube and jacket tube are uniform and constant throughout.

There are three important phenomena in the conjugate condensation heat transfer in vertical tubes cooled by forced turbulent fluid flow. These phenomena

can be classified as condensation process, heat transfer to the turbulent water flow inside the annulus and conjugate heat transfer between the solid and fluid regions. Therefore, in the present study, a stepwise modeling is performed for each phenomenon.

For the first step, the condensation inside a vertical tube is analyzed with known variable tube surface temperature. In Chapter 4, an analytical model for condensation of a vapor flowing downward inside a vertical tube is developed. This model is also compared with the results of three experimental data bases; UCB [Kuhn (1994)], NASA [Goodykontz (1966)] and METU [Tanrikut (1998)].

At the second step, the fluid flow and the heat transfer mechanism is modeled at the outside of the condenser tube. In Chapter 5, inside the annular passage, the velocity and temperature distributions for the turbulent fluid flow are solved with a given variable heat flux ($q''(z)$) from the outer surface of the condenser tube while the cooling water is flowing inside the annular passage. This model is also compared with some experimental results in the literature.

At the final step, these two different problems are combined by the energy balance and the conduction equation for the condenser tube wall and they are coupled via temperatures and heat fluxes at the inner and outer surfaces of the condenser tube wall respectively. In order to solve this identified conjugate problem involving condensation-conduction-convection phenomena, a computer code named ZEC, is developed in Chapter 6. The comparisons between the results of ZEC and the experimental data bases of UCB [Kuhn (1994)], NASA [Goodykontz (1966)] and METU [Tanrikut (1998)] are presented and interpreted. By using computer code ZEC, the effect of some parameters such as inlet pressure and mass flow rate of vapor, inlet temperature and mass flow rate of the coolant on the condensation process are analyzed in Chapter 7.

CHAPTER 3

LITERATURE SURVEY

There are three important phenomena in the conjugate condensation heat transfer in vertical tubes cooled by forced turbulent fluid flow. These phenomena, as previously stated in Chapter 2 are conjugate heat transfer, condensation process and heat transfer to turbulent fluid flow inside an annular channel. So, the literature survey is based on these three classifications.

3.1. Conjugate heat transfer at solid-fluid interfaces

Perelman (1961) is probably the first researcher who suggested the expression “conjugate heat transfer”. He studied the laminar flow over an internally heated flat plate with asymptotic expansions. He identified a parameter that combined the ratio of the conductivities of the fluid and the solid, the Prandtl number and the Reynolds number. This work was followed up by Luikov (1971, 1974). He termed Perelman’s parameter and used it in an approximate analysis involving simplified thin-solid geometry with a linear temperature distribution across the solid, i.e., a one dimensional model.

Karvinen (1978) used the integral method to solve a problem similar to that considered by Luikov. Karvinen presented an approximate method for solving the conjugate heat transfer problem associated with a heat generating plate cooled by forced convection flow, and achieved good agreement with measured data.

Sparrow (1982) studied the conjugate heat transfer problem associated with a vertical plate cooled by laminar forced convection flow. One-dimensional conduction equation for the fin and boundary layer equations for the fluid were solved simultaneously by satisfying the conditions of continuity of temperature and heat flux at the solid–fluid interface. Keeping Prandtl number fixed at 0.7 for air, the numerical results were presented for a range of values of conduction–convection parameter.

Conjugate heat transfer problem of a plate cooled by laminar forced convection boundary layer flow was carried out by Garg (1986). One dimensional conduction equation for the plate and boundary layer equations for fluid were solved simultaneously by similarity solution approach. The results were presented for a wide range of Prandtl number and conduction–convection parameter.

Yu (1991) proposed a very effective solution method for solving the conjugate conduction forced convection problems. For incompressible, laminar boundary layer flow of a fluid with constant thermo-physical properties over a flat plate and a wedge, the interface temperatures and heat transfer rates were computed accurately using finite-difference scheme with marching technique.

Conjugate heat transfer problem associated with forced convection flow over a conducting slab sited in an aligned uniform stream was analyzed analytically as well as numerically by Vynnycky (1998). For the full numerical solutions, the governing equations were first developed in dimensionless stream function–vorticity–temperature form and then solved using a finite difference scheme. The numerical results were presented for a wide range of Reynolds number, Prandtl number, aspect ratio of the slab and thermal conductivity ratio of the slab and the fluid.

Chiu (2001) studied conjugate heat transfer of horizontal channel both experimentally and numerically. He found that the parametric study of

operational parameters related to the conjugate heat transfer revealed that the addition of conjugate heat transfer significantly affects the temperature and heat transfer rates at the surface of the heated region.

Jilani (2002) numerically studied conjugate heat transfer problem associated with a heat generating vertical cylinder cooled by upward forced flow. The two-dimensional conduction equation for the heat generating cylinder and boundary layer equations for the fluid were discretized using finite difference schemes. While the two-dimensional heat conduction equation for the cylinder was solved using Line-by-Line method, marching technique solution procedure was employed to solve the boundary layer equations for the fluid. Results were presented for a wide range of aspect ratio, heat generating and conduction–convection parameters, keeping Prandtl number fixed at 0.005.

Chen (2005) proposed a technique which was used the linear least-squares-error method to estimate the unknown outer-wall heat flux for conjugate heat transfer within a thermally developing, hydrodynamically developed turbulent flow in a circular pipe. The proposed method was applied to solve the steady two-dimensional conduction equation for the pipe wall and the steady two-dimensional convection equation for the flowing fluid simultaneously. The method requires no prior knowledge of the functional form of the unknown wall heat flux, and yields solutions for the unknown conditions within a single computational iteration. The results compared the experimental data confirm that this method is capable of providing precise predictions of the unknown outer-wall temperature, and heat flux.

Jahanger (2007) studied the conjugate heat transfer problem pertinent to rectangular nuclear fuel element dissipating fission heat into upward moving liquid sodium. Introducing boundary layer approximations, the equations governing the flow and thermal fields in the fluid domain were solved simultaneously along with two-dimensional energy equation in the solid domain

by satisfying the continuity of temperature and heat flux at the solid–fluid interface. While the boundary layer equations were discretized using fully implicit finite difference scheme so as to adopt marching technique solution procedure, a second-order central difference scheme was used to discretize the energy equation in the solid domain and the resulting system of finite difference equations were solved employing Line-by-Line Gauss–Seidel iterative solution procedure.

Barletta (2008) studied the conjugate heat transfer problem in a parallel-plane channel. The hydrodynamically developed laminar flow inside the channel was assumed with a boundary condition given by a temperature distribution on the external side of the channel wall, which undergoes a sinusoidal longitudinal change. The local energy balance equation was written with reference to the fully developed region, where the temperature distribution was expressed as a periodic function of the longitudinal coordinate. The temperature field in the solid wall and in the fluid, as well as the local and average Nusselt number, was determined analytically and numerically.

Ramis (2008) presented a comparative study of uniform and non-uniform volumetric energy generation in a rectangular nuclear fuel element cooled by upward moving stream of liquid sodium. Employing finite difference schemes, the boundary layer equations governing the flow and thermal fields in the fluid domain were solved simultaneously with two-dimensional energy equation in the solid domain by satisfying the continuity of temperature and heat flux at the solid–fluid interface. Numerical results were presented for a wide range of aspect ratios, conduction–convection parameters, total energy generation parameters, and flow Reynolds number.

Lin (2008) investigated the conjugate heat transfer characteristics of a single-phase rectangular natural circulation loop numerically. Effects of the wall thermal conductivity and the wall thickness on the heat transfer behavior in a

circulation loop with fixed geometrical configuration were analyzed in detail. It was shown that the presence of axial conduction through thick and highly conductive loop wall tends to strengthen markedly the buoyancy-induced circulating flow in the loop at lower Rayleigh number.

Bilgen (2009) presented a numerical and experimental study of conjugate heat transfer by conduction and natural convection on a heated vertical wall. The system considered was a wall subject to uniform heat flux on one side and cooled on both sides by natural convection of surrounding air. The equations of mass, momentum and energy conservations were solved by the control volume method, Simpler algorithm [Patankar (1980)]. The non-dimensional wall thickness was varied from 0.02 to 0.10, the wall to air conductivity ratio from 1 to 100 and Rayleigh number from 10^3 to 10^9 . The results were presented in terms of Nusselt number on both surfaces as a function of Rayleigh number, and in terms of governing parameters of wall thickness and conductivity ratio. It was found that Nusselt number was a strong function of Rayleigh number and wall thickness, and a weak function of conductivity ratio.

Arıcı (2009) studied the conjugate heat transfer in thermally developing laminar forced convection in a pipe including viscous dissipation and wall conductance, numerically. The constant heat flux was assumed to be imposed at the outer surface of the pipe wall. For the solution of the problem, the finite volume method was used. The distributions for the developing temperature and local Nusselt number in the entrance region were obtained. The dependence of the results on the Brinkman number and the dimensionless thermal conductivity were shown. The viscous heating effect on the wall was also shown. Significant viscous dissipation effects have been observed for large Brinkman numbers.

Ramis (2010) analyzed numerically the steady state fluid flow and conjugate heat transfer characteristics of liquid sodium as a coolant flowing past over rectangular nuclear fuel element having non-uniform volumetric energy

generation. Accordingly, employing stream function-vorticity formulation and using finite difference schemes, the equations governing the flow and thermal fields in the coolant were solved simultaneously with energy equation for the fuel element by satisfying the conditions of continuity of temperature and heat flux at the solid–fluid interface.

Also, a literature survey has been performed for the conjugate coupling heat transfer between a condensation process at one side of a solid body and cooling with a fluid at the another side of this body. However, the theoretical studies related to the conjugate condensation heat transfer problems are limited in the literature.

Patankar and Sparrow (1979) solved the problem of laminar condensation on an extended surface by considering the heat conduction in a plate coupled with the condensation process. Their numerical solution of the governing equations confirms the influence of non-isothermal extended surface over the condensing process.

Wilkins (1980) showed that an explicit analytical solution is possible for the formulation of Patankar and Sparrow.

Neglecting inertia and convection terms in the condensate film, Honda and Fujii (1984) solved the forced flow condensation on a horizontal cylinder as a conjugate heat transfer problem.

Sarma (1988) studied the condensation process on a vertical plate of variable thickness. They studied the effect of the plate geometry on the condensation heat transfer and found that this interaction is very important.

Brouwers (1989) performed an analysis of the condensation of a pure saturated vapor on a cooled channel plate, including the interaction between the

cooling liquid, the condensate and the vapor. He obtained in closed form the solution of the governing equations, confirming that this interaction has to be taken into account in order to have more realistic models for this type of process.

Mendez (1996) analyzed the film condensation process of a saturated vapor in contact with one side of a vertical plate, caused by a forced flow on the other side of the plate. They showed that effects of the heat conduction through the plate substantially modify the classical Nusselt's solution [Nusselt, (1916)].

Trevino (1996) studied the transient conjugate condensation process on one side of a vertical plate, caused by a uniform cooling rate on the other surface of the plate, including the finite thermal inertia. In this work, the transient evolution of the condensed layer thickness and the temperature of the plate were obtained using different realistic limits, including the cases of very good and poor conducting plates. Their main results indicated that the condensed layer thickness evolution is almost insensitive to the longitudinal heat conduction effects through the plate, for a thermally thin plate and that the wall thermal inertia was the controlling factor for the transient condensation process, in most practical cases.

Mendez (1997) solved the problem of the laminar condensation process of a saturated vapor in contact with one side of a vertical thin plate, caused by a natural laminar boundary layer flow on the other surface of the plate. The effects of both longitudinal and transversal heat conduction in the plate were considered in the problem.

Mendez (2000) studied the conjugate condensation-heat conduction process of a saturated vapor in contact with a vertical plate. For the non-isothermal wall conditions, it is considered that the base of the plate is maintained at a uniform temperature. The coupling between the vertical fin and the condensed phase offers a new theoretical perspective to the earlier fundamental works on laminar film condensation. In this work, a perturbation methods and the

boundary layer description for the condensed fluid flow is used to show that the longitudinal and transverse heat conduction through the plate.

Char (2001) studied the conjugate film condensation and natural convection along the vertical plate between a saturated vapor porous medium and a fluid porous medium, theoretically. The solution takes into consideration the effect of heat conduction along the plate. The governing equations along with their corresponding boundary conditions for film condensation and natural convection are first cast into a dimensionless form by a non-similar transformation, and the resulting equations are then solved by the cubic-spline method. The primary parameters studied include the thermal resistance ratio of film to plate, the thermal resistance ratio of natural convection to film, and the Jakob number of the subcooling degree in the film. The effects of these dimensionless parameters on the plate temperature distribution and the local heat transfer rate on both sides of the plate are discussed in detail. In addition, the interesting engineering results regarding the overall heat transfer rate from the film condensation side to the natural convection side are also illustrated.

Raach (2005) developed a solution in one-dimension for a plate, where evaporating seawater is distributed as a falling film one side of the plate, whereas on the other side, the plate is heated by condensing vapor. Evaporating and condensing flows at the both side of the plate are laminar. For the laminar condensation, model is based on Nusselt theory where the plate temperature is assumed to be constant for the design of the multi-effect distillation plant for seawater desalination. In the solution procedure, an adaptive grid was used, i.e., the number of cells was constant whereas their coordinates varied according to the changing film thicknesses. Two years later, this program has been developed in two-dimensions for the simulation of the conjugate heat transfer between the condensing water film on the one side of the plate and the evaporating seawater film on the other side [Raach (2007)].

3.2. Film-wise condensation

The first attempt to analyze the film-wise condensation problem is that of Nusselt (1916). It is assumed that wall temperature is constant, liquid film is laminar, material properties are not changing, vapor is stagnant (i.e., no interfacial shear), convective heat and momentum transfer in liquid film is negligible. With those assumptions, an expression for the local film thickness is derived and it is shown that the condensation heat transfer rate depends on condensate local film thickness.

Since the pioneering analysis of Nusselt, many researchers tried to solve the problem by the boundary layer analysis or by an analytical model. The boundary layer model is based on solving the governing equations for the condensation process including the vapor and liquid film regions with appropriate boundary layer approximations. In the analytical models, mass, momentum and energy balances are established with/without some simplifications, depending on the specified problem.

Rohsenow (1956) analyzed the flow of the liquid film and introduced a correction for latent heat in the Nusselt equation. The use of fluid mechanics to solve the condensation problems was proposed by Cess (1960). Sparrow (1959) solved the boundary layer equations of the condensate film for the laminar vapor flow. For flowing vapor, Shekrladze (1966) assumed that the shear stress at the liquid vapor interface is equal to the loss of momentum of the condensing vapour. The integral method has been used by Jacobs (1966) and Fujii (1972). Dobran (1979) numerically studied the laminar film-wise condensation of pure saturated vapor in forced flow in a vertical tube. Chen (1993) used the modified Nusselt analysis considering interfacial shear for the film and the self-similar velocity profile assumption to solve the governing partial differential equation in the vapor region. Neglecting the pressure gradient Srzic (1999) solved the boundary layer equations for condensation of a mixture of vapor and a lighter gas.

The influence of waves on the condensate film has been treated by Unsal (1988a, 1988b), Hung (1996) and Chou (1997), but the effect of waves on the heat transfer coefficient is not well understood in these studies. Jayanti (1997) has analyzed the influence of waves of a given shape and showed that the heat transfer is mainly due to conduction through the liquid film.

For turbulent condensation inside a tube, Carpenter and Colburn (1951) attributed the resistance to heat transfer to the laminar sublayer. Ueda (1972) measured the film thickness and showed the disagreement with the Carpenter-Colburn theory. Bellinghausen (1992) used k - ϵ turbulence model for condensation inside a vertical tube. Numerical analysis of the condensation of pure and mixed vapors by taking the turbulence in the liquid and vapour phases into account has been presented by Louahlia (1996). Munoz-Cobo (1996) developed a model for condensing flows inside tubes, relying on a coefficient of friction derived from single phase flows. An interfacial shear stress model has been proposed by Narain (1997). The effect of two phase flow regimes on condensation inside tubes is discussed by Dobson (1998). Panday (2003) solved numerically the turbulent film condensation of saturated vapor flowing inside a vertical tube based on the fully coupled liquids and vapor phase boundary layer equations. Oh (2005b) developed a modified Nusselt model with a correction factor and using the Blangetti model [Blangetti (1982)]. Oh (2006) also analyzed the film-wise condensation with the non-condensable gas by using this model.

3.3. Heat transfer in the annular channels

The primary practical interest in turbulent fluid flow in a concentric circular annulus is in connection with convective heat transfer in the outer passage of a double-pipe heat exchanger. Because of the non-linear radial variation of the total shear stress within the fluid, the analysis of flow in an annulus is considerably more complex than in a round tube or parallel-plate channel in the laminar as well as in the turbulent regime. Therefore, numerous analytical and numerical studies of turbulent flow in concentric annular channels

at different thermal boundary conditions have been reported. In the following, some of them related to the hydrodynamically fully developed turbulent flow are reviewed.

Lorenz (1937) discovered experimentally that in turbulent flow the location of the maximum in the time-mean velocity distribution in an annulus differs considerably from that for laminar flow. Kjellstrom (1966) derived integral expressions involving the local turbulent shear stress from which it may be inferred that the location of the maximum in the velocity differs from the location of the zero in the total shear stress as well as from their common location in laminar flow. He was unable to confirm experimentally the difference in location between the maximum in the velocity distribution and the zero in the total shear stress for a smooth annulus, but did succeed for an annulus with a roughened inner surface, for which the difference in locations is magnified. Finally, Lawn (1972) confirmed experimentally the non-coincidence for smooth annuli.

Kays (1963) correlated the experimental data of various investigations for the location of the maximum in the velocity distribution in the turbulent regime with the empirical expression

$$\frac{R_m - R_{iw}}{R_{ow} - R_m} = \left(\frac{R_{iw}}{R_{ow}} \right)^{0.343}$$

Rehme (1974) similarly correlated his own experimental data as well as that of others for the location of the zero total shear stress for $Re = 10^5$ with the expression

$$\frac{R_{o\tau} - R_{iw}}{R_{ow} - R_{o\tau}} = \left(\frac{R_{iw}}{R_{ow}} \right)^{0.386}$$

A lot of experiments to determine velocity and temperature profiles have been performed for different fluids. For instance, Heikal (1976) measured the velocity field and wall heat transfer rate in flow of air. Kuzay (1977) measured the wall heat transfer rate and mean temperature distribution in air flow. Hasan (1992) performed the measurements to obtain the velocity and temperature fields in turbulent upflow of liquid Refrigerant-113 through a vertical concentric annular channel. However, these measurements appeared to have suffered from the probes which were rather large compared to the annulus spacing, precluding the measurements near the wall and quite possibly disturbing the flow field. In order to rectify this shortcoming, Velidandla (1996) used a laser Doppler velocimeter for the velocity measurements and simultaneously, a cold wire for the temperature measurements. Recently, by using this measurement technique, Kang (2001) measured time mean axial and radial velocities, the axial and radial velocity and temperature fluctuations, and radial velocity and temperature profiles precisely. Results were reported for Reynolds numbers at channel inlet of 22,800, 31,500, 46,400 and for the annulus inner wall heat fluxes of 0, 9000 and 16,000 W/m².

A number of numerical studies of turbulent flow in concentric annular channels at different thermal boundary conditions have been reported. Quarmby (1968) carried out an analysis of isothermal flow in a concentric annular channel using the Reynolds number and radius ratio of the channel as parameters. The results including the friction factor, the velocity profiles near at the inner and outer walls, and the maximum mean axial velocity location were reported. Hanjalic (1974) simulated isothermal turbulent flow in a concentric annulus using high Reynolds number versions of the transport equations for axial turbulent shear stress, turbulent kinetic energy, and its dissipation rate. The wall boundary conditions for the mean and turbulence quantities were imposed by means of a modified velocity wall law in which the additive constant is a function of the aspect ratio (inner diameter/outer diameter). Azous (1993) simulated isothermal

flow in concentric and eccentric annuli using a low-Reynolds number two-equation k - τ model of turbulence and a mixing length model as closures.

Numerical simulation of the velocity and thermal fields in turbulent flow through a concentric annular channel with its inner wall heated was performed by Wilson (1968) and Malik (1981). Wilson (1968) used the van Driest model of turbulent viscosity which takes into account the viscous damping in the near-wall region. A constant turbulent Prandtl number, ($Pr_t = 1$), was used for $Pr \geq 0.1$ and an empirical relation for Pr_t . Malik (1981) used three different turbulence models to evaluate the eddy viscosity and a constant turbulent Prandtl number of 0.9.

The authors who have reported numerical simulation of turbulent flow and heat transfer in channels using the k - ε model of turbulence are Abdelmeguid (1979), Pietrzyk (1985) and Cotton (1990).

Churchill (1997) reviewed the prior studies on turbulent flow and convection in annuli. As a result of this review, he found that the most of the prior predictive results were highly uncertain owing to the failure to account for the displacement of the maximum in the velocity from that for laminar flow and/or from the zero in the total shear stress.

After Yu (2001) developed a general expression for the velocity profile in the round tubes, this expression has been developed for the circular annuli by Kaneda (2003), taking account of Churchill's review [Churchill (1997)]. He presented a new, essentially exact, differential model, a set of numerical solutions, and a set of generalized predictive equations for the time-averaged velocity distribution and the mixed-mean velocity. The validity of these results was confirmed by comparisons with prior experimental data and with prior numerically computed values.

Yu (2005a) used this fully developed turbulent flow modeling developed by Kaneda (2003) in his analysis. He developed an analytic solution for fully developed convection extended in concentric circular annuli, with the boundary conditions of uniform heating on the inner wall and an adiabatic outer wall. These conditions correspond to longitudinally and angularly uniform electrical resistance heating of the inner wall as well as to iso-enthalpic counter-current flow through an inner tube and the annulus with perfect insulation on the outer wall. Such conditions may be approached in the heat exchangers far away from the entrance. Also this analytic solution which uses Kaneda's velocity profile has been generalized for some alternative boundary conditions by Yu (2005b, 2005c).

3.4. Concluding comments

Since the pioneering paper of Nusselt (1916) on film-wise condensation, simplifications and idealizations have been re-examined during the past decades in order to improve the simple Nusselt's theory. Well-recognized works totally deal with film condensation over the known thermal boundary conditions at the wall. But, the theoretical studies taking the interaction between the solid wall and the film condensation process into account are very limited.

For the conjugate heat transfer in round tubes, there are many studies in the literature, regarding the coupling of single phase fluid flow heat transfer with the solid heat conduction in the tube wall. However, it is apparent from the review of published literature that, any theoretical study considering the conjugate heat transfer between film-wise condensation processes of the saturated vapor flowing turbulently in contact with a surface of a wall caused by counter current forced or natural flow on the other surface of the wall does not exist.

CHAPTER 4

IN-TUBE CONDENSATION MODEL

The theoretical analysis of the condensation of the vapor in a tube has been carried out by many researchers. The analysis of the vapor condensation process generally involves either the boundary layer model or analytical models. The boundary layer model is referred to the solution of the governing equations for the condensation process including the vapor and liquid film regions with appropriate boundary layer approximations. In the analytical models, mass, momentum and energy balances are established with/without some simplifications, depending on the specified problem.

When the analytical methods are compared with the boundary layer model, the balance equations are solved easier than the boundary layer equations due to their simplicity. But, one of the shortcomings of these methods comes from the question of which correlations would be the most appropriate for a given problem. Researchers suggest different correlations for interfacial friction factors, effect of suction, liquid film model, transition Reynolds number in film, waviness effects in film, etc. Therefore, it needs to be developed a mechanistic model reflecting the transport phenomena of mass, momentum and heat transfer.

4.1 Physical description of the problem

The physical model of the co-current downward flow film condensation in a vertical cylindrical tube is shown in Figure 4.1, where the pure vapor entering

the tube is assumed to be in saturated state and the condensate film forms along the tube surface and it is assumed to be laminar (see page 43, paragraph 3). The inner tube surface is maintained at varying temperature, $T_i(z)$, which is given as boundary condition.

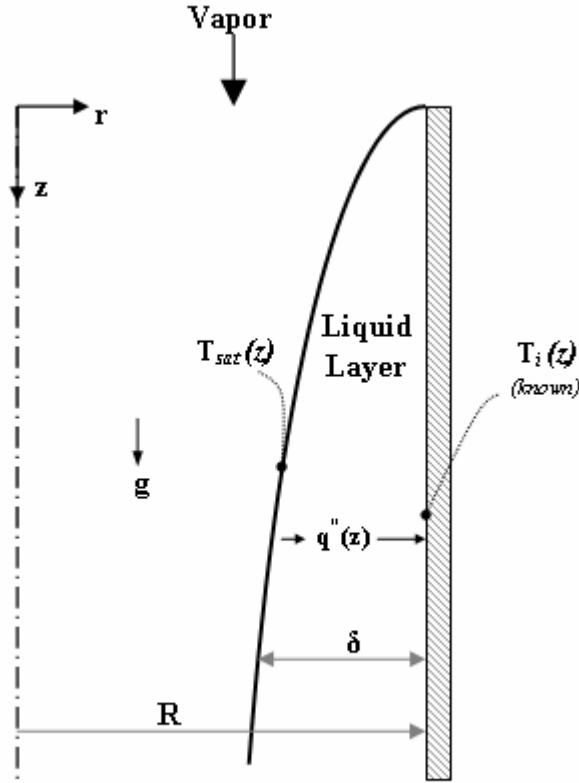


Figure 4.1 Film-wise condensation in a vertical cylindrical tube

An analytical model for the condensation of vapor flowing downward inside a cylindrical tube has been recently studied by Oh, employing the conservation laws [Oh (2006), Oh (2005a, 2005b, 2005c)]. However, OH-model which is summarized in Appendix A has five substantial deficiencies, where;

- Force balance is established for the cartesian geometry, disregarding the area differences in the radial direction for the shear forces,

- Energy balance is constructed and local heat transfer coefficient is calculated in cartesian geometry assuming that the temperature profile in the liquid film is linear.
- Pressure gradient is assumed due to the vapor head only as in the solution of stagnant vapor. But, this is not a good approach if the vapor flow is highly turbulent and the vapor interfacial shear is dominant
- $\frac{\delta}{R_i}$ terms in velocity profile are neglected, assuming that $\frac{\delta}{R_i} \ll 1$ (See Figure A.1 and Eqs. (A.10), (A.11)).
- Shear stress from the liquid to vapor (τ_{IL}) is assumed to be equal to shear stress from the vapor to liquid (τ_{IV}). Namely, $\tau_{IL} = \tau_{IV} = \tau_I$.

Therefore, in this thesis work, an analytical model is developed for the in-tube condensation, overlapping the all above deficiencies. Then, the resulting equations are numerically solved to predict the local condensate film thickness, condensate velocity and local heat transfer coefficients.

4.2 Formulation

Steady, film-wise condensation of a downward vapor flow in a vertical cylindrical tube is considered (Figure 4.1). The vapor flow regime can be either laminar or turbulent, depending on the axial location considered. Near the tube entrance and in the upper region of the tube, the regime may be turbulent. In the lower region, whereas the most of the vapor condenses, the regime might be laminar. It is also assumed that the vapor entering the tube is at saturated state with a fully developed velocity profile.

In order to calculate the local heat fluxes and heat transfer coefficients, the velocity profiles in the liquid and vapor sides have to be determined initially. Therefore, the force balances at both sides should be considered separately.

4.2.1 Liquid layer

An arbitrary distance z , measured from the entrance of the tube is chosen and a force balance is considered on the element of condensate film, lying radially between $R-\delta$ and R , axially between z and $z+dz$ (Figure 4.2).

Force balance inside the liquid layer between z and $z+dz$ can be given as;

$$\tau_{il} P(R-\delta) dz + A_1 p_L + \rho_f g [A_2 (z+dz) - A_1 z] = \tau_L P(r) dz + A_2 \left[p_L + \left(\frac{\partial p_L}{\partial z} \right) dz \right] \quad (4.1)$$

where

$$P(R-\delta) = 2\pi(R-\delta)$$

$$P(r) = 2\pi r$$

$$A_1 = A_2 = A = \pi r^2 - \pi (R-\delta)^2 = \pi [r^2 - (R-\delta)^2]$$

Inserting above expressions into Eq. (4.1);

$$\begin{aligned} & \tau_{il} [2\pi(R-\delta)] dz + \pi [r^2 - (R-\delta)^2] p_L + \rho_f g \pi [r^2 - (R-\delta)^2] dz \\ & = \tau_L [2\pi r] dz + \pi [r^2 - (R-\delta)^2] p_L + \pi [r^2 - (R-\delta)^2] \left[\left(\frac{\partial p_L}{\partial z} \right) dz \right] \end{aligned} \quad (4.2)$$

Eq. (4.2) becomes:

$$2r \tau_L = 2(R-\delta) \tau_{il} + \rho_f g [r^2 - (R-\delta)^2] - [r^2 - (R-\delta)^2] \left(\frac{dp}{dz} \right)_L \quad (4.3)$$

$$\tau_L(r) = \tau_{il} \frac{(R-\delta)}{r} + \frac{[r^2 - (R-\delta)^2]}{2r} \rho_f g - \frac{[r^2 - (R-\delta)^2]}{2r} \left(\frac{dp}{dz} \right)_L \quad (4.4)$$

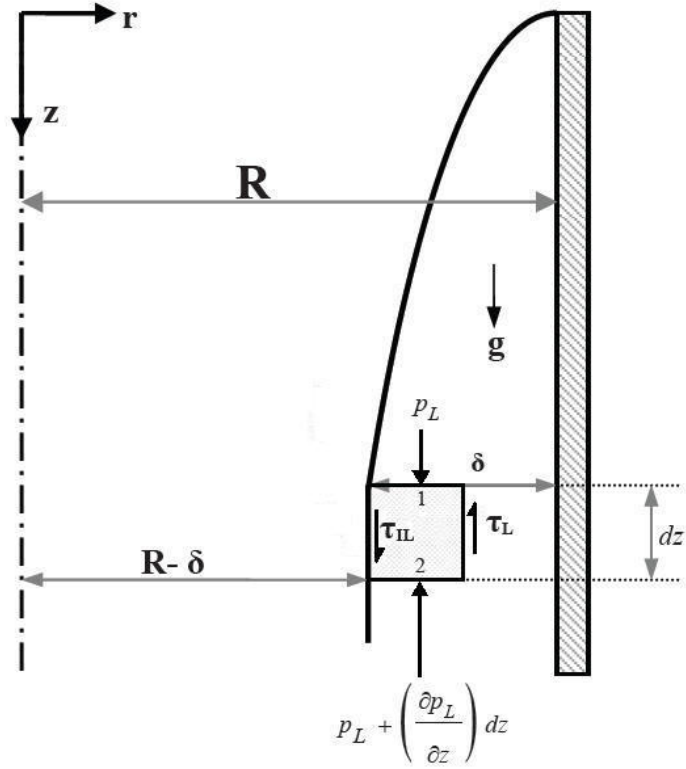


Figure 4.2 Force balance in the condensate liquid layer

Local pressure gradient can be defined with a fictitious vapor density, ρ^* , expressed in the form of [Collier (2001)];

$$\left(\frac{dp}{dz} \right)_L = \rho^* g \quad (4.5)$$

where ρ^* will be determined later.

Defining the shear stress in the liquid layer as;

$$\tau_L(r) = \mu_L \left(\frac{du_L}{dr} \right) \quad (4.6)$$

Inserting Eq. (4.5) and (4.6) into (4.4);

$$\left(\frac{du_L}{dr} \right) = \frac{[r^2 - (R - \delta)^2]}{2r} \frac{(\rho_L - \rho^*)g}{\mu_L} + \frac{(R - \delta)}{r} \frac{\tau_{IL}}{\mu_L} \quad (4.7)$$

Hence, the velocity profile in the laminar liquid film can be obtained from the integration of Eq. (4.7);

$$u_L(r) = \frac{(\rho_L - \rho^*)g}{\mu_L} \left[\frac{r^2}{4} - \frac{(R - \delta)^2}{2} \ln(r) \right] - \frac{\tau_{IL}}{\mu_L} (R - \delta) \ln(r) + C \quad (4.8)$$

In order to find the constant C , the boundary condition $u_L = 0$ at $r = R$ is applied.

$$C = \frac{(\rho_L - \rho^*)g}{\mu_L} \left[\frac{(R - \delta)^2}{2} \ln R - \frac{R^2}{4} \right] - \frac{\tau_{IL}}{\mu_L} (R - \delta) \ln R$$

Condensate liquid velocity profile at any point z , can be given as;

$$u_L(r) = \frac{(\rho_L - \rho^*)g}{\mu_L} \left[\frac{(R - \delta)^2}{2} \ln(R/r) - \frac{(R^2 - r^2)}{4} \right] - \frac{\tau_{IL}}{\mu_L} (R - \delta) \ln(R/r) \quad (4.9)$$

The first term in the right hand side of above equation is the velocity distribution, as in the case of Nusselt analysis with no interfacial shear. The second term is the logarithmic velocity distribution due to the interfacial shear.

For high interfacial shear, the second term is dominant. Hence, the velocity distribution is almost logarithmic. The mass flow rate can be calculated using the velocity profile as follows:

$$\dot{m}_L = \int_{R-\delta}^R \rho_L u_L(r) 2\pi r dr \quad (4.10)$$

The condensation mass flow rate per unit length can be defined as

$$\Gamma(z) = \frac{\dot{m}_L}{2\pi R} \quad (4.11)$$

Integrating Eq. (4.10) by using Eq. (4.9) and inserting this expression into Eq. (4.11); $\Gamma(z)$ becomes;

$$\Gamma(z) = \frac{(\rho_L - \rho^*) \cdot g}{4\nu_L} \left\{ \begin{aligned} &\frac{(R-\delta)^4}{R} \ln\left(\frac{R}{R-\delta}\right) \\ &-\frac{(2R-\delta)(R-\delta)^2 \delta}{2R} - \frac{(2R-\delta)^2 (\delta)^2}{4R} \end{aligned} \right\} \quad (4.12)$$

$$+ \frac{\tau_{IL}}{2\nu_L} \left[\frac{(R-\delta)^3}{R} \ln\left(\frac{R}{R-\delta}\right) - \frac{(2R-\delta)(R-\delta)\delta}{2R} \right]$$

The liquid film Reynolds number and the vapor Reynolds number can be given at any axial location as;

$$\text{Re}_L(z) = \frac{4\Gamma}{\mu_L} \quad (4.13a)$$

$$\text{Re}_v(z) = \frac{2\dot{m}_v}{\pi(R-\delta)\mu_v} \quad (4.13b)$$

In Eq. (4.12), $\Gamma(z)$ is the function of $\delta(z)$, but also there are two unknowns; the fictitious density, ρ^* , and the interfacial shear, τ_{IL} .

Interfacial shear

In the above analysis, the interfacial shear is an unknown parameter, which should be determined by the momentum balance at the film–vapor interface. Two methods are possible for the calculation of the interfacial shear. One method is used to solve the governing equations in the vapor region and to impose the no-slip condition on the tube surface and the continuity of shear at the interface. This method requires relatively long computation time. The other method is used to calculate the interfacial shear with some appropriate correlations as follows:

1. If $\tau_{IL}=0$, it becomes Nusselt solution (no shear at the interface). It works for the stagnant vapor or low vapor flow velocities. However, as the vapor flow velocities increases, interfacial shear becomes dominant. So, $\tau_{IL} \neq 0$.
2. Shear stress from the liquid to vapor (τ_{IL}) is equal to shear stress from the vapor to liquid (τ_{IV}) [Oh (2006)].

$$\tau_{IL} = \tau_{IV} = \tau_I \quad (4.14)$$

$$f = \frac{\tau_I}{\rho_V (\bar{u}_V - \bar{u}_L)^2 / 2} \quad (4.15)$$

where f is the interfacial friction factor given by;

$$\frac{f}{f_0} = \frac{b_f}{\exp(b_f) - 1} \quad (4.16)$$

$$b_f = \frac{\left(\frac{d\Gamma}{dz} \right)}{\rho_V \bar{u}_V (f_0/2)} \quad (4.17)$$

where $\frac{d\Gamma}{dz}$ is called as condensation mass flux.

$$\begin{aligned} f_0 &= 0.079 \text{Re}_V^{-0.25} & \text{Re}_V &\geq 2300 \\ f_0 &= 16/\text{Re}_V & \text{Re}_V &< 2300 \end{aligned} \quad (4.18)$$

3. The interfacial shear stresses, τ_{IV} and τ_{IL} acting on the vapor and liquid are different due to the influence of mass transfer in condensation [Silver (1964), Wallis (1969) and Spalding (1963)].

$$\tau_{IL} \neq \tau_{IV} \quad (4.19)$$

$$\tau_{IV} = \tau_{I0} \frac{a'}{e^{a'} - 1} \quad (4.20)$$

$$\tau_{IL} = \tau_{I0} \frac{a' e^{a'}}{e^{a'} - 1} \quad (4.21)$$

where τ_{I0} is the interfacial shear stress in the absence of phase change, given by;

$$\tau_{I0} = \frac{1}{2} f \rho_V (\bar{u}_V - \bar{u}_L)^2 \quad (4.22)$$

where \bar{u}_V and \bar{u}_L are the mean velocities of the vapor and liquid,

respectively. a' is defined by Wallis (1969) as;

$$a' = \frac{\left(\frac{d\Gamma}{dz} \right)}{f \rho_v (\bar{u}_v - \bar{u}_L)^2 / 2} \quad (4.23)$$

$$f = f_0 \left(1 + 360 \frac{\delta}{2R} \right) \quad (4.24)$$

where f_0 is given in Eq. (4.18).

τ_{IV} and τ_{IL} values obtained from Eq. (4.20) and (4.21) are used in the present analysis.

Pressure drop and fictitious density

The fictitious density is another unknown parameter. It can be determined by solving the governing equations in the vapor region. Since this method requires a large computation time, the following approaches are applied to calculate the pressure drop in liquid layer at any axial location:

1. If only pressure gradient is assumed due to the vapor head [Oh (2005b)], then the fictitious density can be assumed as $\rho^* = \rho_v$, as in the solution of Nusselt. But, this is not a good approach if the vapor flow is highly turbulent and vapor interfacial shear is dominant.
2. One can obtain pressure drop from the force balance at the vapor side assuming average velocities in the radial direction instead of radial velocity profile and then calculate the fictitious density by using single phase approaches [Munoz-Cobo (1996)].

$$\left(\frac{dp}{dz}\right)_V = \left(\frac{dp}{dz}\right)_L = \rho^* g \quad (4.25)$$

So, the fictitious density, ρ^* , can be obtained from the vapor side force balance.

4.2.2 Vapor side

The next step is to apply the conservation of momentum to the vapor volume element shown in Figure 4.3, lying radially $0 < r < (R-\delta)$, and axially between z and $z+dz$.

Force balance at the volume element inside the vapor layer lying between z and $z+dz$;

$$\begin{aligned} A_1 p_V + A_1 (\rho_V \bar{u}_V \bar{u}_V) + \rho_V g [A_2 (z+dz) - A_1 z] = A_{IV} \tau_{IV} \\ + A_2 \left[p_V + \left(\frac{\partial p}{\partial z}\right)_V dz \right] + A_2 \left[(\rho_V \bar{u}_V \bar{u}_V) + \left(\frac{\partial}{\partial z}(\rho_V \bar{u}_V \bar{u}_V)\right) dz \right] \end{aligned} \quad (4.26)$$

where

$$A_{IV} = 2\pi(R-\delta)dz$$

$$A_1 = A_2 = \pi(R-\delta)^2$$

Inserting above expressions into Eq. (4.26), it becomes:

$$(R-\delta) \rho_V g = 2\tau_{IV} + (R-\delta) \left(\frac{dp}{dz}\right)_V + (R-\delta) \left(\frac{d}{dz}(\rho_V \bar{u}_V \bar{u}_V)\right) \quad (4.27)$$

$$\left(\frac{dp}{dz}\right)_V = \rho_V g - \frac{2}{(R-\delta)} \tau_{IV} - \left(\frac{d}{dz}(\rho_V \bar{u}_V \bar{u}_V)\right) \quad (4.28)$$

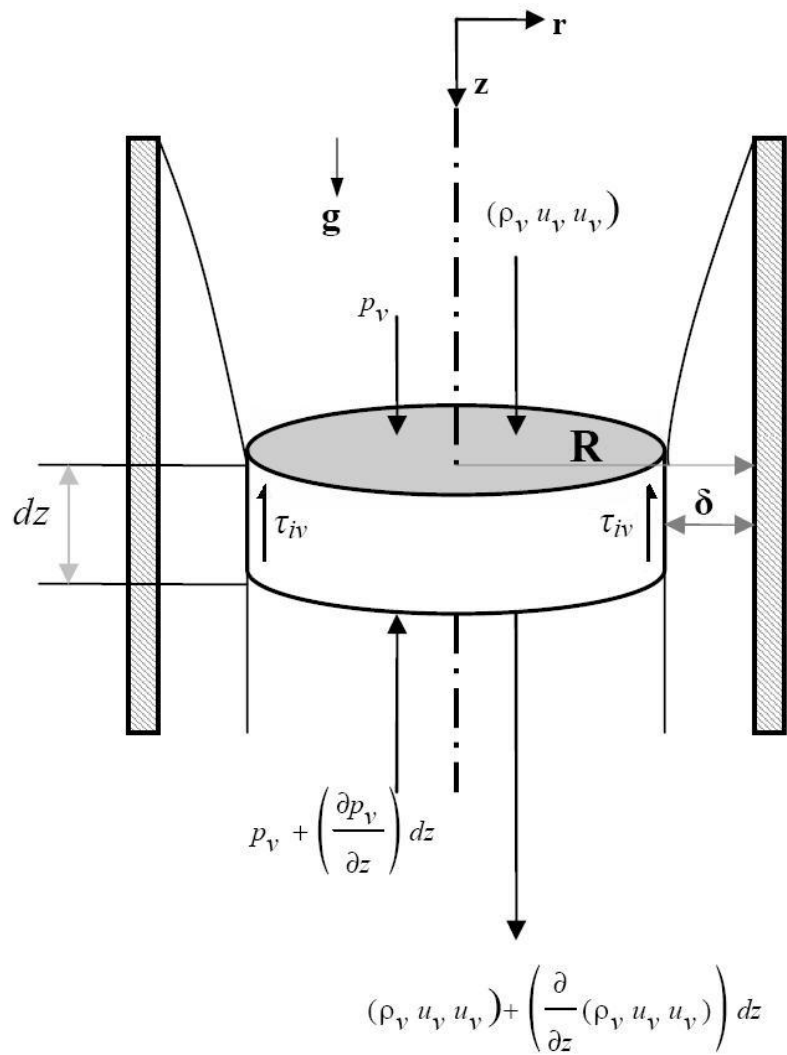


Figure 4.3 Typical vapor volume element, used to apply the momentum conservation

By using the definition of fictitious density given at Eq. (4.25), Eq. (4.28) becomes;

$$\rho^* = \rho_v - \frac{2}{(R-\delta)g} \tau_{IV} - \frac{1}{g} \left(\frac{d}{dz} (\rho_v \bar{u}_v \bar{u}_v) \right) \quad (4.29)$$

For the $\left(\frac{d}{dz} (\rho_v \bar{u}_v \bar{u}_v) \right)$ term, the following expression can be used:

$$\frac{d}{dz} (\rho_v \bar{u}_v \bar{u}_v) = G_v \frac{d\bar{u}_v}{dz} - \frac{R}{(R-\delta)^2} \bar{u}_v \frac{d\Gamma}{dz} \quad (4.30)$$

Inserting above expression into Eq. (4.29), the fictitious density is obtained as;

$$\rho^* = \rho_v \left\{ 1 + \frac{1}{\rho_v g D_H} \left[\frac{4D}{D_H} \bar{u}_v \frac{d\Gamma}{dz} - D_H G_v \frac{d\bar{u}_v}{dz} - 4 \tau_{IV} \right] \right\} \quad (4.31)$$

where the hydraulic diameter (D_H) and the mass flux (G_v) of the vapor are defined as;

$$D_H = 2(R-\delta) \quad (4.31)$$

$$G_v = \rho_v \bar{u}_v \quad (4.31)$$

4.2.3 Energy balance

The heat transfer rate at the vapor and the film region is balanced at the interface as;

$$\left(\frac{d\Gamma}{dz} \right) h_{fg} = h_L (T_{sat} - T_i) \quad (4.32)$$

Heat flux at any axial location in the film region is given as;

$$q'' = h_L \cdot (T_{sat} - T_i) \quad (4.33)$$

$$q'' = -k_L \frac{dT}{dr} \quad (4.34)$$

Since the condensate film flow is assumed to be laminar, heat transfer is by conduction and the temperature profile in the film is similar to that in a hollow cylinder with surface temperatures (T_{sat}, T_i) ;

$$T(r) = \frac{(T_{sat} - T_i)}{\ln\left(\frac{R - \delta}{R}\right)} \ln\left(\frac{r}{R}\right) + T_i \quad (4.35)$$

By using Eq. (4.33), (4.34) and (4.35) at radial point $r = R - \delta$, the film (condensation) heat transfer coefficient can be obtained as;

$$h_L = \frac{k_L}{\left[(R - \delta) \ln\left(\frac{R}{R - \delta}\right) \right]} \quad (4.36)$$

If Eq. (4.32) and (4.36) are combined, the rate of change of the liquid mass flow rate per unit radial length is obtained as;

$$\frac{d\Gamma}{dz} = \frac{k_L \cdot (T_{sat} - T_i)}{h_{fg} \left[(R - \delta) \ln\left(\frac{R}{R - \delta}\right) \right]} \quad (4.37)$$

The liquid film (condensation) Nusselt number can be defined as follow [Tanrikut (1998)];

$$Nu_L = \frac{2h_L R}{k_L} \quad (4.38)$$

4.3 Solution procedure

In order to obtain the local condensation heat transfer coefficient given in Eq. (4.36), it is necessary to determine the local values of five unknown parameters, namely, the liquid film thickness (δ), the condensate mass flow rate per unit length (Γ), the interfacial shears (τ_{ll}, τ_{lv}) and the fictitious density (ρ^*), where these parameters are coupled with five equations given in Eqs. (4.12), (4.20), (4.21), (4.31) and (4.37).

The flowchart of the calculation procedure is summarized as follows (Figure 4.4):

- 1) Specify inlet conditions for vapor (\dot{m}_v, p_v) and the condenser wall temperature profile ($T_i(z)$)
- 2) Start the iteration for the specified node by assuming a condensation mass flux, $\left(\frac{d\Gamma}{dz}\right)_{node}^n$, where n is the index number of iteration and $node$ is the number that shows the axial point for which the calculations are performed. For initial guess of condensation mass flux at $node=1$ and $n=1$

$$\left(\frac{d\Gamma}{dz}\right)_1^1 = 10^{-6}$$

- 3) Calculate the film thickness (δ_{node}^n) from Eq. (4.37).

- 4) Calculate the interfacial shears $\left((\tau_{IL})_{node}^n, (\tau_{IV})_{node}^n \right)$ by using Eqs. (4.18), (4.24), (4.23), (4.22), (4.20) and (4.21).
- 5) Calculate the fictitious density $\left((\rho^*)_{node}^n \right)$ from Eq. (4.31)
- 6) Calculate the condensate mass flow rate per unit length $(\Gamma_{node}^{n+1/2})$ from Eq. (4.12)
- 7) Calculate the condensation mass flux (Γ_{node}^n) from

$$\Gamma_{node}^n = \Gamma_{node-1} + \Delta z \left(\frac{d\Gamma}{dz} \right)_{node}^n$$

- 8) Compare $\Gamma_{node}^{n+1/2}$ and Γ_{node}^n

$$\left\| \frac{\Gamma_{node}^{n+1/2} - \Gamma_{node}^n}{\Gamma_{node}^{n+1/2}} \right\| \leq \varepsilon$$

- 9) Go to next step if the convergence is satisfied. If not, go to Step 2 for the next iteration ($n=n+1$)
- 10) Calculate the local condensation heat transfer coefficient and the local heat flux from Eqs. (4.36) and (4.33) respectively.
- 11) Repeat this calculation procedure from Step 2 through 10 until last node calculation at $z=L$ is performed.

For this calculation procedure, ε is chosen as 10^{-5} and the condenser tube of which the axial length is about 1.5 m is divided into 50 nodes, which is enough for the numerical accuracy (see Appendix B for the verification of 50 nodes).

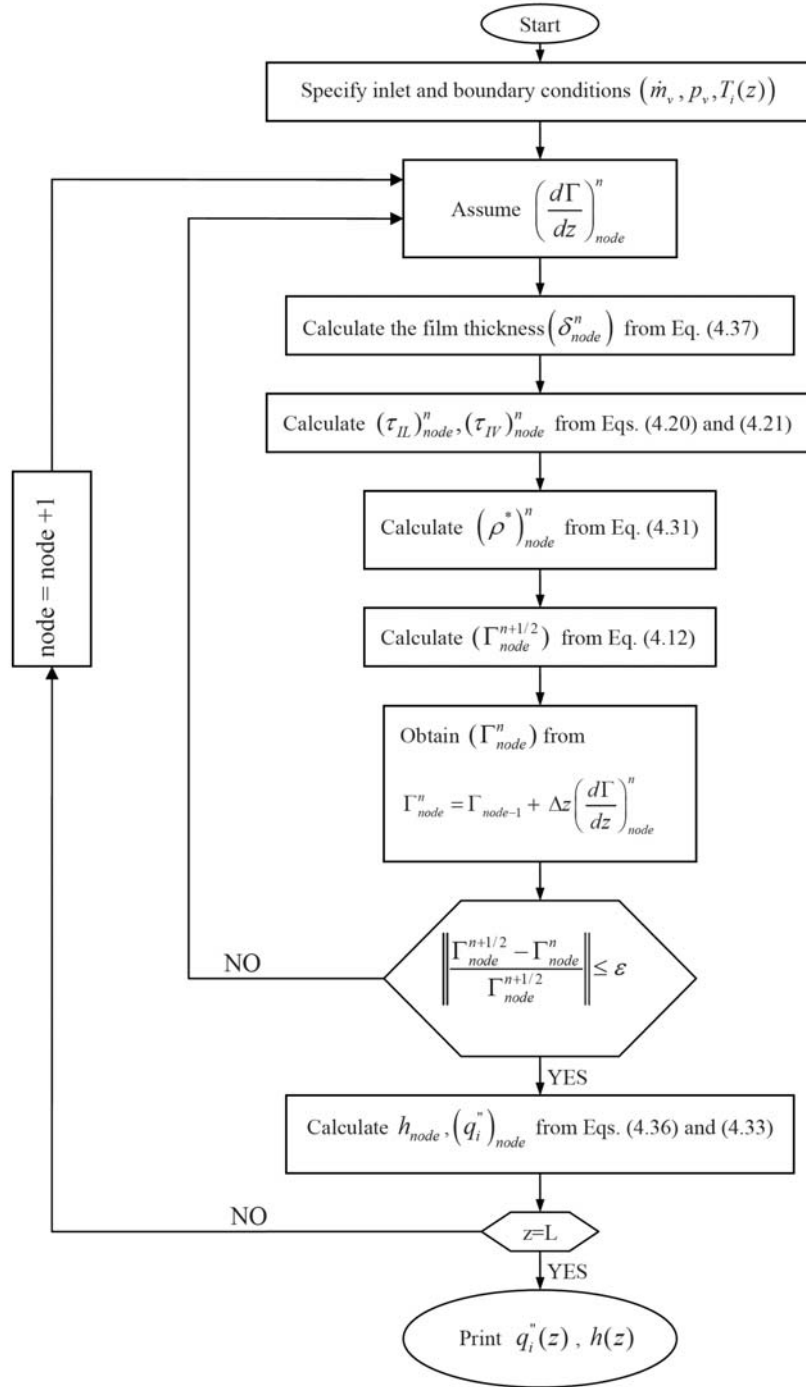


Figure 4.4 Flowchart of the calculation procedure

4.4 Results and discussions

There are some experimental facilities related to in-tube condensation phenomena, where the test sections generally consist of a double-tube annulus. Steam flows and condenses downward inside the condenser tube while the cooling water flows upward in the annulus.

In order to obtain the local heat transfer coefficient from the experiments, steam bulk temperature, local inner wall temperature, and the local heat flux must be known. The thermocouples for certain axial locations are embedded in the wall of the condenser tube to measure the local inner wall surface temperatures. Also, to obtain the local heat flux through the condensate film, an energy balance from the coolant side is used. Another set of thermocouples are mounted into the annulus to measure the coolant bulk temperature.

The local inner wall surface temperature is measured directly and the local heat flux is obtained from the knowledge of the axial coolant temperature profile. From a steady state energy balance on the coolant;

$$q''(z) dA = \dot{m}_{cw} c_{p_{cw}} dT_{cw}, \quad (4.39)$$

or

$$q''(z) = \frac{\dot{m}_{cw} c_{p_{cw}}}{\pi d} \frac{dT_{cw}}{dz} \quad (4.40)$$

From steady state heat balance, the local condensate flow rate is obtained. The heat balance considering only the latent heat transfer is given as;

$$dq = d\dot{m}_{cond} h_{fg} \quad (4.41)$$

The local condensation heat transfer coefficient is obtained as;

$$h(z) = \frac{q''(z)}{(T_{sat} - T_i)} \quad (4.42)$$

The experimental values of local heat transfer coefficient and local condensate flow rate can be compared with the calculated results. Also, experimental values of local liquid film thickness and local liquid Reynolds number can be readily obtained from the local condensate flow rate for the same purpose.

In order to compare the calculated results, there are three available experimental data bases; UCB [Kuhn (1994)], NASA [Goodykontz (1966)] and METU [Tanrikut (1998)]. The parameters of these experimental setups are given in Table 4.1.

The condensate film is reported to be laminar in UCB and METU experiments (no information is reported in NASA experiments). Therefore, in the condensation model developed at the present study, the condensate film is also assumed to be laminar.

From each database, four runs, shown in Table 4.2, 4.3 and 4.4 are selected regarding different steam inlet conditions such as the inlet vapor Reynolds number, the pressure and the mass flow rate.

During the simulation of all experiments, vapor inlet mass flow rates and inlet pressures are selected as tube inlet conditions. Besides this, the condenser tube wall temperature profiles obtained from the experimental databases are directly used as a boundary condition of the simulations. For example, the wall temperatures measured in the UCB experiments are given in Figure 4.5.

Table 4.1 Comparison of the parameters for the pure steam experiments

	UCB [Kuhn (1994)]	NASA [Goodykontz (1966)]	METU [Tanrikut (1998)]
Condenser Tube:			
Inlet steam pressure (kPa)	116-501	112-385	183-545
Inlet steam temperature (°C)	130-151	105- 143	152-168
Inlet steam flow rate (kg/hr)	22-60	15-53	50-123
Inlet Reynolds number	12600-36100	44300-89400	54700-93300
Material	SS.	SS.	SS.
Length (m)	2.42	2.43	2.15
Inner diameter (mm)	47.5	15.875	33.5
Thickness (mm)	1.65	1.5875	4.55
Coolant Side:			
Jacket inner diameter (mm)	73.7	50.8	81.2
Flow rate (kg/hr)	600-1200	492-3483	795-814
Temperature rise (°C)	20-40	5-20	22-35
Inlet Reynolds Number	3000-6500	2000-27000	2000-2200

Table 4.2 Simulated runs and conditions at the tube inlet for UCB tests

Run #	Re_v	\dot{m}_v (kg/s)	p_v (bar)	T_{in} (°C)	T_{sat} (°C)
6.1-2	12614	0.00613889	2.155	130.2	122.6
1.4-1	18083	0.00833333	1.106	126.2	102.5
1.2-4R1	26007	0.01338889	4.093	148.1	144.5
1.1-1	36143	0.01672222	1.161	138.8	103.9

Table 4.3 Simulated runs and conditions at the tube inlet for NASA tests

Run #	Re_v	\dot{m}_v (kg/s)	p_v (bar)	T_{in} (°C)	T_{sat} (°C)
6	44322	0.00743387	3.075	136.02	134.44
14	52132	0.00856786	2.434	127.78	126.67
10	71430	0.01222179	3.847	143.33	142.22
4	89419	0.01474175	2.523	128.10	127.78

Table 4.4 Simulated runs and conditions at the tube inlet for METU tests

Run #	Re_v	\dot{m}_v (kg/s)	p_v (bar)	T_{in} (°C)	T_{sat} (°C)
1.3.1	66875	0.02314	3.03	157.0	133.9
1.4.1	76645	0.02721	3.96	162.7	143.3
1.5.1	85675	0.03101	4.84	165.5	150.6
1.6.1	93365	0.03419	5.45	167.5	155.2

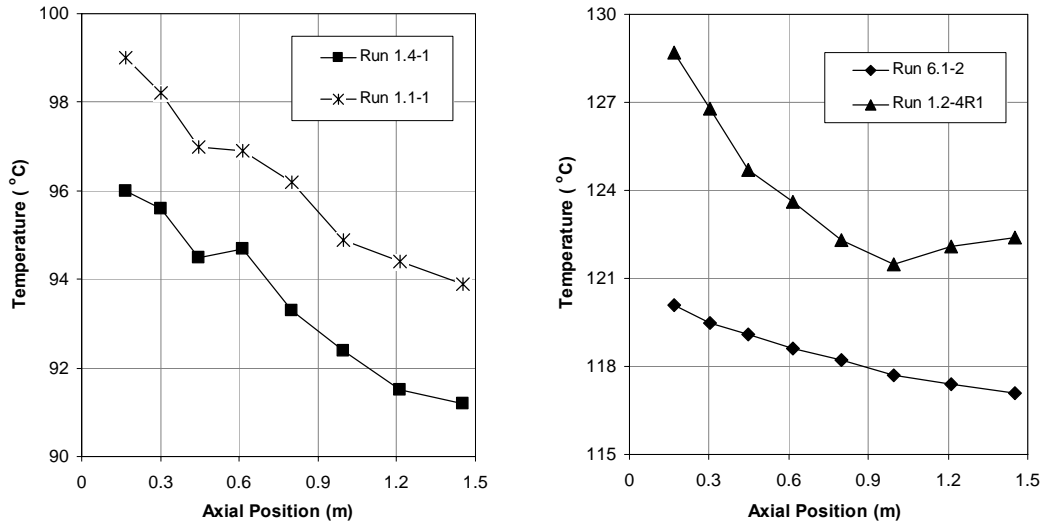


Figure 4.5 Condenser wall temperatures measured in UCB experiments

The liquid film thicknesses, local condensation heat transfer coefficients (HTC) and the local heat fluxes calculated from the present analytical model (SK-model) are compared with the UCB experimental results based on runs in Table 4.2. Also, the calculations for another analytical model, named OH-model given in Appendix B [Oh (2005b)] are performed for the same runs. The comparisons of SK and OH-models with the experimental results are shown in Figure 4.6 through 4.17.

Figures 4.6, 4.7, 4.8 and 4.9 show the variations of the condensate liquid film thicknesses respectively for each case. One can see that the liquid film thickness increases rather steep at the condenser tube inlet. As the steam condenses, the liquid film becomes thicker and so that the thermal resistance increases, leading to slow down of the condensation rate. SK-model model predicts the general trend of experimental data reasonably well while OH-model predicts a thinner film thickness by about less than 15% difference compared to the experimental data.

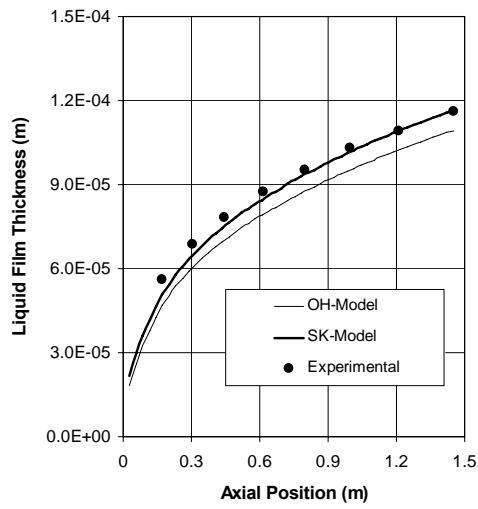


Figure 4.6 Liquid film thickness comparison for UCB Run 6.1-2

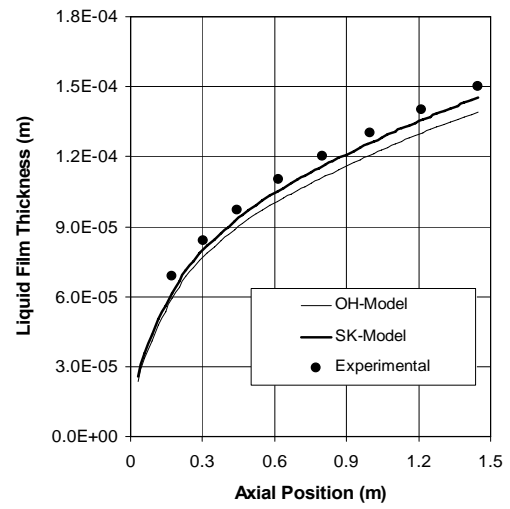


Figure 4.7 Liquid film thickness comparison for UCB Run 1.4-1

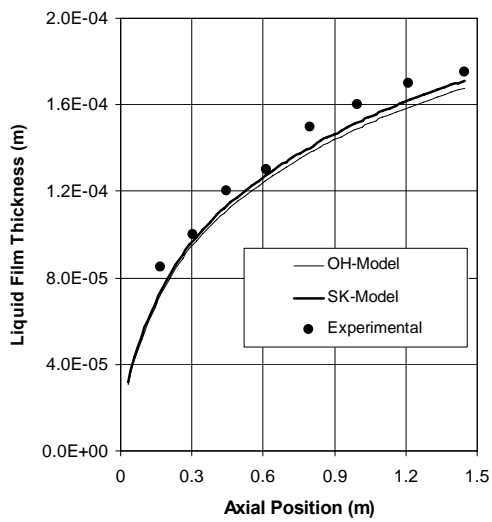


Figure 4.8 Liquid film thickness comparison for UCB Run 1.2-4R1

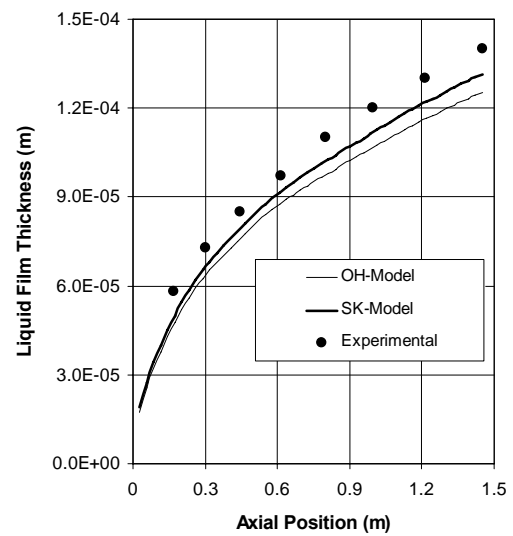


Figure 4.9 Liquid film thickness comparison for UCB Run 1.1-1

In Figures 4.10, 4.11, 4.12, 4.13, the calculated and experimental local heat transfer coefficients are presented for each case. The heat transfer coefficients obtained from SK-model are in agreement with the experimental data. However, OH-model overestimates the local heat transfer coefficients by about less than 20% difference compared to the experimental data for all cases. The calculated local heat transfer coefficient is inversely proportional to the liquid film thickness. SK-model calculates the temperature profile at the liquid layer in radial direction and obtains the local heat transfer coefficients from Eq. (4.36) while the temperature distribution in OH-model is calculated in cartesian geometry and it uses Eq. A.14 to determine the heat transfer coefficients. Therefore, one can say that among these two models, the main reason of the difference in the heat transfer coefficient is undertaken by the error of the calculated liquid film thickness itself and temperature profiles assumed in the liquid layer.

In order to obtain the calculated heat flux values, calculated local heat transfer coefficients and the experimental wall temperatures (Figure 4.5) are used in the following equation:

$$q''_{calc}(z) = h_{calc}(z) \left[T_{sat} - (T_i(z))_{exp} \right] \quad (4.43)$$

It is also noted that the experimental local heat fluxes are obtained from the temperature measurements in the jacket side given in Eq. (4.40). So, in Figures 4.14, 4.15, 4.16, 4.17, the calculated and experimental local heat fluxes are compared for each case. SK-model predicts the general trend of experimental data reasonably well while OH model overestimates the heat fluxes compared to the experimental data for all cases.

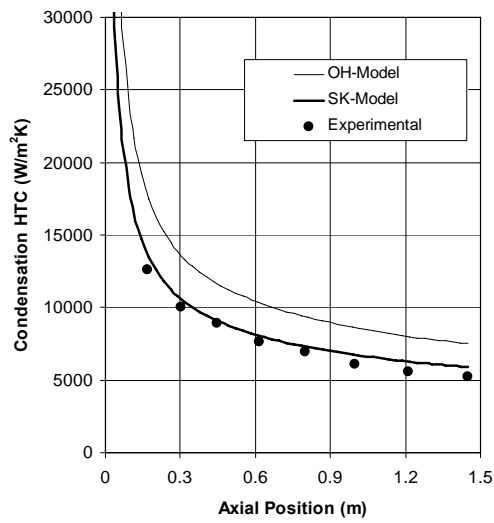


Figure 4.10 Comparison of condensation HTC for UCB Run 6.1-2

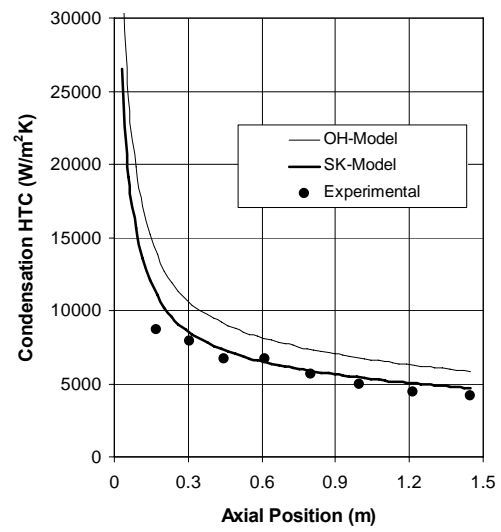


Figure 4.11 Comparison of condensation HTC for UCB Run 1.4-1

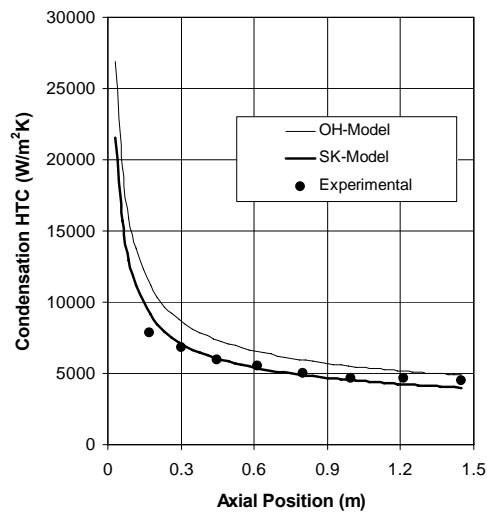


Figure 4.12 Comparison of condensation HTC for UCB Run 1.2-4R1

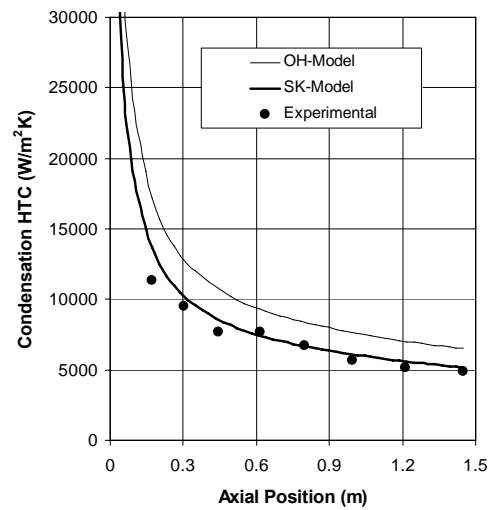


Figure 4.13 Comparison of condensation HTC for UCB Run 1.1-1

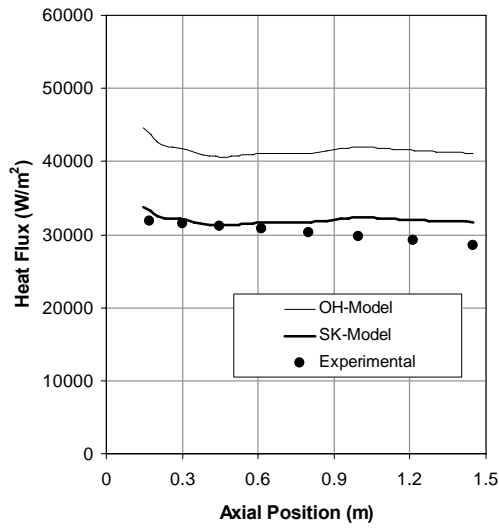


Figure 4.14 Calculated and experimental heat fluxes for UCB Run 6.1-2

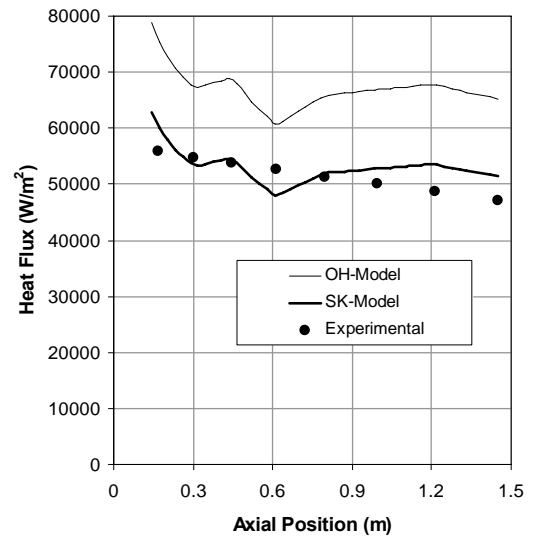


Figure 4.15 Calculated and experimental heat fluxes for UCB Run 1.4-1

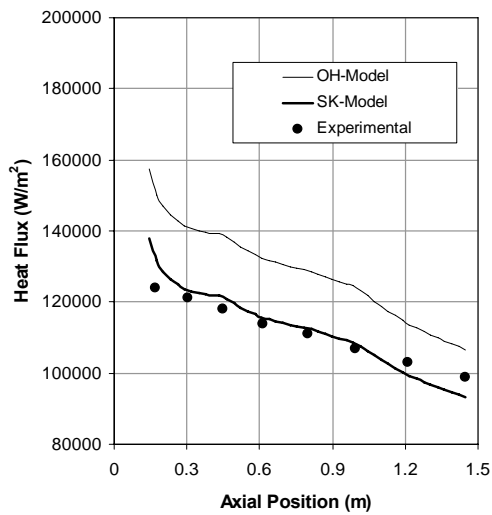


Figure 4.16 Calculated and experimental heat fluxes for UCB Run 1.2-4R1

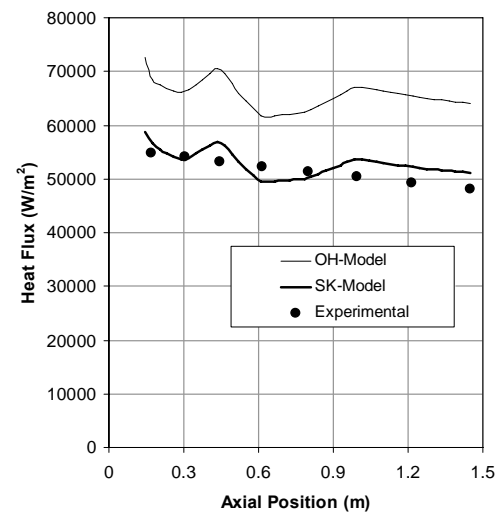


Figure 4.17 Calculated and experimental heat fluxes for UCB Run 1.1-1

The predictions of SK-model are found in favorable agreement over the whole range of UCB experimental results. Although results of OH-model are satisfactory and this model also predicts the general trends, the results of this model are not as accurate as SK-model due to its inherent deficiencies as mentioned before.

Similar comparisons are performed for the NASA experiments. Since there is only experimental information about the local condensation heat transfer coefficients, the results of analytical SK and OH-models for heat transfer coefficients are compared with the experimental data from Figures 4.18 to 4.21. The figures show that both models achieve good agreement with experimental data within $\pm 25\%$ deviation, except at the inlet of the tube. This difference may arise from the high inlet steam Reynolds numbers that does not allow film-wise liquid layer formation at the inlet of tube. This situation may sweep the condensate liquid particles from the tube surface and inhibits the liquid film formation at the entrance of the condenser tube. Since both analytical models disregard the misty flow, the analytical results are very poor at the tube inlet.

Finally, the analytical models are compared with METU experimental results for the liquid film Reynolds numbers and the condensate heat fluxes given in figures from 4.22 to 4.29. SK-model predicts the liquid film Reynolds numbers within $\pm 30\%$ deviation whereas OH-model significantly underestimates the liquid film Reynolds numbers (Figures 4.22, 4.23, 4.24 and 4.25). In the case of heat flux comparisons (Figures 4.26, 4.27, 4.28 and 4.29), SK and OH models underestimate the experimental data within $\pm 40\%$ deviation. In METU experiments, it is reported that the maximum uncertainty associated with the heat flux is $\pm 11\%$ [Tanrikut (1998)].

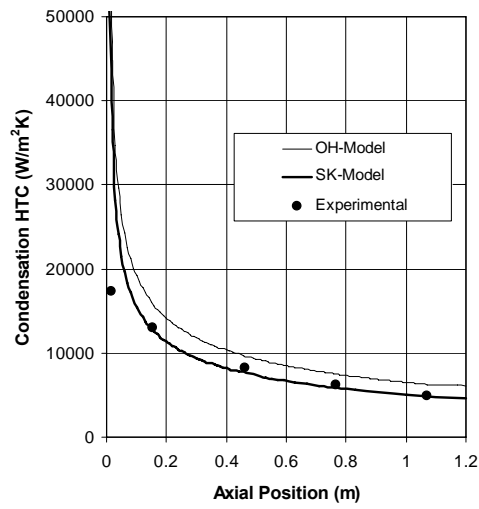


Figure 4.18 Comparison of condensation HTC for NASA Run 6

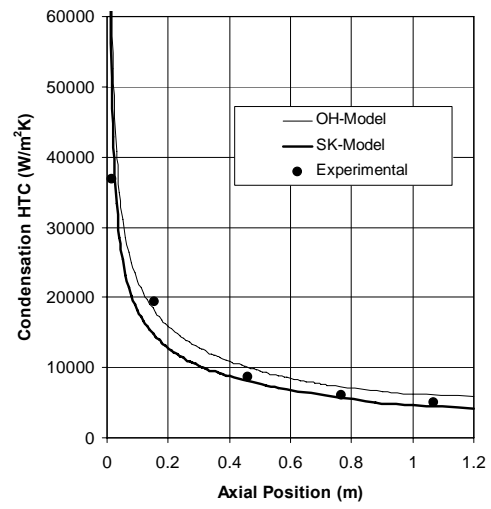


Figure 4.19 Comparison of condensation HTC for NASA Run 14

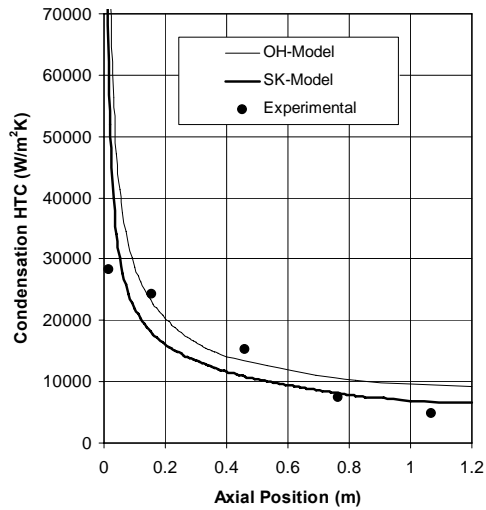


Figure 4.20 Comparison of condensation HTC for NASA Run 10

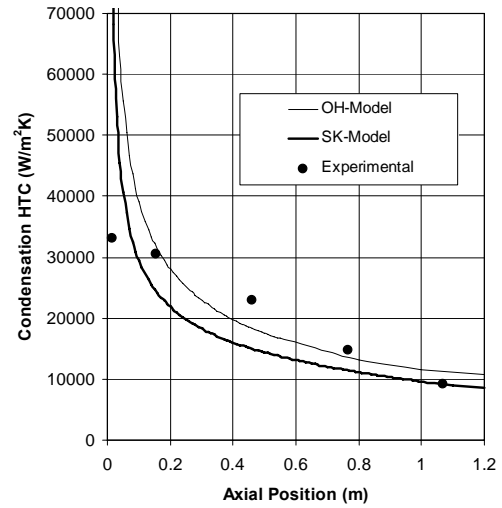


Figure 4.21 Comparison of condensation HTC for NASA Run 4

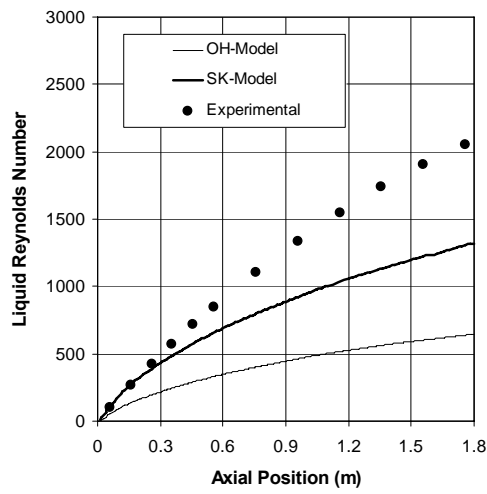


Figure 4.22 Liquid film Reynolds number comparison for METU Run 1.3.1

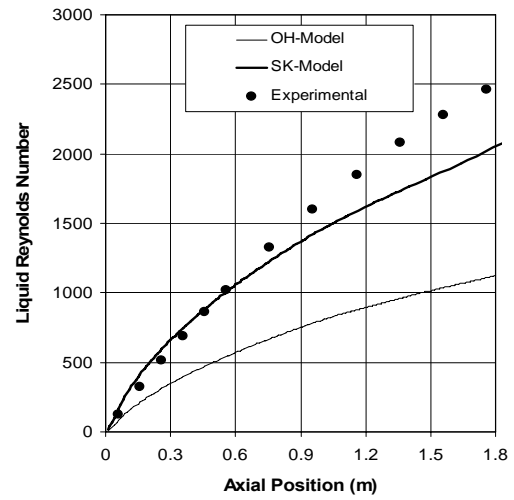


Figure 4.23 Liquid film Reynolds number comparison for METU Run 1.4.1

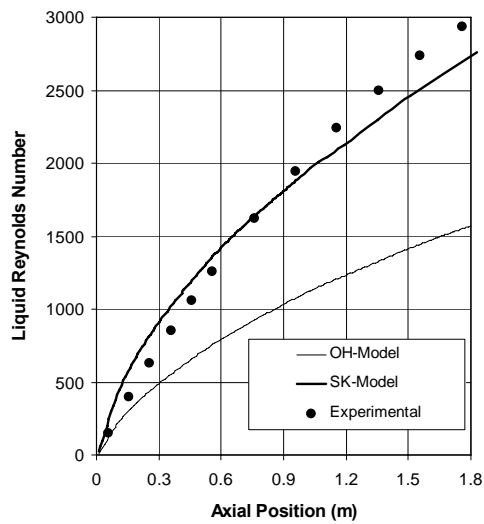


Figure 4.24 Liquid film Reynolds number comparison for METU Run 1.5.1

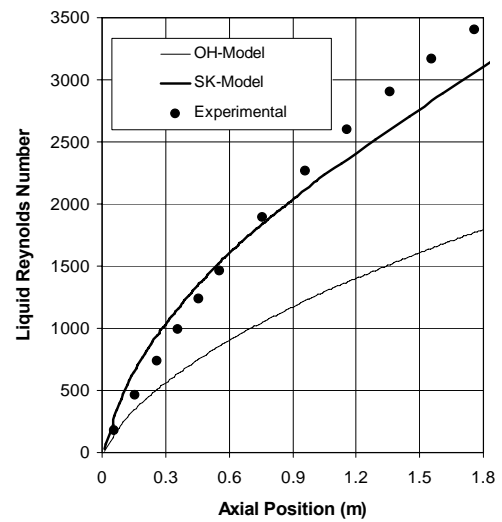


Figure 4.25 Liquid film Reynolds number comparison for METU Run 1.6.1

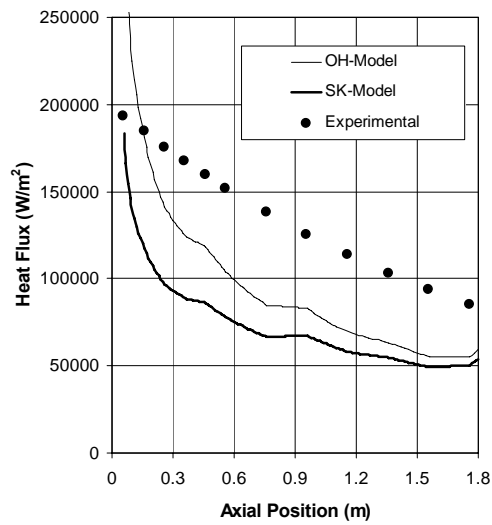


Figure 4.26 Comparison of heat fluxes for METU Run 1.3.1

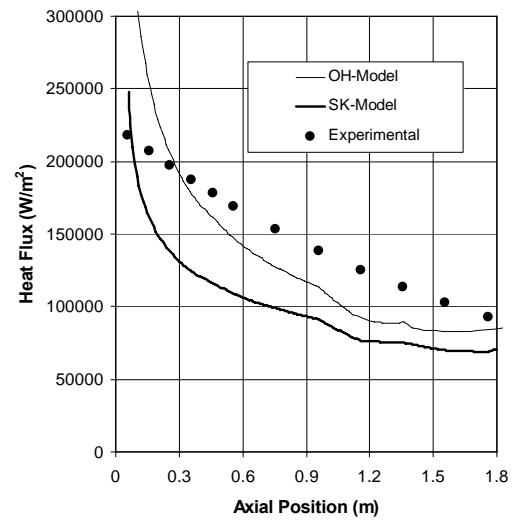


Figure 4.27 Comparison of heat fluxes for METU Run 1.4.1

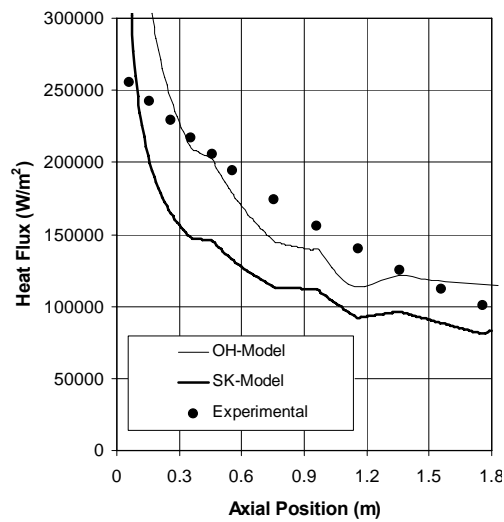


Figure 4.28 Comparison of heat fluxes for METU Run 1.5.1

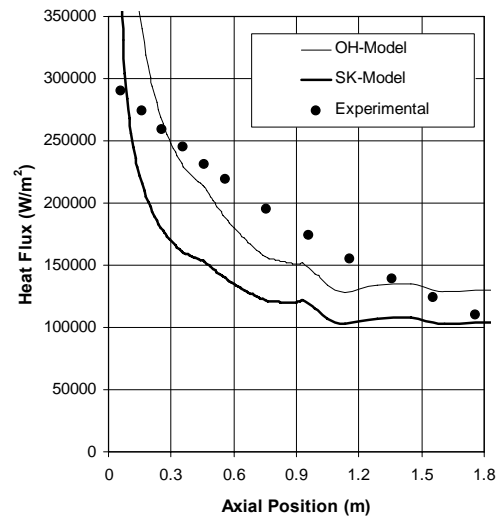


Figure 4.29 Comparison of heat fluxes for METU Run 1.6.1

CHAPTER 5

HEAT TRANSFER IN THE ANNULAR FLOW

Turbulent flow and heat transfer in concentric annular channels have been studied extensively because of its many applications in engineering equipment. The primary practical interest in turbulent flow in a concentric circular annulus is in connection with convective heat transfer in the outer passage of a double pipe heat exchanger. Because of the non-linear radial variation of the total shear stress within the fluid, the analysis of flow in an annulus is considerably more complex than in a round tube or parallel-plate channel in the laminar as well as in the turbulent regime. As the aspect ratio (inner diameter/outer diameter) increases toward unity, the velocity distribution and the friction factor approach to those for a parallel-plate channel in turbulent as well as in laminar flow. As the aspect ratio decreases toward zero, the velocity distribution approaches to that for a round tube but never quite attains it, because the velocity remains zero and the velocity gradient is finite at the inner wall.

As a consequence of its relative complexity, the behavior of both flow and convective heat transfer in an annulus in the fully developed turbulent regime should be characterized and generalized theoretically. The objective of this chapter is to improve a model in a quantitative sense by a combination of theoretical and correlative methodologies. The specific plan is; first to derive the correlating equations for the turbulent shear stress distribution, second to utilize such expressions to calculate the total shear stress distribution, as well as to obtain correlating equations for the time-average product of fluctuating velocity

components in radial and axial directions, third to utilize these values to predict the velocity profile, fourth to utilize these predictive and correlative expressions to determine the heat flux distribution in the annulus. This mission is finally accomplished with the calculation of turbulent thermal conductivity and the temperature distribution in the annular channel.

5.1 Formulation

In this section, a system in which a Newtonian fluid flows with steady motion in an annular pipe is considered (Figure 5.1). It is analogous to the cooling water flow inside the jacket tube for the conjugate condensation heat transfer problem. The fluid temperature, mass flow rate and the pressure at the inlet of the annular pipe are known. A spatially non-uniform heat flux ($q''(z)$) which is distributed along the outer surface of the condenser tube wall is removed by the coolant passing through the annulus. During the solution of the heat transfer problem inside the annular tube, the following conditions and assumptions are considered:

- a) The flow inside the annular tube is steady and potential flow.
- b) Hydrodynamic fully developed flow is established for coolant entering the annulus.
- c) The coolant flow might be laminar or turbulent.
- d) The jacket tube wall is thermally insulated.
- e) Heat is only transferred from the condensate to the coolant inside the annulus through the condenser tube wall. Therefore, the heat flux ($q''(z)$) at the outer surface of the condenser tube (i.e. at the inner wall of the annulus) is a function of axial location only.
- f) Cross sectional areas of the condenser and jacket tubes are uniform and constant.

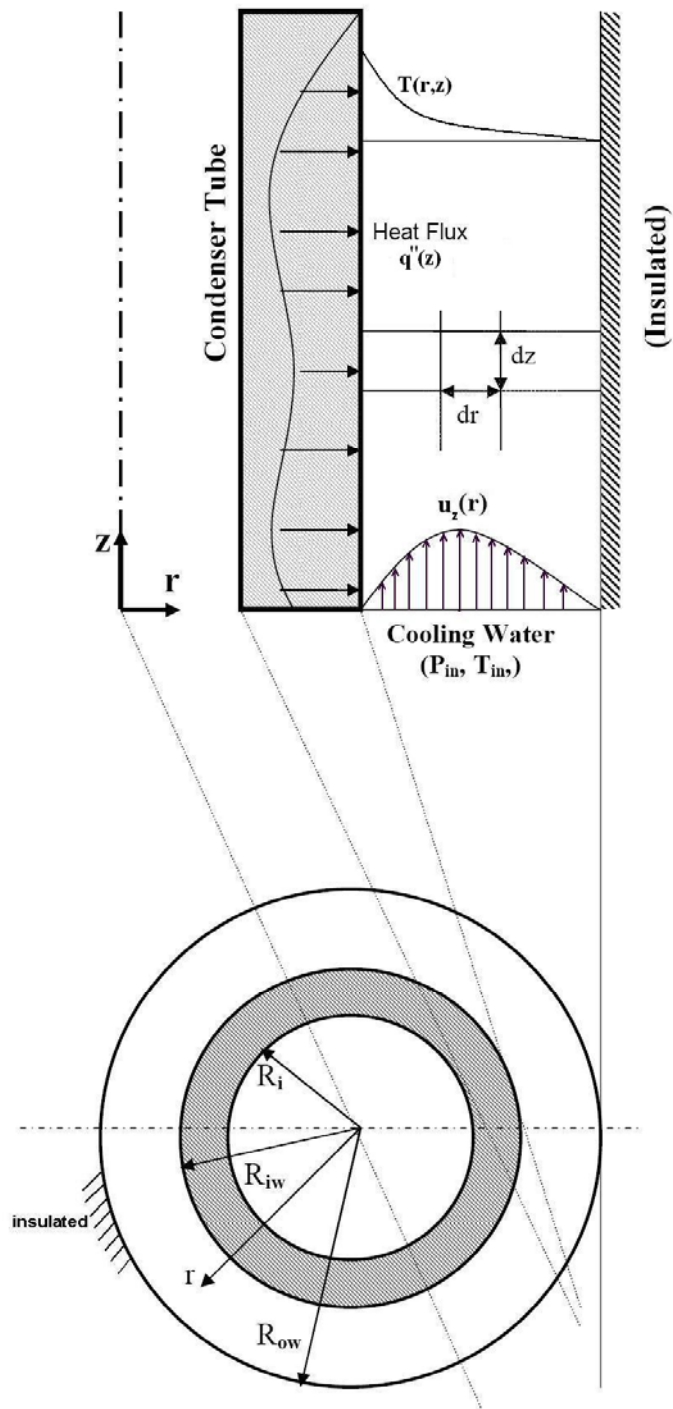


Figure 5.1 The annular flow and heat transfer inside the jacket tube

Figure 5.1 is a schematic representation of the considered annular pipe flow and heat transfer. The governing differential equation for the temperature field of the annular pipe flow can be expressed as:

$$\rho c_p u_z \frac{\partial T}{\partial z} = \frac{1}{r} \frac{\partial}{\partial r} \left(r k_{eff} \frac{\partial T}{\partial r} \right) \quad (5.1)$$

The appropriate boundary conditions are as follows:

- $T(r, z) = T_{in}$ at $z = 0$
- $\left(\frac{\partial T}{\partial r} \right)_{r=R_{ow}} = 0$ at $r = R_{ow}$ ($0 \leq z \leq L$) (L is the tube length.)
- $q''(z) = \left(-k_{eff} \frac{\partial T}{\partial r} \right)_{r=R_{iw}}$ at $r = R_{iw}$ ($0 \leq z \leq L$)

where k_{eff} is the effective thermal conductivity given as;

$$k_{eff} = \begin{cases} k(r) & , \text{ for laminar flow (thermal conductivity } k(T)) \\ k(r) + k_{tur}(r) & , \text{ for turbulent flow} \end{cases}$$

For turbulent flow, Eq. (5.1) has three unknowns, namely, u_z , k_{tur} and T . The fluid properties (ρ, c_p, k) can be calculated from the polynomials given in Appendix C.

If the flow is laminar, number of unknowns drops to two since k_{tur} is equal to zero. In this case, one can solve Eq. (5.1) and obtain the temperature distribution if the velocity profile, $u_z(r)$, is known. So, for the fully developed laminar flow in an annular passage, the velocity profile is specified using the analytical expression obtained by Kays (1993):

$$\frac{u}{u_m} = \frac{2}{M} \left[1 - \left(\frac{R}{R_{ow}} \right)^2 + B \ln \frac{R}{R_{ow}} \right] \quad (5.2)$$

where u_m is the mean velocity and

$$B = \frac{\left(\frac{R_{iw}}{R_{ow}} \right)^2 - 1}{\ln \frac{R_{iw}}{R_{ow}}}$$

$$M = 1 + \left(\frac{R_{iw}}{R_{ow}} \right)^2 - B$$

For the fully developed turbulent case, velocity profile is calculated in Section 5.2. The calculation of turbulent viscosities (eddy diffusivities) and k_{tur} are performed in Section 5.3.

Finally, in Section 5.3, the solution methodology of the energy equation, Eq (5.1), is presented for the annular passages where the inner surface is heated and the outer surface is insulated. Also, the predicted results are compared to some experimental results.

5.2 Velocity profile for the turbulent flow in an annulus

The axial velocity profile, $u_z(r)$, of the turbulent flow in the cylindrical geometry can be written from the definition of total shear stress as;

$$\tau = \mu \frac{du_z}{dr} - \rho \overline{u'_r u'_z} \quad (5.3)$$

where $\overline{u'_r u'_z}$ is the time-average product of fluctuating velocity components in radial and axial directions. Eq. (5.3) may be re-expressed in a dimensionless form which is proposed by Churchill (1995);

$$\frac{\tau}{\tau_w} = \frac{du^+}{dy^+} + \left(\overline{u'_r u'_z} \right)^+ \quad (5.4a)$$

where

$$\begin{aligned} \left(\overline{u'_r u'_z} \right)^+ &= -\rho \overline{u'_r u'_z} / \tau_w \\ u^+ &= u_z (\rho / \tau_w)^{1/2} \\ y^+ &= y (\rho \tau_w)^{1/2} / \mu \\ y &= r - R_{iw} \\ r^+ &= r (\rho \tau_w)^{1/2} / \mu \\ R^+ &= R (\rho \tau_w)^{1/2} / \mu \end{aligned} \quad (5.4b)$$

If one can calculate $\left(\overline{u'_r u'_z} \right)^+$ and τ / τ_w precisely in a circular annulus, the dimensionless velocity profile, u^+ , for fully developed turbulent flow can be obtained by stepwise integration of Eq. (5.4a).

5.2.1 Shear stress distribution

In order to find the distribution of shear stress, $\tau(r)$, the force balance for the cylindrical control element shown in Figure 5.2 can be given as:

$$\begin{aligned} \tau(2\pi r dz) + \left\{ p + \left(\frac{\partial p}{\partial z} \right) dz \right\} (2\pi r dr) &= \left\{ \tau(2\pi r dz) + \frac{\partial}{\partial r} [\tau(2\pi r dz)] dr \right\} \\ &+ p(2\pi r dr) \end{aligned} \quad (5.5)$$

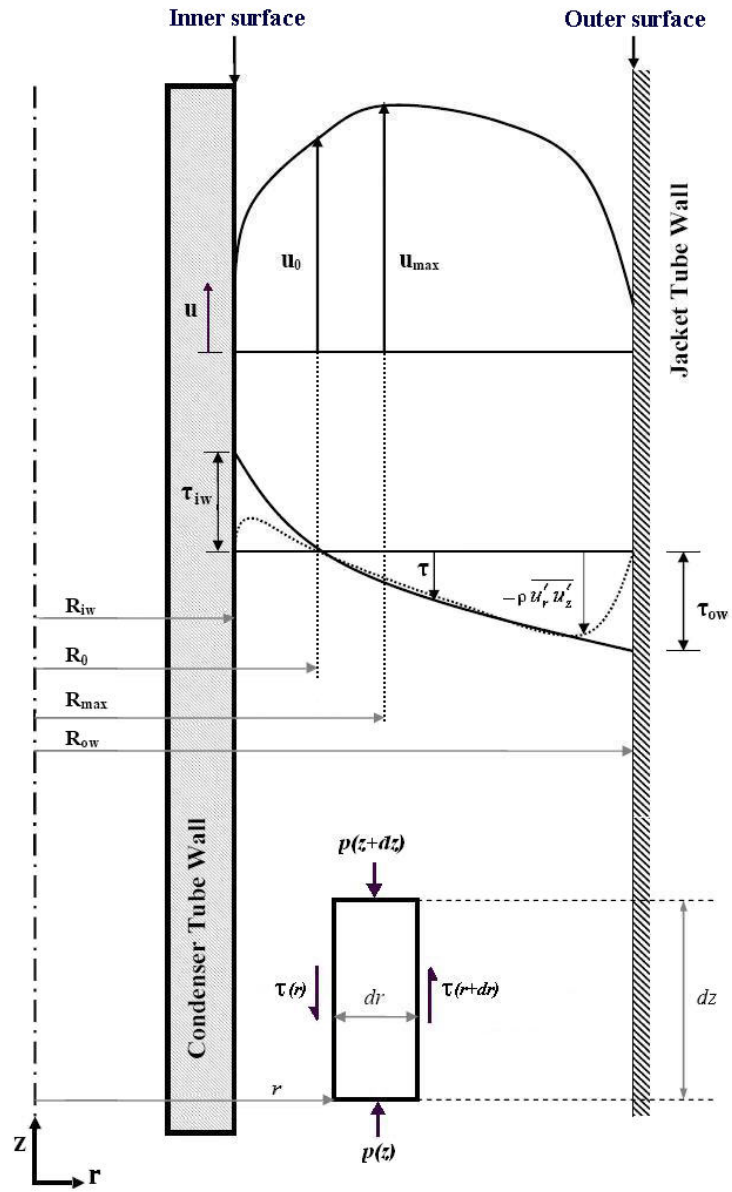


Figure 5.2 Schematic representation of velocity, turbulent shear stress, total shear stress and the force balance in an annulus

Rearranging Eq. (5.5), it becomes

$$\frac{\partial}{\partial r}(\tau r) = r \frac{\partial p}{\partial z} \quad (5.6)$$

The annulus is divided into two regions as inner region, $(R_{iw} \leq r \leq R_0)$, and outer region, $(R_0 \leq r \leq R_{ow})$, where R_0 is the location of zero in the total shear stress. The shear stresses can be calculated for both regions as follows:

Inner Region (i)

Integrating Eq. (5.6) to obtain;

$$\begin{aligned} (\tau_i r) &= \left(\frac{\partial p}{\partial z} \right) \int_{R_{iw}}^r r dr, \quad R_{iw} \leq r \leq R_0 \\ \Rightarrow (\tau_i r) &= \frac{1}{2} \left(\frac{\partial p}{\partial z} \right) (r^2 - R_{iw}^2) + C \end{aligned}$$

where C is the integration constant and it can be obtained from the boundary condition at,

$$r = R_0 \Rightarrow \tau_i = 0 \Rightarrow C = -\frac{1}{2} \left(\frac{\partial p}{\partial z} \right) (R_0^2 - R_{iw}^2)$$

and hence

$$\tau_i(r) = \frac{1}{2r} \left(\frac{\partial p}{\partial z} \right) (r^2 - R_0^2) \quad (5.7)$$

Shear stress at the inner surface ($r = R_{iw}$);

$$\tau_{iw} = \frac{1}{2R_{iw}} \left(\frac{\partial p}{\partial z} \right) (R_{iw}^2 - R_0^2) \quad (5.8)$$

Dividing Eq. (5.7) by (5.8), the following equation is obtained:

$$\left(\frac{\tau}{\tau_w} \right)_i = \frac{R_{iw}}{r} \frac{(r^2 - R_0^2)}{(R_{iw}^2 - R_0^2)} \quad (5.9)$$

Outer Region (o)

By the same way, Eq. (5.6) can be written for the outer region as;

$$\begin{aligned} (\tau_o r) &= \left(\frac{\partial p}{\partial z} \right) \int_r^{R_{ow}} r dr, \quad R_0 \leq r \leq R_{ow} \\ \Rightarrow (\tau_o r) &= \frac{1}{2} \left(\frac{\partial p}{\partial z} \right) (R_{ow}^2 - r^2) + C \end{aligned}$$

Using the boundary condition at

$$r = R_0 \Rightarrow \tau_o = 0 \Rightarrow C = -\frac{1}{2} \left(\frac{\partial p}{\partial z} \right) (R_{ow}^2 - R_0^2)$$

and hence

$$\tau_o(r) = \frac{1}{2r} \left(\frac{\partial p}{\partial z} \right) (R_0^2 - r^2) \quad (5.10)$$

Shear stress at the outer surface ($r = R_{ow}$);

$$\tau_{ow} = \frac{1}{2R_{ow}} \left(\frac{\partial p}{\partial z} \right) (R_0^2 - R_{ow}^2) \quad (5.11)$$

Dividing Eq. (5.10) by (5.11), the following equation is obtained:

$$\left(\frac{\tau}{\tau_w} \right)_o = \frac{R_{ow}}{r} \frac{(r^2 - R_0^2)}{(R_{ow}^2 - R_0^2)} \quad (5.12)$$

And finally, the surface shear stress ratio, τ^* , is defined by using Eq.(5.9) and (5.12);

$$\tau^* = \frac{\tau_{iw}}{\tau_{ow}} = \frac{R_{ow}}{R_{iw}} \frac{(R_{iw}^2 - R_0^2)}{(R_0^2 - R_{ow}^2)} \quad (5.13)$$

Rehme (1974) correlated his own experimental data for the location of zero in the total shear stress (R_0) for the turbulent flow in an annulus with the following empirical expression;

$$\frac{R_0 - R_{iw}}{R_{ow} - R_0} = \left(\frac{R_{iw}}{R_{ow}} \right)^{0.386} \quad (5.14)$$

Kays (1963) similarly correlated the experimental data of various investigations for the location of the maximum in the velocity distribution (R_{max}) in an annulus for the turbulent regime with the following empirical expression;

$$\frac{R_{max} - R_{iw}}{R_{ow} - R_{max}} = \left(\frac{R_{iw}}{R_{ow}} \right)^{0.343} \quad (5.15)$$

These two empirical expressions which are independent of the flow rate and fluid properties can be used to find the radial locations where the shear stress is zero and the axial velocity is maximum.

One can easily obtain the surface shear stress ratio, τ^* , by using Eq. (5.13) and (5.14). But in order to find the shear stress distribution, the definition of mean friction factor can be used;

$$f_{wm} = \frac{2\tau_{wm}}{\rho u_m^2} \quad (5.16)$$

Kaneda (2003) proposed an expression for τ_{wm} as the weighted mean of the shear stresses at both inner and outer surfaces of the annulus:

$$\tau_{wm} = \frac{R_{iw}\tau_{iw} + R_{ow}\tau_{ow}}{(R_{iw} + R_{ow})} \quad (5.17)$$

Kaneda (2003) also proposed a mean friction factor (f_{wm}) correlation as;

$$(2/f_{wm})^{1/2} = 3.2 + \frac{1}{0.436} \ln \left[\text{Re}(f_{wm}/8)^{1/2} \right] - \frac{275}{\text{Re}(f_{wm}/8)^{1/2}} \quad (5.18)$$

where Reynolds number for an annular flow (Re) is defined as;

$$\text{Re} = \frac{2\rho(R_{ow} - R_{iw})u_m}{\mu} \quad (5.19)$$

τ_{iw} and τ_{ow} can be obtained by using Eqs. (5.13) and (5.17);

$$\tau_{iw} = \frac{R_{iw} + R_{ow}}{R_{iw}} \left[\frac{(R_0^2 - R_{iw}^2)/(R_{ow}^2 - R_0^2)}{1 + \{(R_0^2 - R_{iw}^2)/(R_{ow}^2 - R_0^2)\}} \right] \tau_{wm} \quad (5.20)$$

$$\tau_{ow} = \frac{R_{iw} + R_{ow}}{R_{ow}} \left[\frac{(R_{ow}^2 - R_0^2)/(R_0^2 - R_{iw}^2)}{1 + \{(R_{ow}^2 - R_0^2)/(R_0^2 - R_{iw}^2)\}} \right] \tau_{wm} \quad (5.21)$$

By using Eqs. (5.18), (5.19) and (5.16), the weighted mean of the shear stresses (τ_{wm}) can be calculated. Then, shear stress distribution in the annulus can be obtained from Eq. (5.9) and (5.20) for inner region and Eq. (5.12) and (5.21) for outer region.

5.2.2 Fluctuating velocity distribution

Churchill (1995) developed an equation of the non-dimensional time-average product of fluctuating velocity components in radial and axial directions $(\overline{u'_r u'_z})^+$ for a round tube and for a parallel plate channel. This equation was adopted by Kaneda (2003) for annuli, defining two regions inside the annulus as inner region ($R_{iw} \leq r \leq R_{\max}$) and outer region ($R_{\max} \leq r \leq R_{ow}$), where R_{\max} is given in Eq. (5.15). Both of these adopted equations have the following form:

$$\left[(\overline{u'_r u'_z})^+ \right]^n = \left[(\overline{u'_r u'_z})_0^+ \right]^n + \left[(\overline{u'_r u'_z})_\infty^+ \right]^n \quad (5.22)$$

with a combining exponent n of -8/7. In this correlative model, it is assumed that flow regime in radial direction is divided into two sections shown with the subscript 0 and ∞ . $(\overline{u'_r u'_z})_0^+$ denotes the dimensionless velocity profile for the sublayer near the inner and outer surfaces while $(\overline{u'_r u'_z})_\infty^+$ denotes the

dimensionless velocity profile for the fully turbulent region from the sublayers near the surfaces to the point of maximum velocity.

The following asymptotic expression for small values of y^+ is presumed to be applicable for all shear flows for both the inner region ($R_{iw} \leq r \leq R_{\max}$) and outer region ($R_{\max} \leq r \leq R_{ow}$) of an annulus [Kaneda (2003)]:

$$\left(\overline{u'_r u'_z}\right)_0^+ = 0.7 \left(\frac{y^+}{10}\right)^3 \left(\frac{\tau}{\tau_w}\right) \quad (5.23)$$

$$\left(\overline{u'_r u'_z}\right)_\infty^+ = \left(\frac{\tau}{\tau_w}\right) - \left(1 - \frac{y^+}{R^+}\right) \left[\frac{B}{y^+} + \frac{B}{R^+} \left\{ 1 + \left(1 + \frac{2C}{B}\right) \left(\frac{y^+}{R^+}\right) \right\} \right] \quad (5.24)$$

For the arbitrary constants B and C , Zagarola (1996) suggested the values 2.294 and 6.824, respectively for round tubes. Kaneda (2003) claims that these constants are also applicable to the annular passages.

When Eqs. (5.23) and (5.24) are written for the inner region of annulus ($R_{iw} \leq r \leq R_{\max}$), the dimensionless distance from the wall, y^+ is replaced by $r^+ - R_{iw}^+$, the radius R^+ by $R_{\max}^+ - R_{iw}^+$, the shear stress at the wall, τ_w by τ_{iw} and the shear stress ratio τ/τ_w by τ/τ_{iw} given in Eq. (5.9). Then, these two equations become;

$$\left(\overline{u'_r u'_z}\right)_0^+ = 0.7 \left(\frac{r^+ - R_{iw}^+}{10}\right)^{0.8} \frac{R_{iw}}{r} \frac{(R_0^2 - r^2)}{(R_0^2 - R_{iw}^2)} \quad (5.25)$$

$$\begin{aligned} \left(\overline{u'_r u'_z}\right)_\infty^+ &= \frac{R_{iw}}{r} \frac{(R_0^2 - r^2)}{(R_0^2 - R_{iw}^2)} - \left(\frac{R_{\max} - r}{R_{\max} - R_{iw}} \right) \\ &\times \left[\frac{B}{r^+ - R_{iw}^+} + \frac{B}{R_{\max}^+ - R_{iw}^+} \left\{ 1 + \left(1 + \frac{2C}{B} \right) \left(\frac{r - R_{iw}}{R_{\max} - R_{iw}} \right) \right\} \right] \end{aligned} \quad (5.26)$$

Here; $\left(\overline{u'_r u'_z}\right)_0^+$, $\left(\overline{u'_r u'_z}\right)_\infty^+$, r^+ , R_{iw}^+ and R_{\max}^+ are normalized with respect to τ_{iw} (Eq. (5.4b)). For the outer region ($R_{\max} \leq r \leq R_{ow}$), Eqs. (5.23) and (5.24) are directly applicable in terms of $\tau/\tau_w = \tau/\tau_{ow}$, i.e., $\left(\overline{u'_r u'_z}\right)_0^+$, $\left(\overline{u'_r u'_z}\right)_\infty^+$, $y^+ = R_{ow}^+ - r^+$ and $R^+ = R_{ow}^+ - R_{\max}^+$ are all normalized in terms of τ_{ow} . If Eq. (5.23) is written by using Eq. (5.4b), $\left(\overline{u'_r u'_z}\right)_0^+$ for the outer region becomes;

$$\left(\overline{u'_r u'_z}\right)_0^+ = -\rho \left(\overline{u'_r u'_z}\right)_0 / \tau_{ow} = 0.7 \left(\frac{1}{10} y \frac{(\rho \tau_{ow})^{1/2}}{\mu} \right)^3 \left(\frac{\tau}{\tau_w} \right)_0 \quad (5.27)$$

It is noted that the fluctuating velocity is normalized in terms of τ_{ow} . In order to be compatible numerically with the values of $\left(\overline{u'_r u'_z}\right)_0^+$ for the inner region, it is convenient to renormalize the equation in terms of τ_{iw} . If Eq. (5.27) is rewritten, $\left(\overline{u'_r u'_z}\right)_0^+$ for the outer region becomes;

$$\left(\overline{u'_r u'_z}\right)_0^+ = -\rho \left(\overline{u'_r u'_z}\right)_0 / \tau_{iw} = 0.7 \left(\frac{1}{10} y \frac{(\rho \tau_{iw})^{1/2}}{\mu} \right)^3 \left(\frac{\tau}{\tau_w} \right)_i \left(\frac{\tau_{ow}}{\tau_{iw}} \right)^{3/2} \quad (5.28)$$

$$\left(\overline{u'_r u'_z}\right)_0^+ = 0.7 \left(\frac{y^+}{10} \right)^3 \left(\frac{\tau}{\tau_w} \right)_i \left(\frac{1}{\tau^*} \right)^{3/2} \quad (5.29)$$

Using Eqs. (5.9) and (5.13), Eq. (5.29) becomes;

$$\left(\overline{u'_r u'_z}\right)_0^+ = 0.7 \left(\frac{R_{ow}^+ - r^+}{10}\right)^3 \left(\frac{R_{iw}}{r}\right) \left(\frac{R_{ow}^2 - r^2}{R_{ow}^2 - R_{iw}^2}\right) \left(\frac{R_{iw}^2}{R_{ow}^2}\right)^{3/2} \left(\frac{R_{ow}^2 - R_0^2}{R_0^2 - R_{iw}^2}\right)^{3/2} \quad (5.30)$$

By the same way, if Eq. (5.24) is rewritten by inserting Eqs.(5.13) and (5.9), $\left(\overline{u'_r u'_z}\right)_\infty^+$ for the outer region becomes;

$$\begin{aligned} \left(\overline{u'_r u'_z}\right)_\infty^+ &= \left(\frac{R_{iw}}{r}\right) \frac{(R_0^2 - r^2)}{(R_0^2 - R_{iw}^2)} + \left(\frac{R_{iw}^2}{R_{ow}^2}\right)^{1/2} \left(\frac{R_{ow}^2 - R_0^2}{R_0^2 - R_{iw}^2}\right) \left(\frac{r - R_{\max}}{R_{ow} - R_{\max}}\right) \\ &\times \left[\frac{B}{R_{ow}^+ - r^+} + \frac{B}{R_{ow}^+ - R_{\max}^+} \left\{ 1 + \left(1 + \frac{2C}{B}\right) \left(\frac{R_{ow} - r}{R_{ow} - R_{\max}}\right) \right\} \right] \end{aligned} \quad (5.31)$$

For the inner region ($r \leq R_{\max}$), a different value of C used in Eq.(5.26), designated as C' is proposed by Kaneda (2003) in order to force the expression for the velocity distribution in the inner region and outer region to match at the point $r = R_{\max}$. Hence, C' is evaluated as;

$$\begin{aligned} C' &= B - \frac{3}{2} \left[A + B \ln(R_{\max}^+ - R_{in}^+) \right] \\ &+ \frac{3}{2} \left(\frac{R_{ow}^2}{R_{iw}^2}\right)^{1/2} \left(\frac{R_0^2 - R_{iw}^2}{R_{ow}^2 - R_0^2}\right)^{1/2} \\ &\times \left[\frac{2(C - B)}{3} + A + B \ln \left\{ (R_{ow}^+ - R_0^+) \right\} \left(\frac{R_{iw}^2}{R_{ow}^2}\right)^{1/2} \left(\frac{R_{ow}^2 - R_0^2}{R_0^2 - R_{iw}^2}\right) \right] \end{aligned} \quad (5.32)$$

where the constant A is taken as 6.18.

5.2.3 Numerical evaluation

Since non-dimensional time-average product of fluctuating velocity components in radial and axial directions $\left(\overline{u'_r u'_z}\right)^+$ is the most important variable to obtain the solution of the velocity profile in the annulus, it is necessary to present the variation of this quantity. As an illustration of this behavior, computed values of $\left(\overline{u'_r u'_z}\right)^+$ from Eq. (5.22) are plotted in Figure 5.3 for four different values of aspect ratio (R_{iw}/R_{ow}) and for three different values of $R_{ow}^+ - R_{iw}^+$. At both surfaces of the annulus, the absolute value of $\left(\overline{u'_r u'_z}\right)^+$ increases rapidly, whereas it shows almost linear variation across the central part of the annulus.

Since $\left(\overline{u'_r u'_z}\right)^+$ and τ/τ_w are calculated readily in a circular annulus, the non-dimensional velocity profile, u^+ can be obtained by a stepwise integration of Eq. (5.4a);

$$u^+ = \int_0^{y^+} \left[\left(\frac{\tau}{\tau_w} \right) - \left(\overline{u'_r u'_z} \right)^+ \right] dy^+ \quad (5.33)$$

For an annulus, non-dimensional mean velocity, u_m^+ , is defined as;

$$u_m^+ = \frac{\int_0^{(R_{ow}^+ - R_{iw}^+)} u^+ y^+ dy^+}{\int_0^{(R_{ow}^+ - R_{iw}^+)} y^+ dy^+} = \frac{2}{(R_{ow}^+ - R_{iw}^+)^2} \int_0^{(R_{ow}^+ - R_{iw}^+)} u^+ y^+ dy^+ \quad (5.34)$$

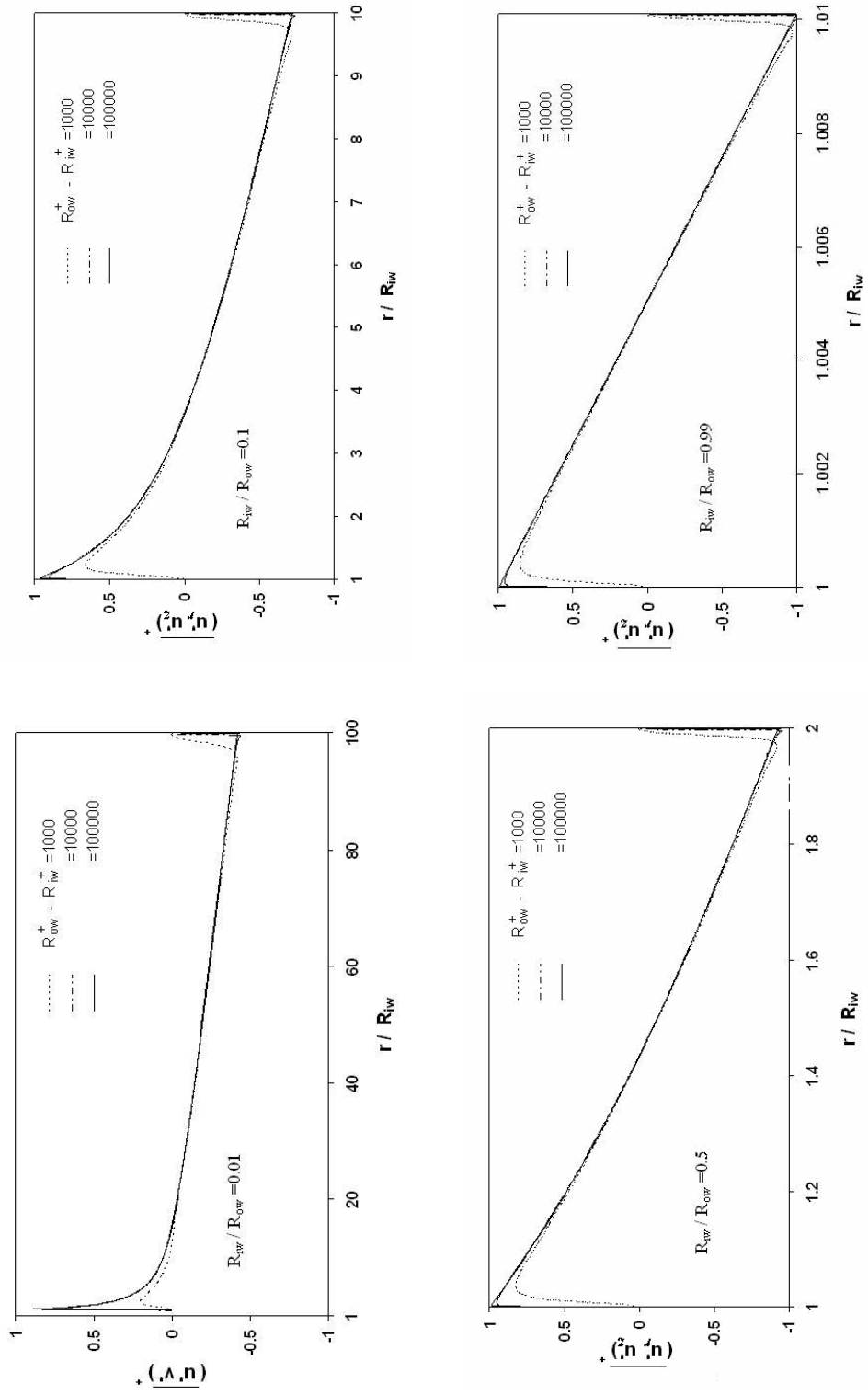


Figure 5.3 Computed radial variation of the non-dimensional fluctuating velocities in an annulus

For illustrative purposes, values of u/u_m computed from the Eqs. (5.33) and (5.34) for u^+ and u_m^+ , respectively, are plotted versus the non-dimensional radial location $((r - R_{iw})/(R_{ow} - R_{iw}))$ across the annulus in Figure 5.4 for three different values of aspect ratio (R_{iw}/R_{ow}) and for three different values of $R_{ow}^+ - R_{iw}^+$. For a particular value of $R_{ow}^+ - R_{iw}^+$, as R_{iw}/R_{ow} decreases from unity to zero, the maximum value of the ratio u/u_m moves from mid-point of the annulus to the inner surface. This result confirms that as $R_{iw}/R_{ow} \rightarrow 1$, the velocity distribution approaches to that for a parallel-plate channel while the velocity distribution approaches to that for a round tube as the aspect ratio decreases toward zero. For a constant value of R_{iw}/R_{ow} , as $R_{ow}^+ - R_{iw}^+$ increases, the maximum value of the ratio u/u_m decreases and u/u_m becomes flatter. This result confirms that as $R_{ow}^+ - R_{iw}^+$ increases, the effect of turbulence in the flow channel increases.

In order to verify this annular flow model, it has to be compared to some experimental data for the developed turbulent annular flows. Figure 5.5 shows the calculated fully developed velocity profile and the experimental results obtained from the Kuzay (1973) data for an annulus of aspect ratio 0.556. Another comparison is shown in Figure 5.6 for an annulus of aspect ratio 0.25 where the experimental data from Ball (1972) are used.

On the basis of comparisons with the experimental data, the computed values are seen to be in reasonable agreement for the turbulent annular flow.

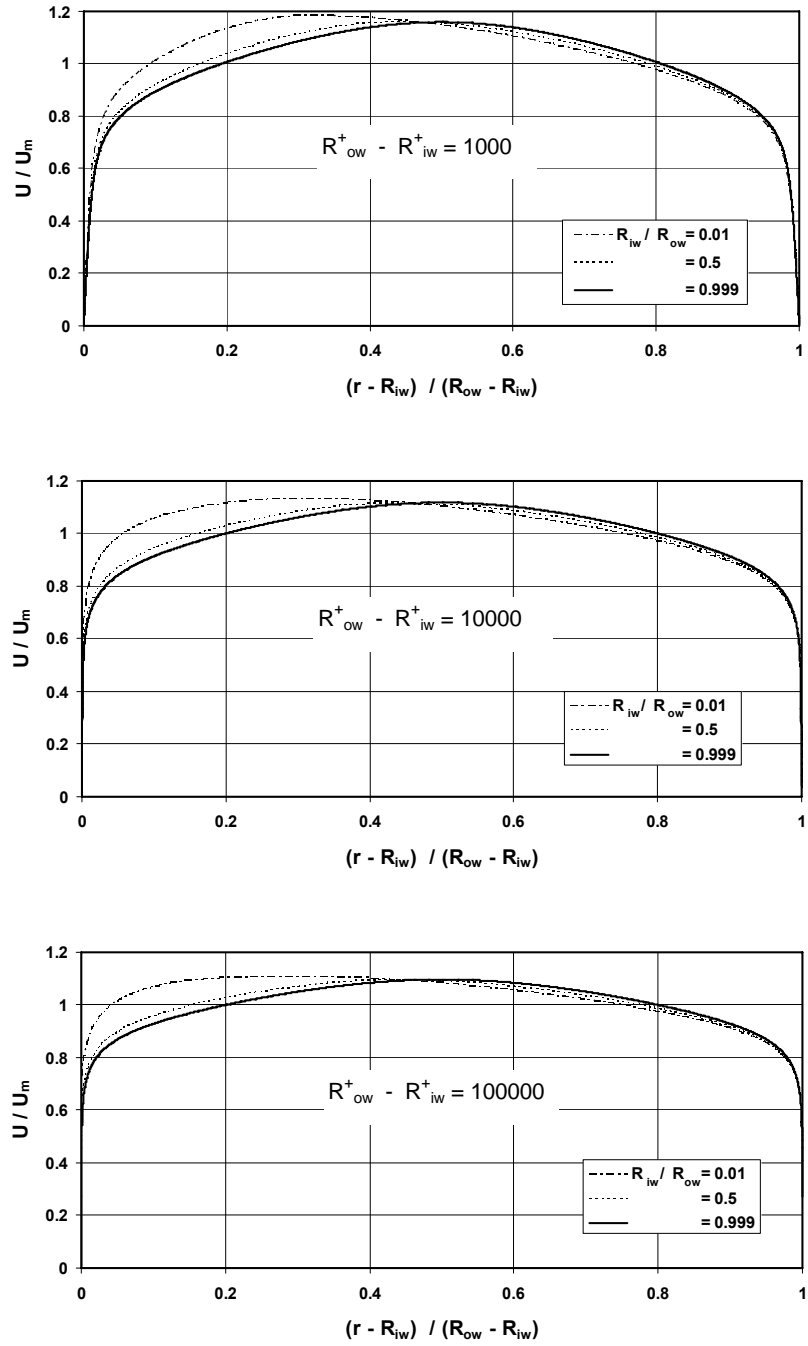


Figure 5.4 Predicted velocity profiles for different flow and aspect ratios.

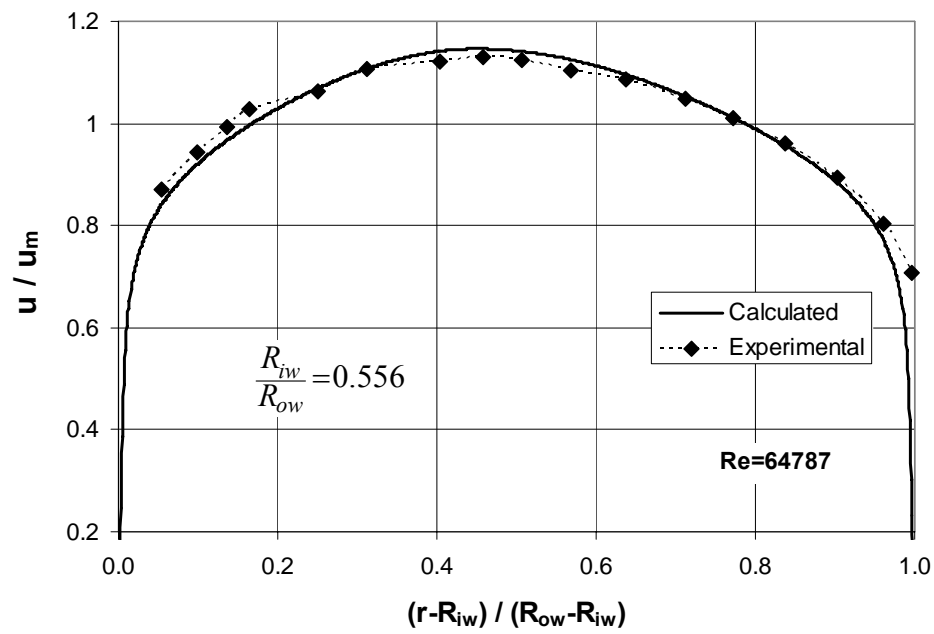


Figure 5.5 Measured and calculated velocity profiles [Kuzay (1973)]

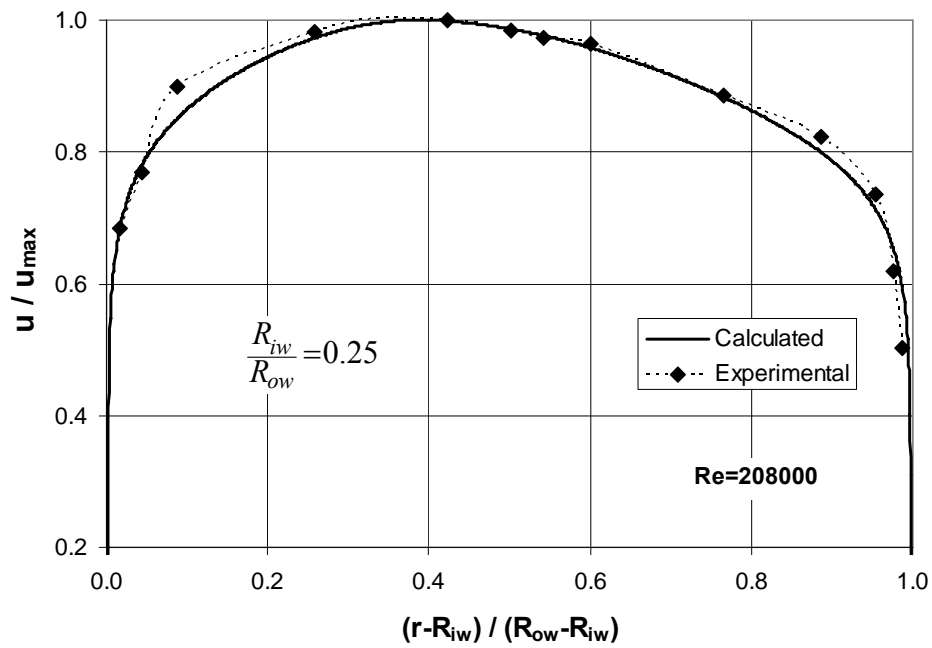


Figure 5.6 Measured and calculated velocity profiles [Ball (1972)]

5.3 Temperature profile in an annular flow

For steady, axisymmetric, fully developed two dimensional flow in a pipe or in a concentric annulus, the energy equation is written as;

$$\rho c_p u_z \frac{\partial T}{\partial z} = \frac{1}{r} \frac{\partial}{\partial r} \left(r k_{eff} \frac{\partial T}{\partial r} \right) \quad (5.35)$$

Eq. (5.35) can be solved for the appropriate thermal boundary conditions given in Section 5.1 in case of known velocity profile and the effective thermal conductivity, k_{eff} as well. The velocity profiles are given in Eq.(5.2) for laminar flow and in Section 5.2 for the turbulent flow respectively. If the flow is laminar, k_{eff} is directly equal to thermal conductivity ($k(T)$) of the coolant. But if the flow is turbulent, k_{tur} should be taken into account. From the definition of effective thermal conductivity, k_{eff} can be written as follow:

$$\begin{aligned} k_{eff} &= k + k_{tur} = k \left[1 + \frac{k_{tur}}{k} \right] = k \left[1 + \underbrace{\left(\frac{k_{tur}}{c_p \mu_{tur}} \right)}^{1/Pr_{tur}} \underbrace{\left(\frac{c_p \mu}{k} \right)}^{Pr} \left(\frac{\mu_{tur}}{\mu} \right) \right] \\ &= k \left[1 + \left(\frac{Pr}{Pr_{tur}} \right) \left(\frac{\mu_{tur}}{\mu} \right) \right] \end{aligned} \quad (5.36)$$

Many empirical and semi-theoretical correlating equations are proposed in the literature for the turbulent Prandtl number (Pr_{tur}). In this study, the following numerically modified empirical equation of Jischa (1979) is used:

$$Pr_{tur} = 0.85 + \frac{0.015}{Pr}, \quad Pr \geq 0.7 \quad (5.37)$$

The eddy viscosity for the turbulent flow is defined as;

$$\mu_{tur} = \frac{-\rho \overline{u'_r u'_z}}{du/dr} \quad (5.38)$$

From Figure 5.2, the eddy viscosity is positive for $r \geq R_{\max}$, infinite for $r = R_{\max}$, negative for $R_0 \leq r \leq R_{\max}$, zero for $r = R_0$ and positive again for r smaller than R_0 . Due to infinite and negative values of eddy viscosity, μ_{tur} given in Eq. (5.38) is not applicable for an annulus. Yu (2005a, 2005b, 2005c) suggested an equation for the annular heat transfer to avoid the singularity and the negative values as follows:

$$\frac{\mu_{tur}}{\mu} = \left(\frac{(\overline{u'_r u'_z})^+}{\tau/\tau_w - (\overline{u'_r u'_z})^+} \right) \quad (5.39)$$

5.3.1 Heat transfer model

In a concentric annulus, the inner surface is assumed to be heated and the outer surface is insulated. The heat transfer analysis can be carried out by a thermal energy balance. The thermal energy balance for the cylindrical control volume in Figure 5.7 can be given as;

$$\begin{aligned} q_r''(2\pi r dz) + \rho c_p u T(2\pi r dr) = & \left[q_r''(2\pi r dz) + \frac{\partial}{\partial r} [q_r''(2\pi r dz)] dr \right] \\ & + \left[\rho c_p u T(2\pi r dr) + \frac{\partial}{\partial z} [\rho c_p u T(2\pi r dr)] dz \right] \end{aligned} \quad (5.40)$$

where q_r'' is the heat flux in the radial direction. From Eq. (5.40);

$$-\frac{\partial}{\partial r}(q_r'' r) = \rho c_p u r \frac{\partial T}{\partial z} \quad (5.41)$$

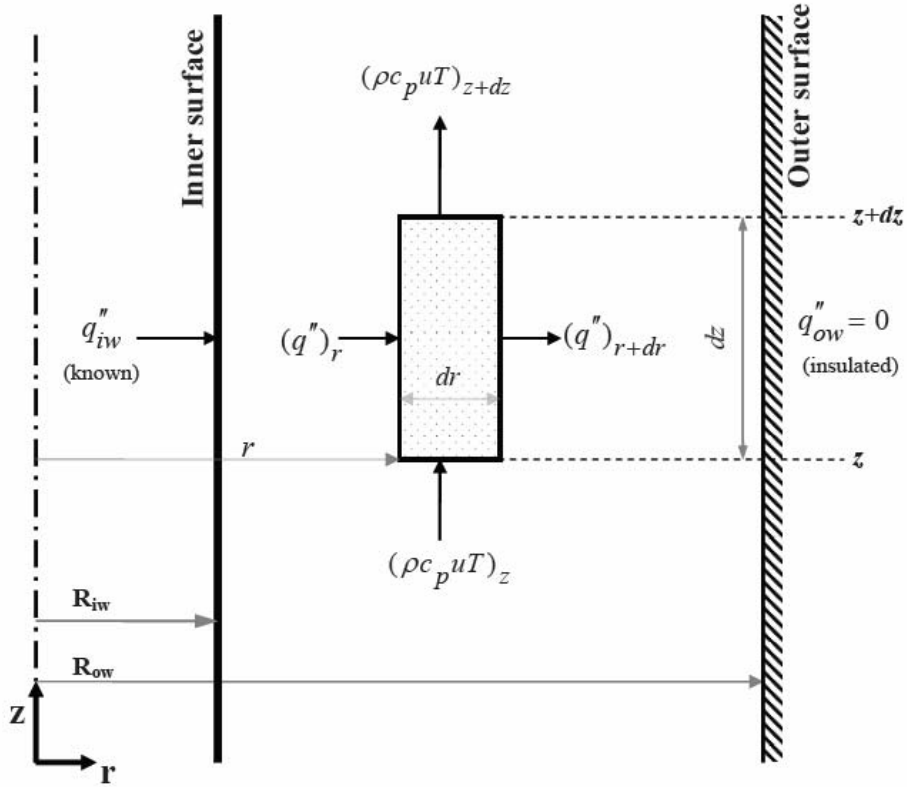


Figure 5.7 Schematic representation of thermal energy balance in the annulus

Integrating Eq. (5.41);

$$(q''_r r) = - \int_r^{R_{ow}} \rho c_p u \left(\frac{\partial T}{\partial z} \right) r dr + C \quad (5.42)$$

where C is the integration constant and $C=0$ since $q'' = 0$ at $r = R_{ow}$.

It is assumed that there exists constant heat flux at the inner wall and constant heat transfer coefficient between z and $z+dz$. The temperature gradients in axial direction can be shown that

$$\frac{\partial T_m}{\partial z} = \frac{\partial T_{iw}}{\partial z} = \frac{\partial T}{\partial z} \quad (5.43)$$

By using Eq. (5.43), Eq. (5.42) can be rewritten as;

$$q_r'' = \left(-\frac{\partial T}{\partial z} \right) \frac{1}{r} \int_r^{R_{ow}} \rho c_p u r dr \quad (5.44)$$

If Eq.(5.44) is rewritten for the inner surface with known uniform and constant heat flux, q_{iw}'' , between z and $z+dz$

$$q_{iw}'' = \left(-\frac{\partial T_{iw}}{\partial z} \right) \frac{1}{R_{iw}} \left[\int_{R_{iw}}^{R_{ow}} \rho c_p u r dr \right] \quad (5.45)$$

Dividing Eq. (5.44) with Eq. (5.45), one can obtain the heat flux ratios as;

$$\frac{q_r''}{q_{iw}''} = \frac{R_{iw}}{r} \left[\frac{\int_r^{R_{ow}} \rho c_p u r dr}{\int_{R_{iw}}^{R_{ow}} \rho c_p u r dr} \right] \quad (5.46)$$

After determination of heat flux distribution along the radial direction, the temperature profile at any axial point, z , can be derived from the basic heat conduction equation:

$$q_r'' = -k_{eff} \frac{\partial T_z}{\partial r} \quad (5.47)$$

It should be noted that there is only conduction heat transfer in radial direction since advection can be disregarded in radial direction. Radial temperature distribution at point z ($T_z(r)$) can be obtained by integrating Eq.(5.47);

$$\int_{R_{iw}}^r dT_z = - \int_{R_{iw}}^r \frac{q_r''}{k_{eff}} dr \quad (5.48)$$

So, Eq.(5.48) yields;

$$T_z(r) = T_z(R_{iw}) - \int_{R_{iw}}^r \frac{q_r''}{k_{eff}} dr \quad (5.49)$$

If Eq.(5.46) is substituted into Eq.(5.49), the radial temperature profile at any axial point z is given as;

$$T_z(r) = T_z(R_{iw}) - \int_{R_{iw}}^r \frac{1}{k_{eff}} \left[\frac{q_{iw}'' R_{iw}}{r} \frac{\int_{R_{ow}}^{R_{ow}} \rho c_p u r dr}{\int_{R_{iw}}^{R_{ow}} \rho c_p u r dr} \right] dr \quad (5.50)$$

The mean temperature ($\bar{T}(z)$) at any axial point z is given as;

$$\bar{T}_z = \frac{2\pi}{(\dot{m} c_p)} \int_{R_{iw}}^{R_{ow}} (\rho c_p u r T) dr \quad (5.51)$$

The local heat transfer coefficient (h) and Nusselt number (Nu) at any axial point z is given as;

$$h_z = \frac{q_{iw}''(z)}{(T_z(R_{iw}) - \bar{T}_z)} \quad (5.52)$$

$$Nu_z = \frac{2 h_z (R_{ow} - R_{iw})}{k_z} \quad (5.53)$$

5.3.2 Solution procedure

In order to determine the value of $T_z(R_{iw})$, i.e., the temperature (T_{iw}) at the inner surface and at axial point $z+\Delta z$, conservation of energy between the axial points z and $z+\Delta z$ can be used;

$$\int_{R_{iw}}^{R_{ow}} (\rho c_p u r T)_{z+\Delta z} dr = \int_{R_{iw}}^{R_{ow}} (\rho c_p u r T)_z dr + R_{iw} \Delta z q''_{iw} \quad (5.54)$$

Since Eq. (5.50) is a double integral, it can be solved by simultaneous stepwise integration.

The calculation procedure to be performed is summarized as follows:

- (1) Specify inlet conditions ($\dot{m}_{in}, \bar{T}_{in}$) and heat flux profile at the inner surface of the annulus ($q''_{iw}(z)$) as boundary condition
- (2) Calculate velocity distribution, $u_z(r)$, from Section 5.2
- (3) At axial point z , calculate the fluid properties (ρ, c_p, k, μ) for the mean temperature (\bar{T}_z) from Eq.(5.51)
- (4) Calculate $\int_{R_{iw}}^{R_{ow}} (\rho c_p u r T)_z dr$
- (5) Calculate $E_1 = \int_{R_{iw}}^{R_{ow}} (\rho c_p u r T)_{z+\Delta z} dr$ from Eq.(5.54)
- (6) Assume the temperature at the inner surface for the axial point z ; $T_z(R_{iw})$
- (7) Calculate the heat flux distribution from Eq.(5.46)
- (8) Calculate k_{eff} from Eqs.(5.36), (5.37) and (5.39)
- (9) Calculate the temperature distribution from Eq.(5.50)
- (10) Obtain $E_2 = \int_{R_{iw}}^{R_{ow}} (\rho c_p u r T)_{z+\Delta z} dr$ from calculated temperature distribution

(11) If $T_z(R_{iw})$ converges, i.e., $\left(\frac{\|E_2 - E_1\|}{E_1} \leq \varepsilon\right)$, go to the next step. If not, go to

Step 6 for the next iteration.

(12) Go to Step 3 for the next axial node. Repeat this calculation procedure from Step 3 through 12 until last node calculation at $z=L$ is performed.

The flow chart of the temperature distribution calculation in the annulus ($T_z(r)$) is given in Figure 5.8. For this calculation procedure, ε is chosen as 10^{-5} and the annulus is divided into 50 nodes, which is the same number of nodes in condensation model given in Chapter 4.

5.4 Results and discussions

Turbulent flow and heat transfer in concentric annular channels where the inner surface of the channel is heated and the outer surface is insulated have been studied experimentally by many researchers such as Carpenter (1946), McMillan (1946), Dufinescz (1938), Monrad (1942) and Miller (1955) for water ($2 \leq Pr \leq 10$), Leung (1962), Petukhov (1963), Roberts (1968), Quarmby (1967) and Vilemas (1987) for air ($Pr \cong 0.70$), and Trefethan (1951) for mercury ($0.01 \leq Pr \leq 0.03$).

In these earlier studies, sufficient information such as the local values of wall temperatures and mean temperatures or the local values of Nu number is not given. Instead of these, the average values of Nu and Re numbers are given by the authors due to inadequacy of the measuring instrumentation. But, one of the recent experimental studies performed by Kang (2001) covers all information for the velocity and thermal fields, where these values are measured in heated and unheated turbulent upflow of liquid R-113 through a vertical annular channel of inner to outer radius ratio 0.415. These experiments are conducted at test section inlet temperature of 42.7°C , three different flow rates and inner surface heat fluxes. Table 5.1 contains the experimental conditions and associated parameters.

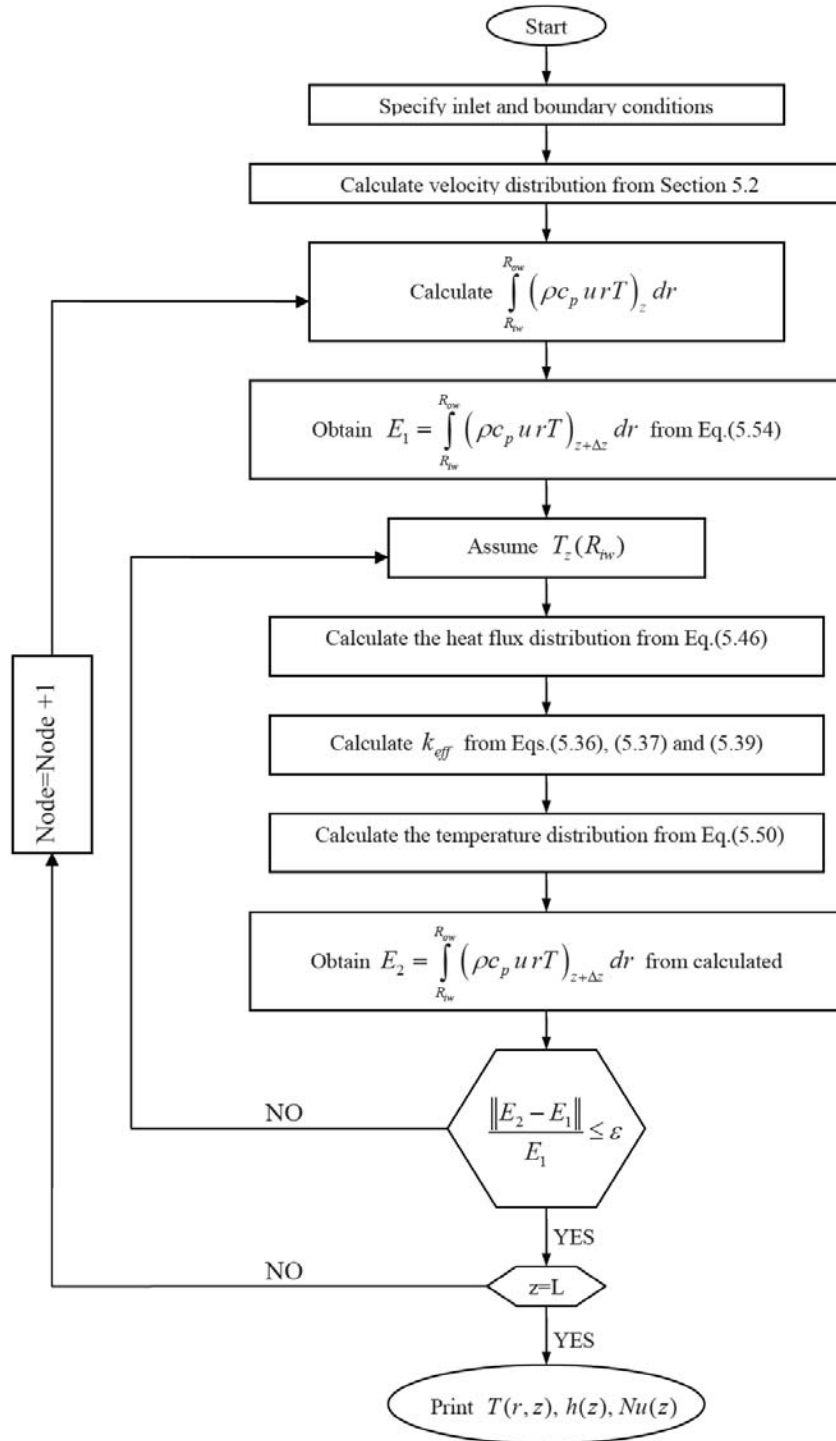


Figure 5.8 Flow chart of the temperature distribution calculation in the annulus

Table 5.1 Inlet conditions and parameters for Kang's experiments [Kang (2001)]

Parameter	Experiment							
	1	2	3	4	5	6	7	8
u_m (m/s)	0.374	0.374	0.374	0.516	0.516	0.516	0.760	0.760
Re	22800	22800	22800	31500	31500	31500	46400	46400
P (kPa)	269	269	269	269	269	269	269	269
T_{inlet} (°C)	42.7	42.7	42.7	42.7	42.7	42.7	42.7	42.7
q''_{iw} (W/m ²)	0.0	9000	16000	0.0	9000	16000	0.0	16000
Pr	7.25	7.15	7.07	7.25	7.18	7.12	7.25	7.16

Figures 5.9, 5.10 and 5.11 show the radial velocity profiles at the exit of the test section for each experiment and the corresponding calculated velocity profiles. It is observed that the velocity profile does not change significantly for heated and unheated channels in case of same inlet flow conditions.

The comparisons of the measured and calculated temperature profiles for different heating cases are shown in Figures 5.12-5.16. On the basis of comparisons with the experimental data, the calculated values are seen to be in good agreement with them. One can conclude that the heat transfer model for the annular flow presented in this section seems to be reasonably well. Moreover, the calculated and measured inner surface temperatures are sufficiently close to each other, where it has vital importance for the conjugate condensation heat transfer analysis to be performed in the following chapter.

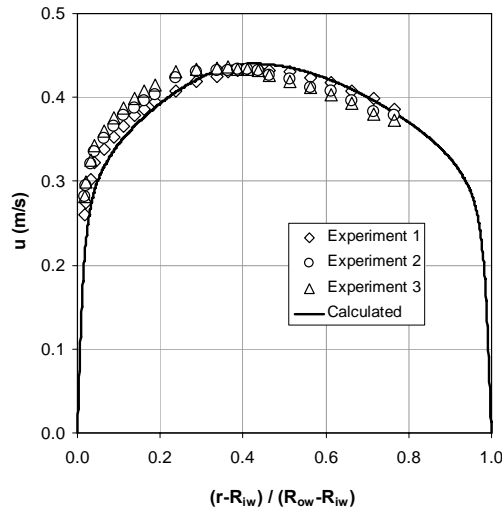


Figure 5.9 Comparison of measured and calculated velocity profiles [Kang (2001)]

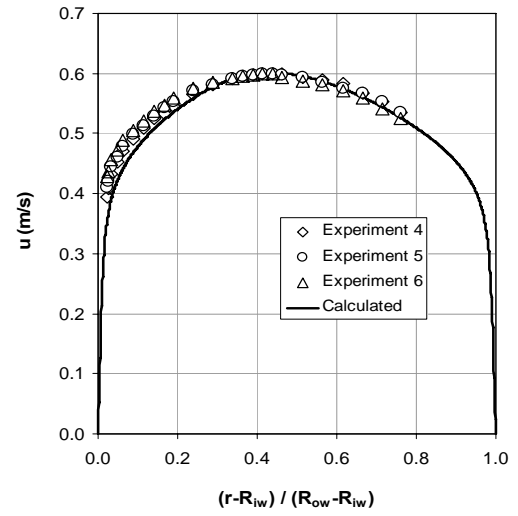


Figure 5.10 Comparison of measured and calculated velocity profiles [Kang (2001)]

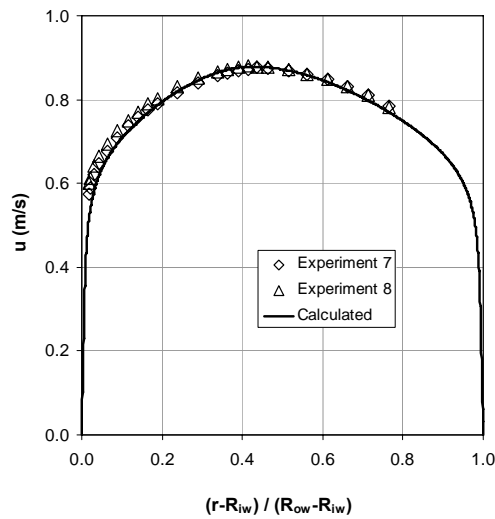


Figure 5.11 Comparison of measured and calculated velocity profiles [Kang (2001)]

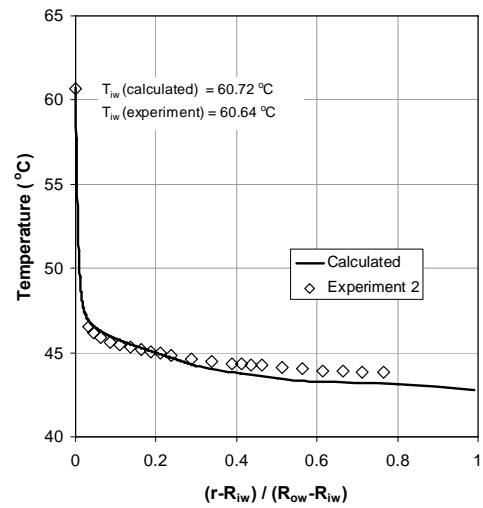


Figure 5.12 Comparison of measured and calculated temperature profiles for experiment 2 [Kang (2001)]

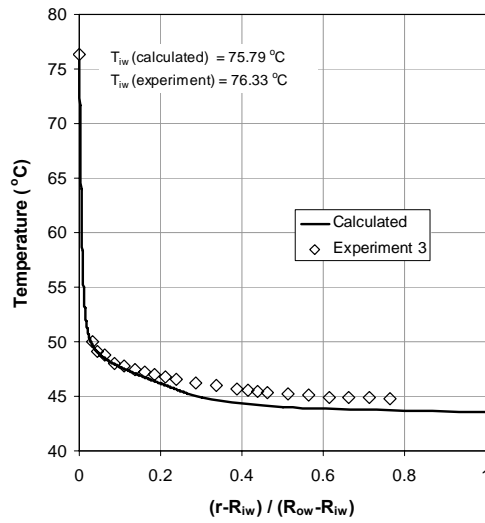


Figure 5.13 Comparison of measured and calculated temperature profiles for experiment 3 [Kang (2001)]

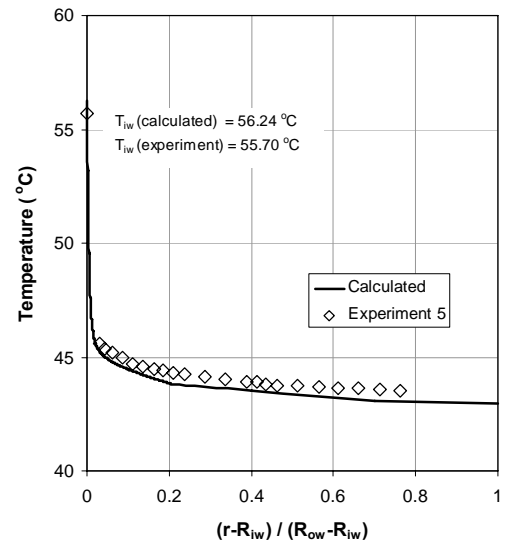


Figure 5.14 Comparison of measured and calculated temperature profiles for experiment 5 [Kang (2001)]

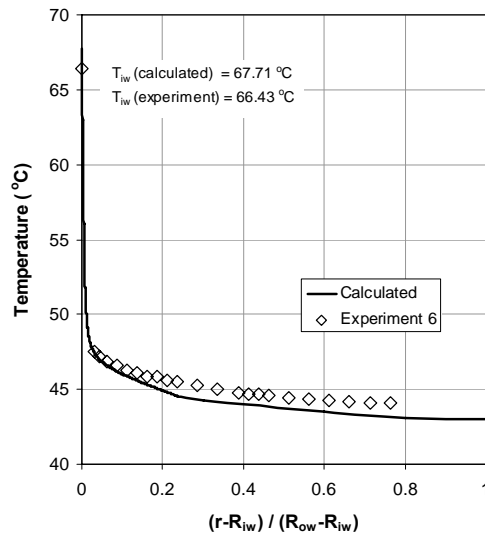


Figure 5.15 Comparison of measured and calculated temperature profiles for experiment 6 [Kang (2001)]

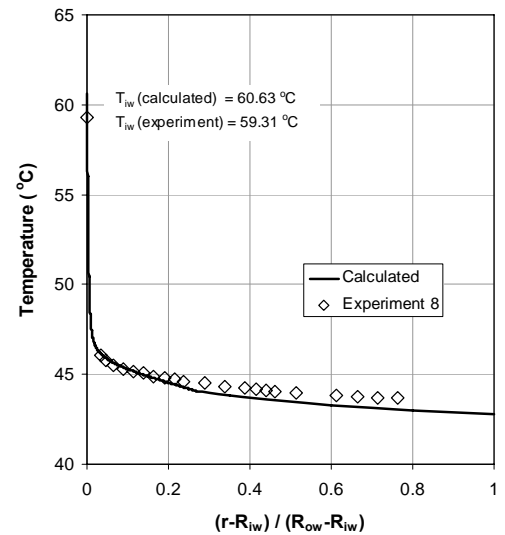


Figure 5.16 Comparison of measured and calculated temperature profiles for experiment 8 [Kang (2001)]

CHAPTER 6

CONJUGATE CONDENSATION HEAT TRANSFER

The heat transfer mechanism and thermal boundary layer formation for a fluid flowing inside a tube is directly influenced by the tube wall boundary conditions. In common applications, the wall boundary conditions are prescribed as either known temperature distribution or known heat flux values at the wall surface along the tube. But, there might be a case where the fluid convection and conduction through the wall interact and the wall surface temperature or wall surface heat flux are not known. The unknown temperature or heat flux profiles are determined by taking account of this fluid convection and wall conduction interaction. Therefore, the heat conduction through the wall and heat convection to/from the fluid flow should be coupled. This coupling procedure is called conjugate heat transfer between the wall and fluid flow.

In the conjugate condensation heat transfer process considered in this thesis work, there are two concentric tubes as shown in Figure 2.1, where the steam flows downward and condenses inside the condenser tube. The latent heat of condensation process is transferred out of the tube by the coolant flowing upward outside of the condenser tube. Because of the fact that only the inlet boundary conditions of steam and coolant are known, the conjugate solution should be applied to determine the outlet conditions of both condensed steam and heated coolant. In order to obtain these outlet conditions, an energy balance taking the heat transfer interactions into account should be established and the

parameters such as local temperatures and local heat fluxes along the condenser tube and annular passage should be calculated.

6.1 Coupling of two different fluid flows separated by a solid wall

Since the heat transfer characteristics of both annular side convection and steam condensation inside the condenser tube are directly dependent on the local heat fluxes and the local wall temperatures of the condenser tube respectively, the interaction between these two heat transfer mechanisms through the tube wall is important. Due to unknown wall temperature of the condenser tube, formation of condensate liquid layer thickness inside the tube and the fluid temperature distribution in the annulus are effected by the other's local conditions. Therefore, film-wise condensation, heat conduction through the condenser tube wall and heat removal from the outer surface of the condenser tube by cooling water flow should be coupled and solved simultaneously.

Two different and independent heat transfer models, namely “condensation model” and “convection model of annular flow” are previously given in Chapters 4 and 5, respectively. The solution of condensation model requires the local inner surface temperatures of the condenser tube wall as boundary condition while the convection model of annular flow solution uses the local heat flux values at the outer surface of the condenser tube wall as boundary condition. Therefore, it is essential to couple these two separate models via heat conduction through the condenser tube wall (Figure 6.1).

Disregarding the axial conduction in the tube wall (see Appendix C), the heat balance through the condenser tube wall is given by;

$$q''_{iw}(z) = \frac{R_i}{R_{iw}} q''_i(z) \quad (6.1)$$

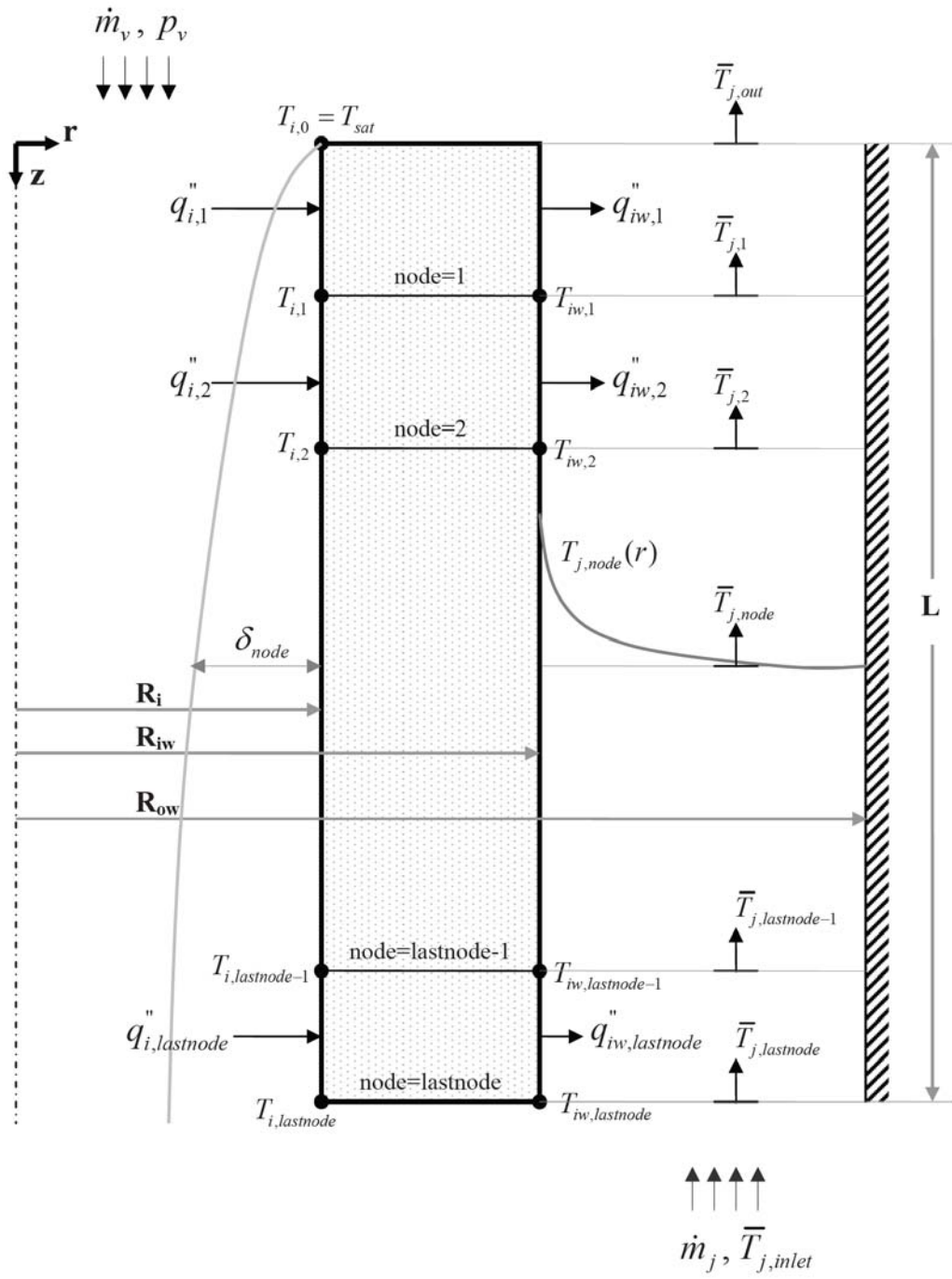


Figure 6.1 Schematic representation of the coupling procedure

It should be noted that $q''_{iw}(z)$ is the same as the local heat flux value which is taken as boundary condition at Section 5.3.1.

A general expression for the inner surface temperature of the condenser tube wall at any location in axial direction for constant thermal conductivity of tube material can be written as;

$$T_i(z) = T_{iw}(z) + \frac{R_i}{k_w} \ln [R_{iw} / R_i] q''_i(z) \quad (6.2)$$

which satisfies the boundary conditions:

$$T = T_{iw}(z) \quad \text{at } r = R_{iw}$$

$$q'' = q''_i(z) \quad \text{at } r = R_i$$

If the thermal conductivity is considered as a linear function of temperature, it can be presented as follows:

$$k_w(T) = a + bT \quad (6.3)$$

where the parameters a and b can be determined for the specified material. The energy balance at any axial point of the condenser tube can be written as;

$$2\pi R_i q''_i dz = 2\pi r q'' dz \quad \Rightarrow \quad R_i q''_i = r \left(-k_w \frac{\partial T}{\partial r} \right)$$

$$\int_{T_{iw}}^{T_i} k_w(T) dT = - \int_{R_{iw}}^{R_i} q''_i \frac{R_i}{r} dr \quad (6.4)$$

The solution of Eq. (6.4) by using Eq. (6.3) is given by,

$$T_i(z) = \frac{\left(\sqrt{a^2 - 2bc}\right) - a}{b} \quad (6.5)$$

where parameter c is expressed as;

$$c = q_i''(z)R_i \ln[R_{iw}/R_i] - \left[\frac{b}{2}T_{iw}^2 + aT_{iw} \right]$$

Also, the following interface conditions should be applied for coupling:

- At $r = R_{iw}$ and $0 \leq z \leq L$, where L is the tube length;

$$k_w \left(\frac{\partial T_w}{\partial r} \right) = k_j \left(\frac{\partial T_j}{\partial r} \right)$$

$$T_w(R_{iw}, z) = T_j(R_{iw}, z)$$

where subscript j refers to cooling fluid in the annulus (jacket side).

- At $r = R_{ow}$ and $0 \leq z \leq L$;

$$q''(R_{ow}, z) = 0 \Rightarrow \left(\frac{\partial T_j}{\partial r} \right) = 0$$

For the complete solution of the conjugate problem, Eq. (6.1) and Eq.(6.2) (or Eq.(6.5)), as well as the interface conditions should be consistent all along the tube. Coupling between the condensate heat flux (q_i'') and the temperature profile in the coolant flow (T_j) is constituted by using the energy balance and thermal resistances at the inner and outer surfaces of the condenser tube wall. And then,

the ultimate solution must also be satisfied by the interface conditions [Chen (2005)]. Therefore, an iterative procedure should be sought for the solution of this conjugate problem.

During the solution of the conjugate condensation heat transfer problem inside the concentric tubes, the following conditions and assumptions are accepted:

- a) The vapor and the coolant flows inside and outside of the condenser tube are steady.
- b) Hydrodynamically fully developed flows are established for the vapor and external coolant entering the tube and the annulus, respectively.
- c) Thermo-physical conditions of the vapor and external coolant are both known at their respective inlets. The vapor entering the tube is at saturated or superheated state.
- d) The vapor and external coolant flows are turbulent. But the condensate film flow inside the tube is laminar.
- e) Only film-wise condensation occurs inside the condenser tube; mist formation and wavy effects are disregarded.
- f) The jacket tube wall is insulated.
- g) The interfacial shear stresses acting on the condensate film and the vapor are not equal due to the condensation process inside the tube.
- h) Heat is transferred out from the condensate to the external coolant through the condenser tube only in the radial direction. In another words, heat conduction along the condenser tube in the axial direction is disregarded (see Appendix C).
- i) Dimensions of the condenser tube and jacket tube are uniform and constant throughout.

6.2 Solution procedure

Condensation process inside the condenser tube and external turbulent flow outside the condenser tube are coupled by using the Eqs. (6.1) and (6.5) (or Eq.(6.2)) and interface conditions given in the previous section. Also, the solution methodologies for the condensation and turbulent flow heat transfer phenomena, developed in Chapter 4 and Chapter 5 are arranged according to the boundary and interface conditions at the inner and outer surfaces of the condenser tube wall.

A computer code named ZEC covering an iterative solution scheme to solve the condensation-conduction-convection problem based on the conjugate heat transfer is developed in Fortran-90 language. During the iterative solution, the iteration to obtain the coolant flow outlet temperature is called “outer iteration” and the iteration to determine the inner surface temperature of the condenser tube wall is called “inner iteration”. The iteration procedure of ZEC can be summarized as follows:

1. Specify inlet conditions for vapor (\dot{m}_v, p_v) and coolant flow ($\dot{m}_j, \bar{T}_{j,inlet}$)
2. Start outer iteration by assuming an outlet mean bulk temperature for the coolant flow ($\bar{T}_{j,out}^{(l)}$) at $z=0$ where l is the index number of outer iteration.

For the first outer iteration ($l=1$);

$$\bar{T}_{j,out}^{(1)} = \frac{T_{sat} + \bar{T}_{j,inlet}}{2}$$

Take $\bar{T}_{j,0}^{(1)} = \bar{T}_{j,out}^{(1)}$

3. Start inner iteration for the specified node by assuming a temperature for the inner surface of the condenser tube wall ($T_{i,node}^{(n)}$), where n is the index number of inner iteration and *node* is the number that shows the axial

point for which the calculations are performed. For $node=1$ and $n=1$, $T_{i,1}^{(1)}$ is assumed to be slightly less than the saturation temperature of vapor.

4. Apply the solution procedure of condensation model given in section 4.3 to calculate the heat flux value $(q_{i,node}^{(n)})$ at the inner surface of the condenser tube by using $T_{i,node}^{(n)}$ value designated in Step 3 as boundary condition.
5. Obtain the heat flux value $(q_{iw,node}^{(n)})$ at the outer surface of the condenser tube wall from Eq.(6.1).
6. Designate this heat flux as boundary condition for the coolant flow.
7. Calculate the temperature distribution in the coolant flow $(T_{j,node}^{(n)}(r))$ by using the solution procedure of heat transfer model of annular flow given in section 5.3.2.
8. Obtain the outer surface temperature of the condenser tube wall $(T_{iw,node}^{(n)} = T_{j,node}^{(n)}(R_{iw}))$
9. Calculate the updated inner surface temperature of the condenser tube wall $(T_{i,node}^{(n)})_{updated}$ from Eq. (6.5) (or from Eq.(6.2))
10. Compare the updated and the previous values of inner surface temperatures of the wall, i.e.,

$$\left[\frac{\left\| (T_{i,node}^{(n)})_{updated} - T_{i,node}^{(n)} \right\|}{(T_{i,node}^{(n)})_{updated}} \leq \varepsilon_1 \right]$$

Go to next step if the convergence is satisfied. If not, go to Step 3 for the next inner iteration ($n=n+1$) by using Secant Method [Cheney (1999)].

11. Calculate the coolant mean temperature for the specified node $(\bar{T}_{j,node}^{(l)})$ from

$$\bar{T}_{j,node}^{(l)} = \frac{2\pi}{(\dot{m}c_p)_{j,node}} \int_{R_{iw}}^{R_{ow}} (\rho c_p u r T)_{j,node}^{(n)} dr \quad (6.6)$$

12. Repeat this calculation procedure from Step 3 through Step 11 until last node calculation at $z=L$, $(\bar{T}_{j,lastnode}^{(l)})$, is performed.
13. When the last node is reached, compare the calculated mean temperature $(\bar{T}_{j,lastnode}^{(l)})$ and inlet mean temperature $(\bar{T}_{j,inlet})$ given as boundary condition for the flow in annular jacket side

$$\frac{\|\bar{T}_{j,lastnode}^{(l)} - \bar{T}_{j,inlet}\|}{\bar{T}_{j,inlet}} \leq \varepsilon_2$$

14. If convergence is satisfied, stop the calculation. If not, go to Step 2 ($l=l+1$) until outer iteration is converged.

The complete flow chart for the calculations is given in Figure 6.2. The flow chart for the “condensation model” and “heat transfer model of annular flow” are previously depicted in Figures 4.4 and 5.8, respectively. These two models given in Chapters 4 and 5 are used in the conjugate solution where condensation model uses inner surface temperatures of the condenser tube wall as boundary condition obtained from the solution of annular flow model whereas annular flow model uses the heat flux values at the outer surface of the condenser tube wall as boundary condition obtained from the solution of condensation model for each node and for each iteration.

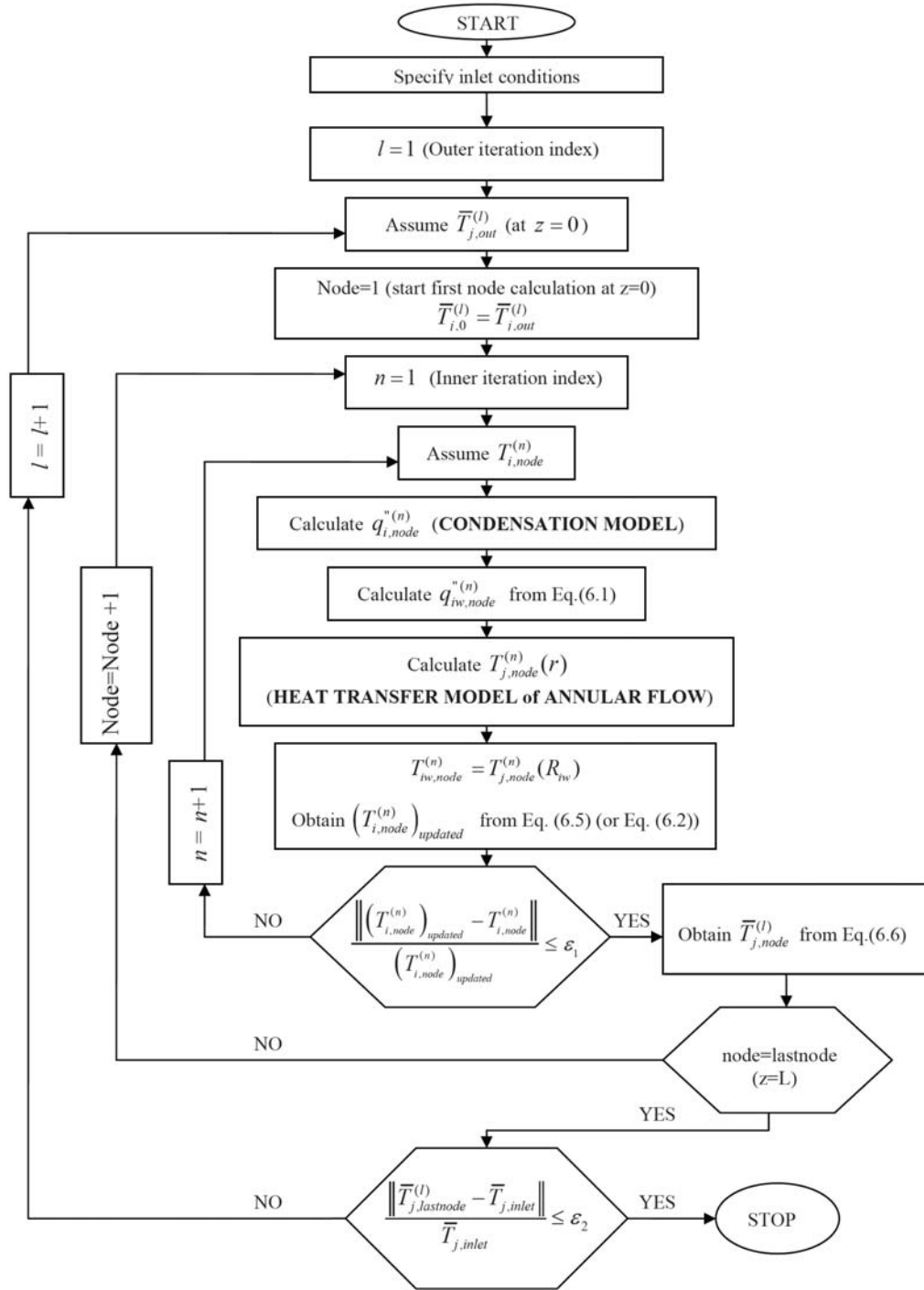


Figure 6.2 Flow chart of the whole calculational procedure

6.3 Numerical results and discussions

The numerical calculation results are compared to three available experimental databases; UCB [Kuhn (1994)], NASA [Goodykontz (1966)] and METU [Tanrikut (1998)]. The parameters of these experimental setups are previously given in Table 4.1.

In these experimental setups, the condenser tubes are made of SS304. The thermal conductivity (k_w) of this material is not constant for the operational temperatures of the experiments (Figure 6.3). Therefore, in numeric calculations, k_w is taken as the linear function of temperature, which is given in Eq. (6.3). Figure 6.3 shows the temperature dependent thermal conductivity variation of SS304 given by Assael (2004) and Incropera (1985). The study of Assael (2004) is used in the calculations, where the constants a and b in Eq. (6.3) are as follows:

$$a = 13.96048 \quad \text{and} \quad b = 0.01857 \quad 50^\circ\text{C} < T < 150^\circ\text{C} \quad (6.7)$$

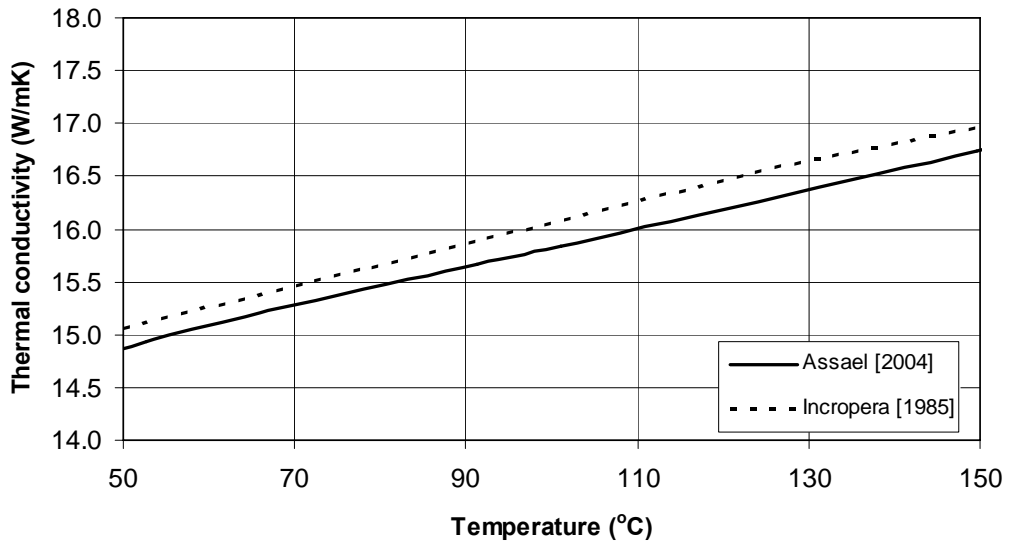


Figure 6.3 Thermal conductivity variation of SS304

In all code calculations, the condenser tube is divided into 50 axial nodes, which is enough for the numerical accuracy. The convergence criteria, ε_1 and ε_2 are chosen as 10^{-4} and 10^{-3} , respectively.

6.3.1 Comparison of numerical calculations with UCB experiments

UCB experimental data [Kuhn (1994)] contains sufficient information such as local coolant mean temperatures, local outer and inner surface temperatures of the condenser tube wall, local condensate liquid boundary layer thickness and the local heat transfer coefficients. Therefore, the numerical calculation results are compared to all these parameters.

In UCB database, the steam inlet Reynolds number varies from 12600 to 36100 for different pressures while coolant (jacket) side inlet Reynolds number changes between 3000 and 6500. Therefore, six runs, shown in Table 6.1 are selected, from the database, regarding different steam and coolant inlet conditions covering the whole range of experiments.

Table 6.1 Inlet conditions for UCB tests

Run #	Condenser Side (vapor)					Jacket Side (coolant)		
	Re	\dot{m} (kg/hr)	p_v (KPa)	T_{in} (°C)	T_{sat} (°C)	Re	\dot{m} (kg/hr)	T_{in} (°C)
6.1-2	12614	22.1	215.5	130.2	122.6	4356.3	494.0	87.9
1.4-1	18083	30.0	110.6	126.2	102.5	3466.4	828.7	37.4
1.3-2	23213	40.4	199.2	136.7	120.1	3946.4	932.5	38.2
1.2-4R1	26007	48.2	409.3	148.1	144.4	6426.1	1095.8	40.4
1.2-1	29926	49.7	112.7	135.1	102.8	4872.5	1082.4	42.0
1.1-1	36143	60.2	116.1	138.8	103.9	4565.9	999.8	42.7

For each case, the calculated values of the inner and the outer surface temperatures of the condenser tube wall, coolant axial mean temperatures inside the jacket tube, vapor Reynolds number, condensate liquid film thickness inside the condenser tube and local condensation heat transfer coefficients are compared with the experimental data from Figure 6.4 through Figure 6.39.

The calculated coolant mean temperatures (Figures 6.4, 6.5, 6.6, 6.7, 6.8 and 6.9) for each run predict the general trend of experimental data reasonably well. The code ZEC calculates the coolant mean temperatures by about less than 5% deviation, compared to the experimental data. The comparisons for the outer and the inner surface temperatures of the condenser tube wall are given in Figures 6.10, 6.11, 6.12, 6.13, 6.14, 6.15 and Figures 6.16, 6.17, 6.18, 6.19, 6.20, 6.21, respectively for each case. The code ZEC predicts the outer and the inner surface temperatures of the condenser tube wall by about less than 8% difference compared to the experimental data for all case. In UCB experiments, a constant thermal conductivity value is used to calculate the inner and outer surface temperatures from the measured wall temperatures by means of embedded thermocouples into the condenser tube wall at certain axial locations while the temperature dependent function given in Eq.(6.3) is used during the code calculations.

Figures 6.22, 6.23, 6.24, 6.25, 6.26, 6.27 and Figures 6.28, 6.29, 6.30, 6.31, 6.32, 6.33 show the variations of the vapor Reynolds numbers (Eq. (4.13b)) and condensate liquid film thicknesses respectively for each case. One can see that the liquid film thickness increases rather steep at the condenser tube inlet. As the steam condenses and its Reynolds number decreases, the liquid film becomes thicker and so that the thermal resistance increases, leading to slow down of the condensation rate. The ZEC model predicts a thinner film thickness by about 10% less than experimental data for all cases.

Finally, in Figures 6.34, 6.35, 6.36, 6.37, 6.38 and 6.39, the calculated and experimental local heat transfer coefficients are presented for each case. The heat transfer coefficients are in agreement with the experimental data. The code ZEC predicts the local heat transfer coefficients by about less than $\pm 15\%$ difference compared to the experimental data for all cases. The calculated local heat transfer coefficient is inversely proportional to the condensate liquid film thickness (Eq. (4.36)). Therefore one can say that the main reason of the difference in the heat transfer coefficient is undertaken by the deviation of the calculated liquid film thickness.

In UCB experiments [Kuhn (1994)], it is reported that the maximum uncertainty for the condensation heat transfer coefficient is $\pm 18.7\%$. Regarding the experimental uncertainty, the numerical results of code ZEC seem to be satisfactory.

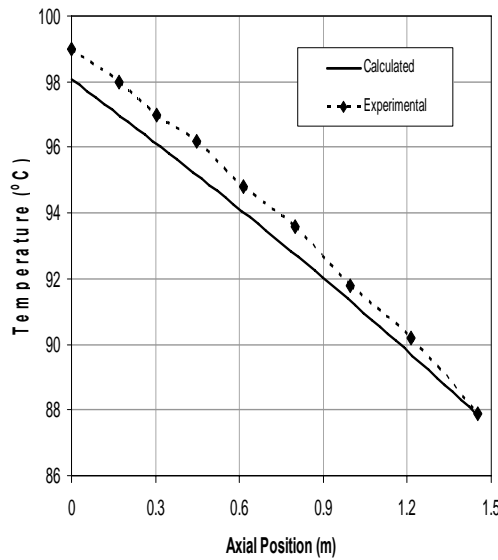


Figure 6.4 Mean temperature variation of coolant inside the jacket for Run 6.1-2

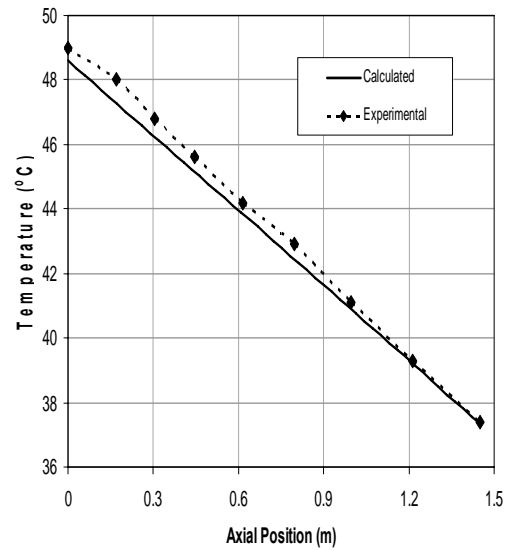


Figure 6.5 Mean temperature variation of coolant inside the jacket for Run 1.4-1

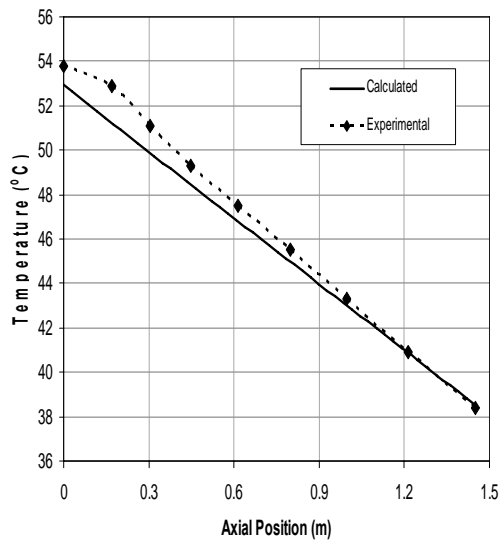


Figure 6.6 Mean temperature variation of coolant inside the jacket for Run 1.3-2

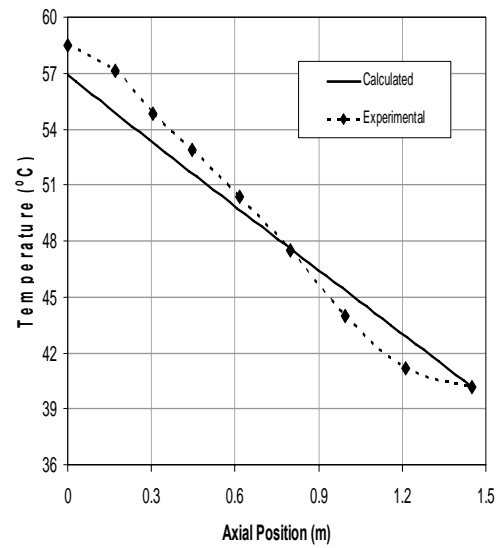


Figure 6.7 Mean temperature variation of coolant inside the jacket for Run 1.2-4R1

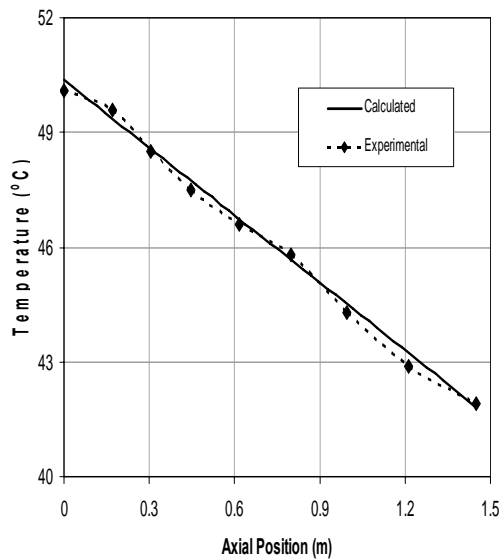


Figure 6.8 Mean temperature variation of coolant inside the jacket for Run 1.2-1

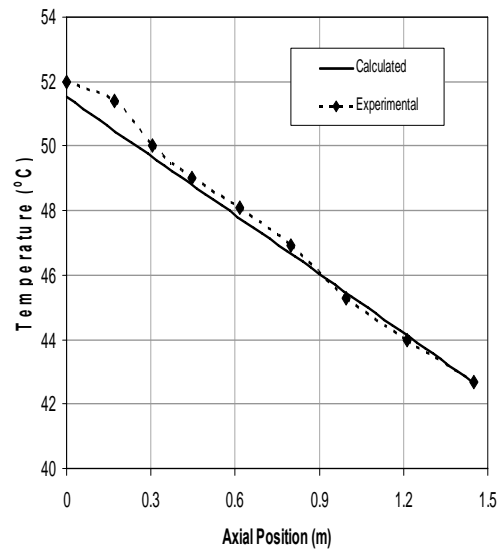


Figure 6.9 Mean temperature variation of coolant inside the jacket for Run 1.1-1

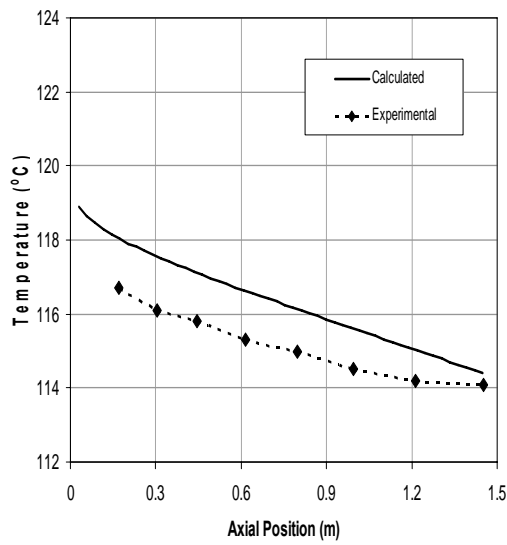


Figure 6.10 Outer surface temperature variation of the condenser tube wall for Run 6.1-2

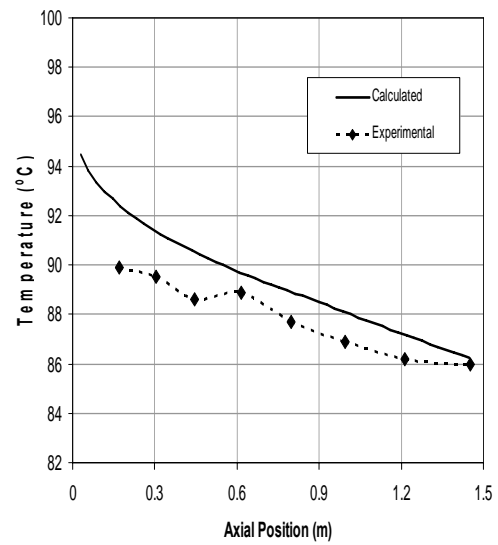


Figure 6.11 Outer surface temperature variation of the condenser tube wall for Run 1.4-1

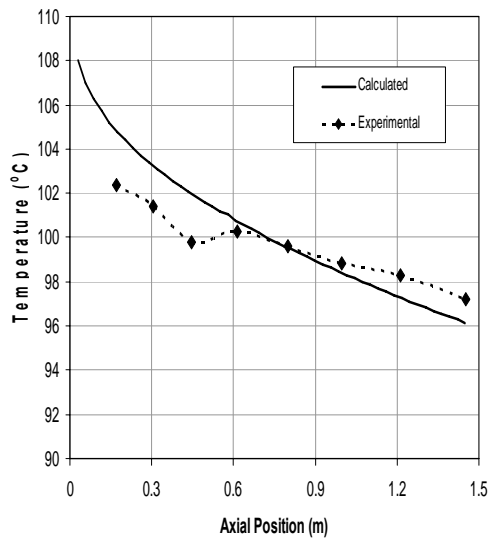


Figure 6.12 Outer surface temperature variation of the condenser tube wall for Run 1.3-2

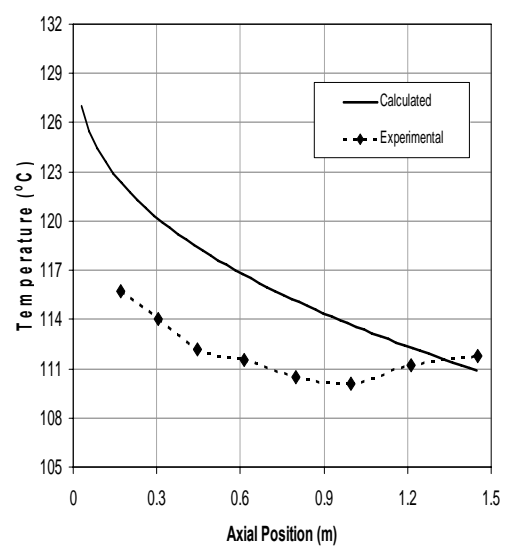


Figure 6.13 Outer surface temperature variation of the condenser tube wall for Run 1.2-4R1

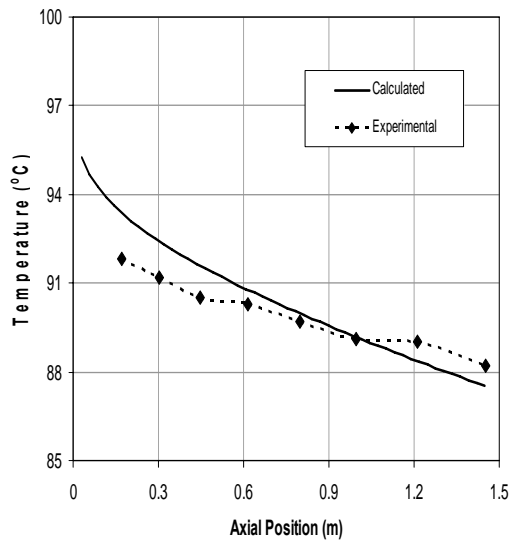


Figure 6.14 Outer surface temperature variation of the condenser tube wall for Run 1.2-1

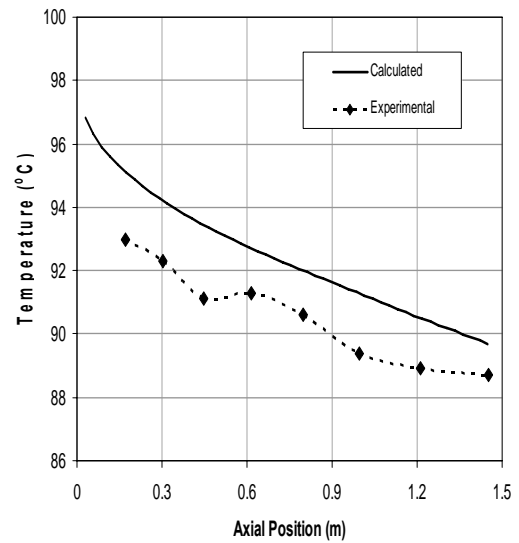


Figure 6.15 Outer surface temperature variation of the condenser tube wall for Run 1.1-1

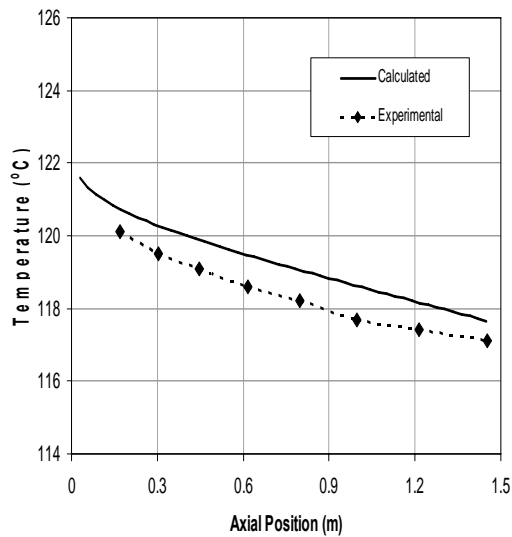


Figure 6.16 Inner surface temperature variation of the condenser tube wall for Run 6.1-2

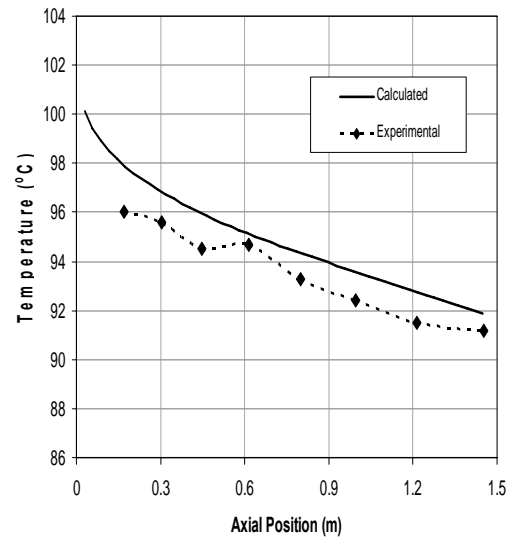


Figure 6.17 Inner surface temperature variation of the condenser tube wall for Run 1.4-1

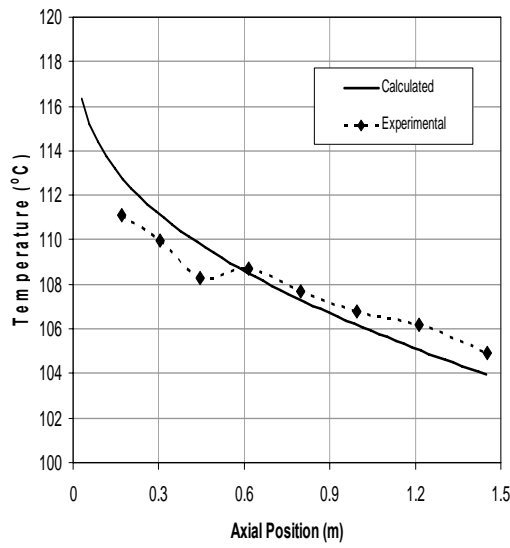


Figure 6.18 Inner surface temperature variation of the condenser tube wall for Run 1.3-2

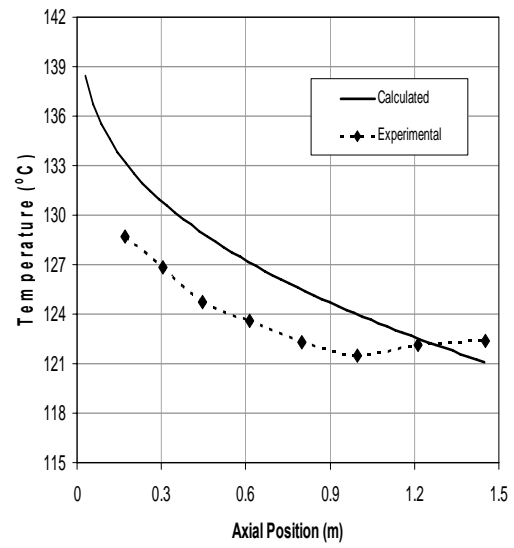


Figure 6.19 Inner surface temperature variation of the condenser tube wall for Run 1.2-4R1

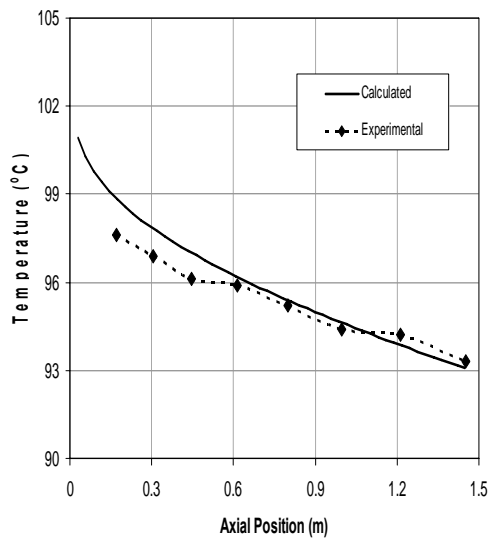


Figure 6.20 Inner surface temperature variation of the condenser tube wall for Run 1.2-1

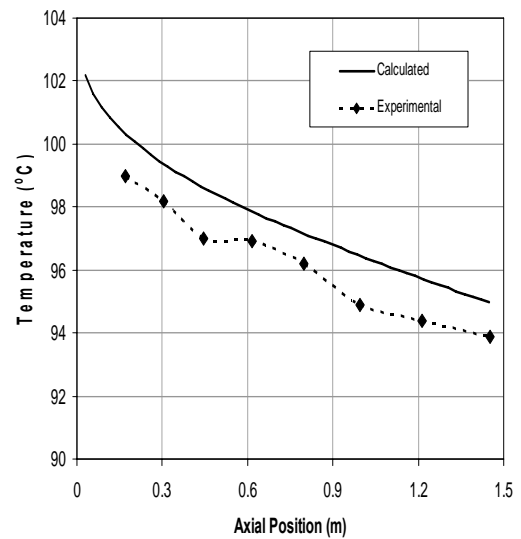


Figure 6.21 Inner surface temperature variation of the condenser tube wall for Run 1.1-1

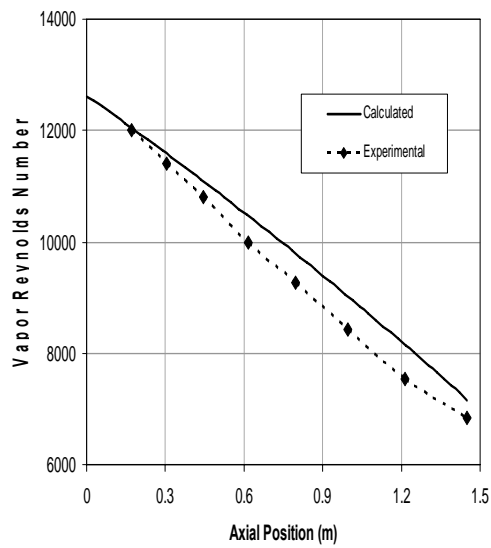


Figure 6.22 Vapor Reynolds number variation for Run 6.1-2

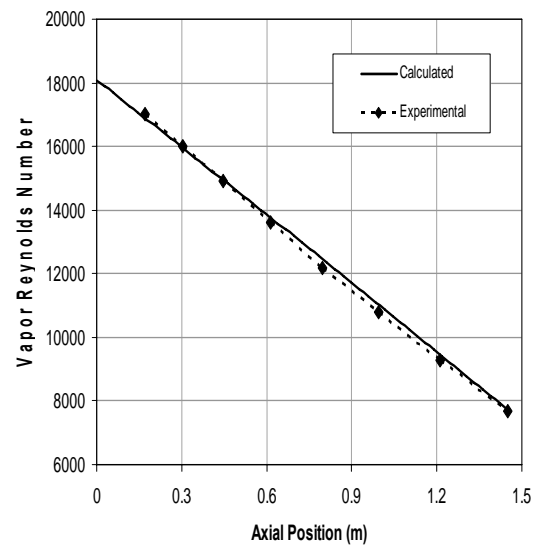


Figure 6.23 Vapor Reynolds number variation for Run 1.4-1

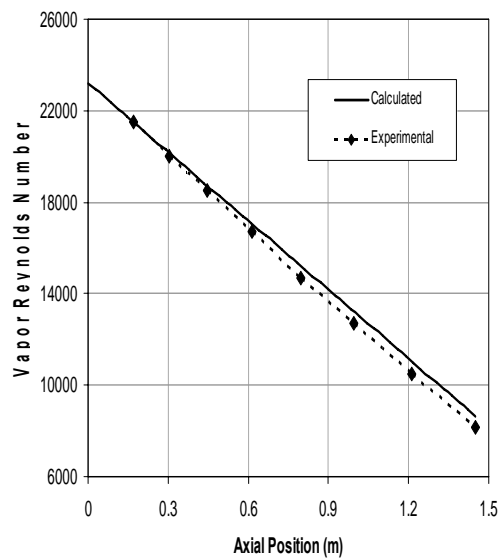


Figure 6.24 Vapor Reynolds number variation for Run 1.3-2

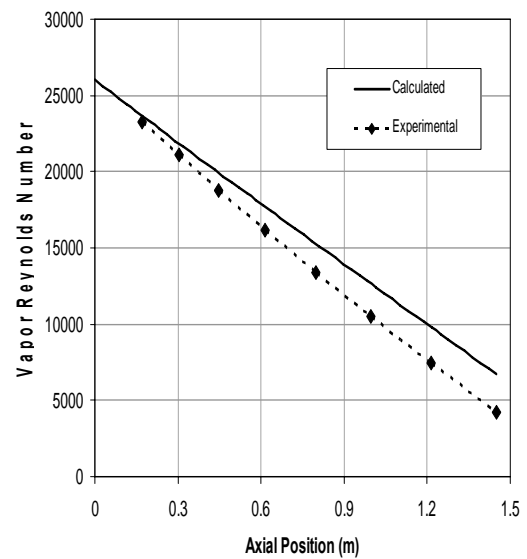


Figure 6.25 Vapor Reynolds number variation for Run 1.2-4R1

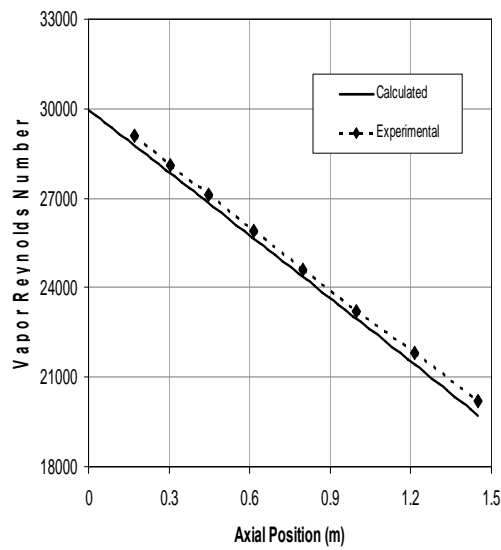


Figure 6.26 Vapor Reynolds number variation for Run 1.2-1

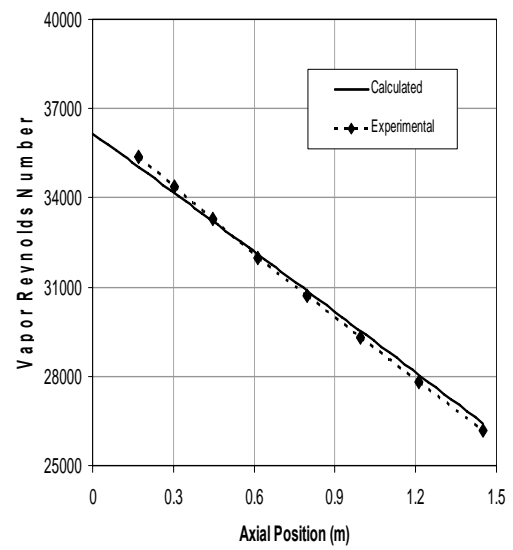


Figure 6.27 Vapor Reynolds number variation for Run 1.1-1

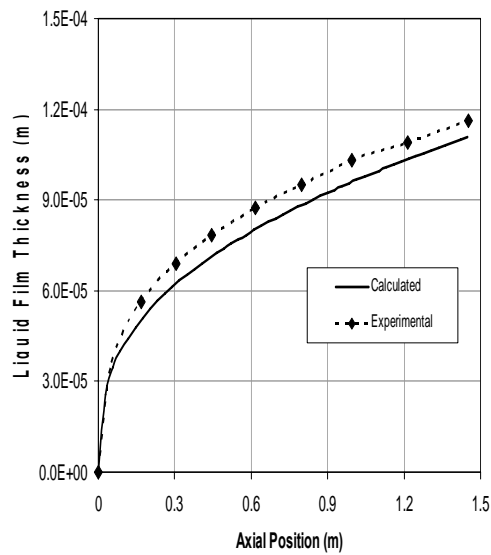


Figure 6.28 Condensate liquid film thickness comparison for Run 6.1-2

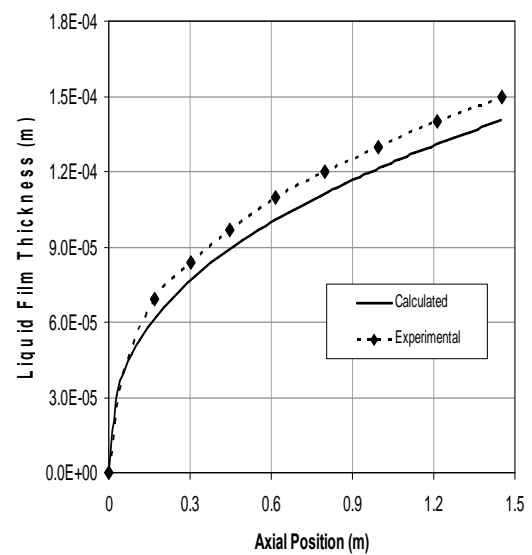


Figure 6.29 Condensate liquid film thickness comparison for Run 1.4-1

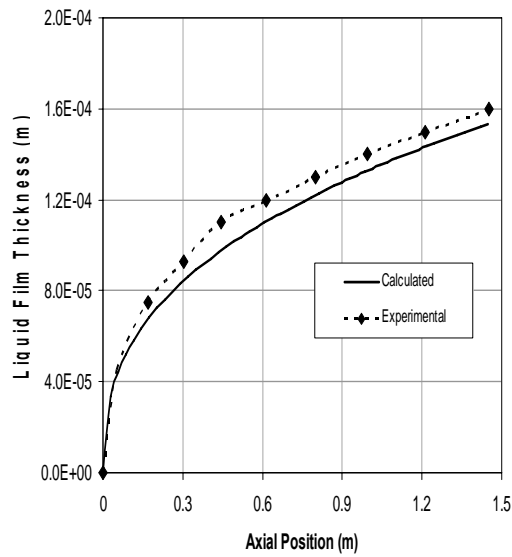


Figure 6.30 Condensate liquid film thickness comparison for Run 1.3-2

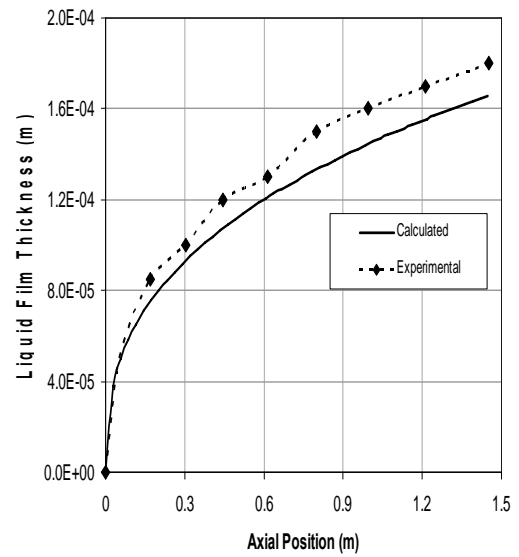


Figure 6.31 Condensate liquid film thickness comparison for Run 1.2-4R1

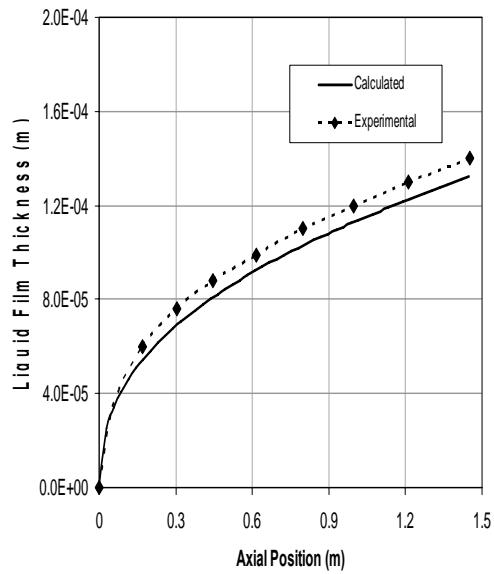


Figure 6.32 Condensate liquid film thickness comparison for Run 1.2-1

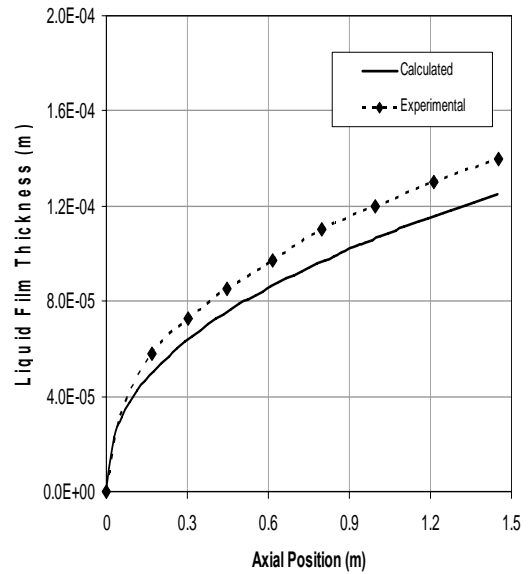


Figure 6.33 Condensate liquid film thickness comparison for Run 1.1-1

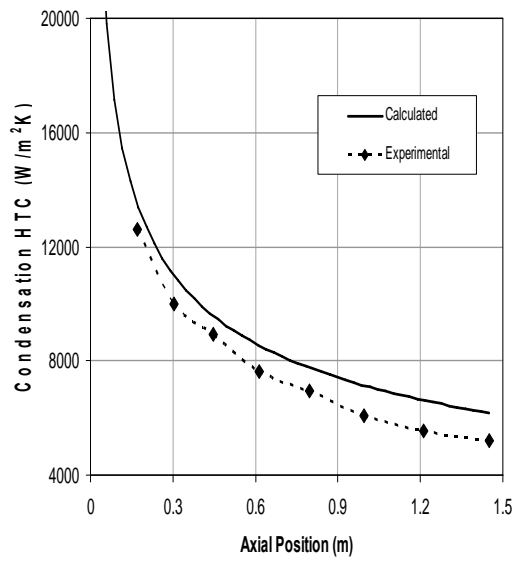


Figure 6.34 Local condensation heat transfer coefficients for Run 6.1-2

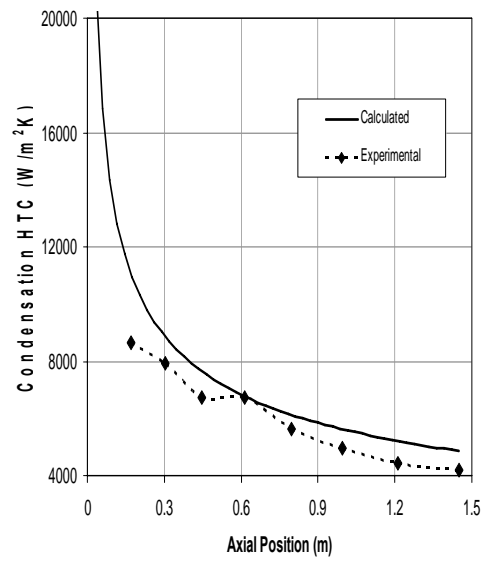


Figure 6.35 Local condensation heat transfer coefficients for Run 1.4-1

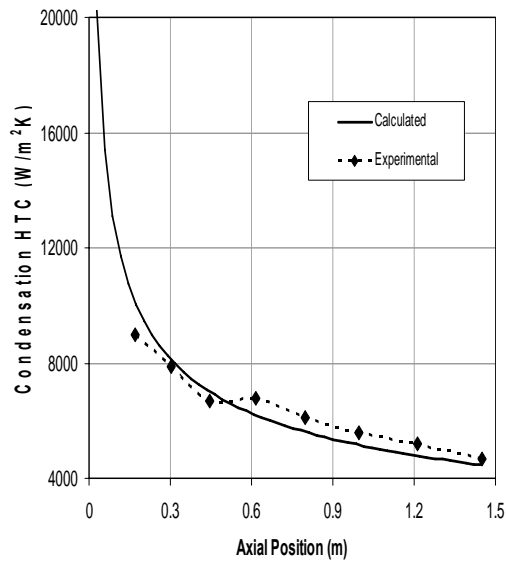


Figure 6.36 Local condensation heat transfer coefficients for Run 1.3-2

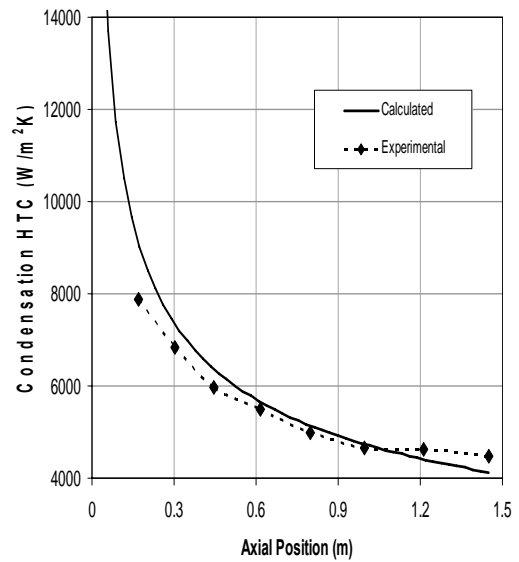


Figure 6.37 Local condensation heat transfer coefficients for Run 1.2-4R1

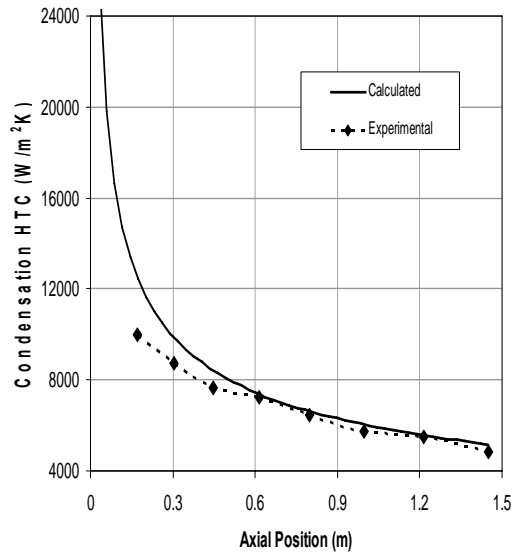


Figure 6.38 Local condensation heat transfer coefficients for Run 1.2-1

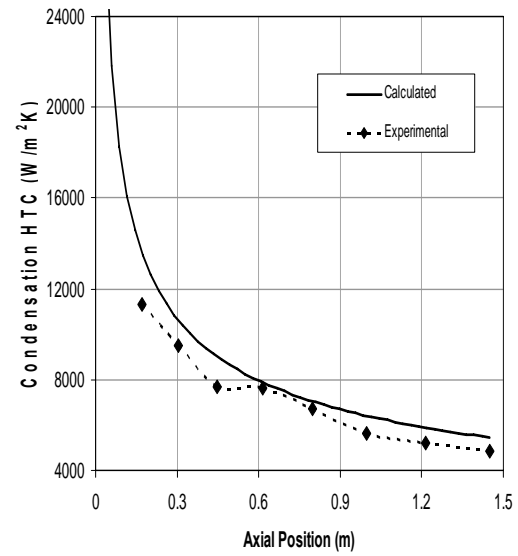


Figure 6.39 Local condensation heat transfer coefficients for Run 1.1-1

6.3.2 Comparison of numerical calculations with NASA experiments

NASA experimental data [Goodykontz (1966)] contains the local coolant mean temperatures, local inner surface temperatures of the condenser tube wall and the local condensation heat transfer coefficients. Therefore, the numerical calculation results are compared to the experimental data in terms of these parameters.

From NASA experiments, two runs are chosen for comparison. Inlet conditions of these NASA experiments are summarized in Table 6.2. For each case, the calculated values of coolant axial mean temperatures inside the jacket tube, the inner surface temperatures of the condenser tube wall and local condensation heat transfer coefficients are compared with the experimental data from Figure 6.40 through Figure 6.45.

Table 6.2 Inlet boundary conditions for NASA tests

Run #	Condenser Side (vapor)					Jacket Side (coolant)		
	Re	\dot{m} (kg/hr)	p_v (KPa)	T_{in} (°C)	T_{sat} (°C)	Re	\dot{m} (kg/hr)	T_{in} (°C)
6	44322	26.8	307.5	136.0	134.4	5728.2	670.9	45.3
10	71430	44.0	384.1	143.3	142.2	25455	3016.4	39.4

The code ZEC predicts the calculated coolant mean temperatures, given in Figures 6.40 and 6.41, by about less than 10% deviation compared with the experimental data. The calculated coolant mean temperatures reflect the general trend of experimental data reasonably well.

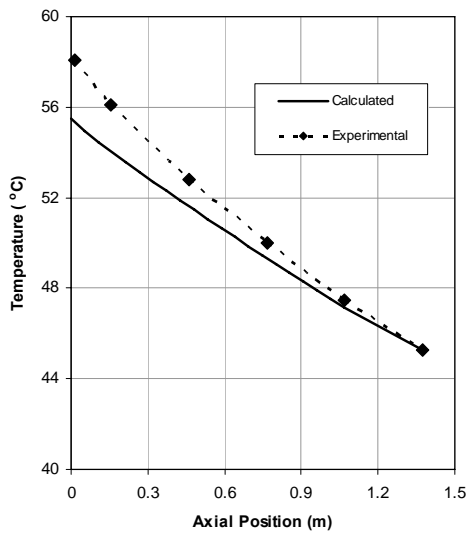


Figure 6.40 Mean temperature variation of coolant inside the jacket for Run 6

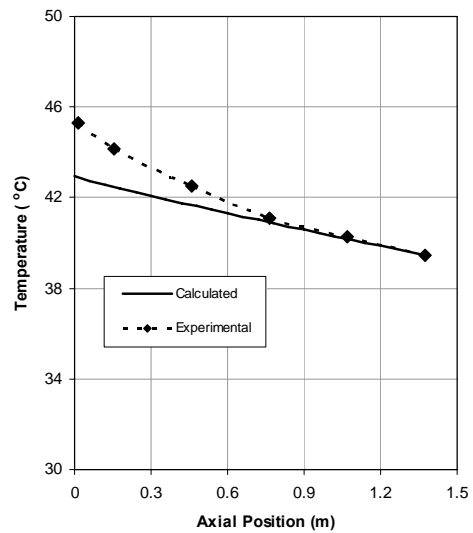


Figure 6.41 Mean temperature variation of coolant inside the jacket for Run 10

The comparisons for the inner surface temperatures of the condenser tube wall are given in Figures 6.42 and 6.43 for each case. For NASA experiments, there is not detailed information about how to obtain the surface temperatures and which thermal conductivity value is used. However, during the code calculations, the temperature dependent function given in Eq.(6.3) is used. The code ZEC calculates the inner surface temperatures of the condenser tube wall by about less than $\pm 25\%$ difference compared to the experimental data for these two cases.

In Figures 6.44 and 6.45, the calculated and experimental local heat transfer coefficients are presented for each case. The code ZEC predicts the local heat transfer coefficients by about less than 30% difference compared to the experimental results for all cases. The results of code ZEC are found to be satisfactory, compared with the NASA experiments.

It should be noted that an error analysis for the NASA experiments does not exist in the reference report [Goodykontz (1966)].

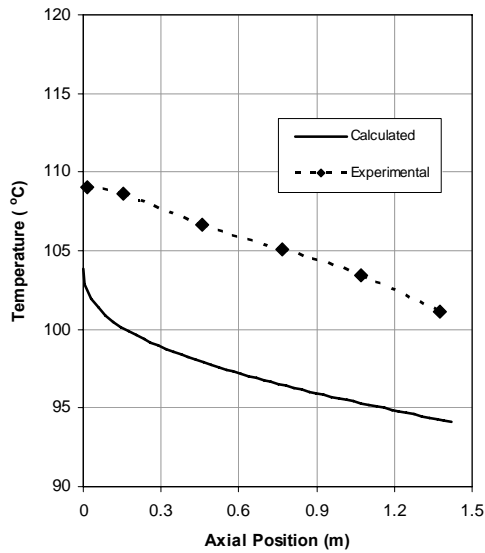


Figure 6.42 Inner surface temperature variation of the condenser tube wall for Run 6

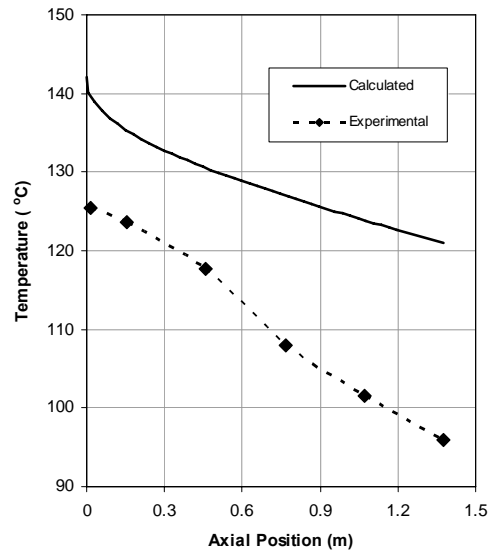


Figure 6.43 Inner surface temperature variation of the condenser tube wall for Run 10

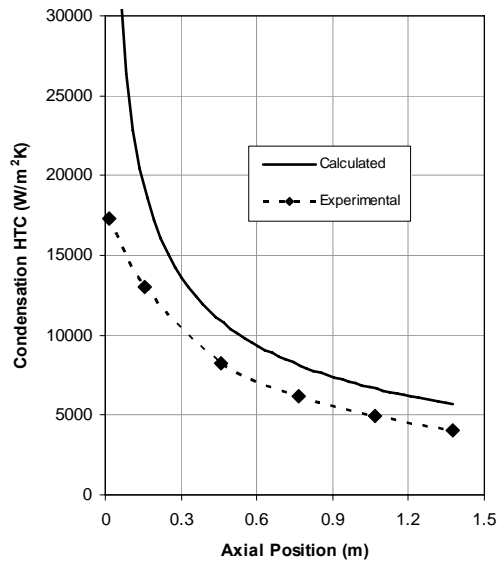


Figure 6.44 Local condensation heat transfer coefficients for Run 6

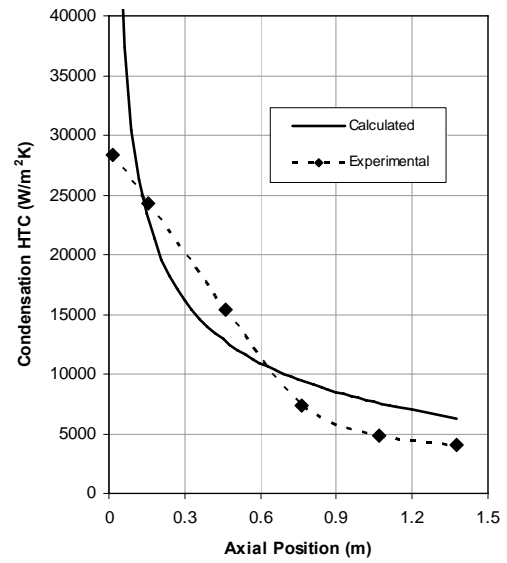


Figure 6.45 Local condensation heat transfer coefficients for Run 10

6.3.3 Comparison of numerical calculations with METU experiments

The local coolant mean temperatures, local inner surface temperatures of the condenser tube wall and the local condensation heat transfer coefficients in METU experimental data [Tanrikut (1998)] are used to compare to the numerical calculations of the code ZEC.

From METU experiments, two runs are chosen for comparison. Inlet conditions of these METU runs are summarized in Table 6.3. For each case, the calculated values are compared to the experimental data from Figure 6.46 through Figure 6.51.

Table 6.3 Inlet boundary conditions for METU tests

Run #	Condenser Side (vapor)					Jacket Side (coolant)		
	Re	\dot{m} (kg/hr)	p_v (KPa)	T_{in} (°C)	T_{sat} (°C)	Re	\dot{m} (kg/hr)	T_{in} (°C)
1.3.1	66875	83.30	303	157.0	133.9	2115.1	802.8	20.2
1.4.1	76645	97.96	396	162.7	143.3	2143.5	813.6	21.4

The code ZEC predicts the calculated coolant mean temperatures given in Figures 6.46 and 6.47 by a deviation about 45% compared to the experimental data. Especially, the considerable deviations between the experimental and calculated values occur at the inlet region of the test section where the condensation process starts.

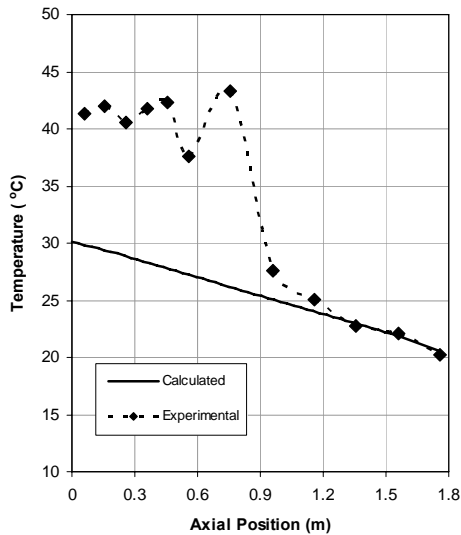


Figure 6.46 Mean temperature variation of coolant inside the jacket for Run 1.3.1

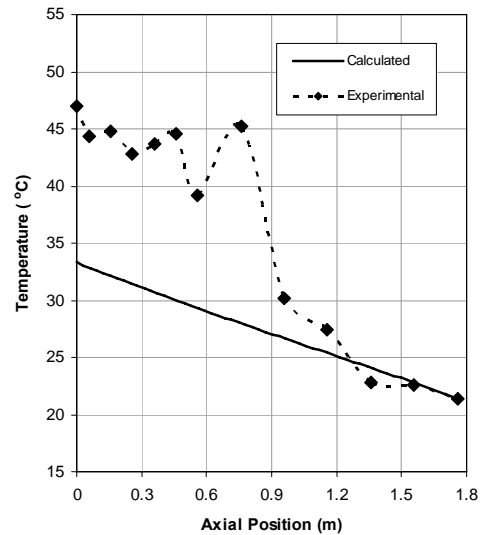


Figure 6.47 Mean temperature variation of coolant inside the jacket for Run 1.4.1

The comparisons for the inner surface temperatures of the condenser tube wall are given in Figures 6.48 and 6.49 for each case. In METU experiments, a constant thermal conductivity value is used to calculate inner surface temperatures of the condenser tube wall from the measured temperatures by means of embedded thermocouples into the condenser tube wall at certain axial locations while the temperature dependent function given in Eq.(6.3) is used during the code calculations. The code ZEC predicts the surface temperatures by about less than 10% difference compared to the experimental results for these two cases.

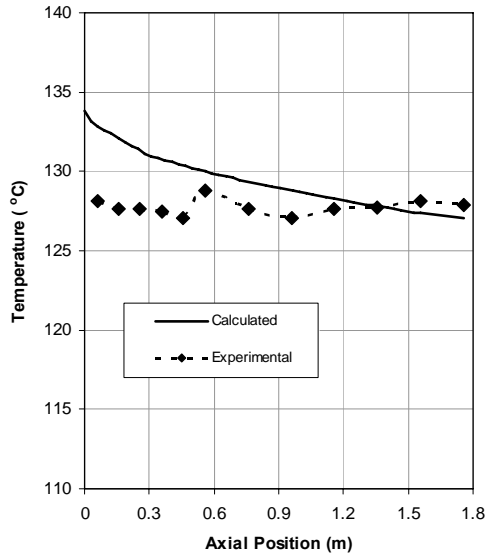


Figure 6.48 Inner surface temperature variation of the condenser tube wall for Run 1.3.1

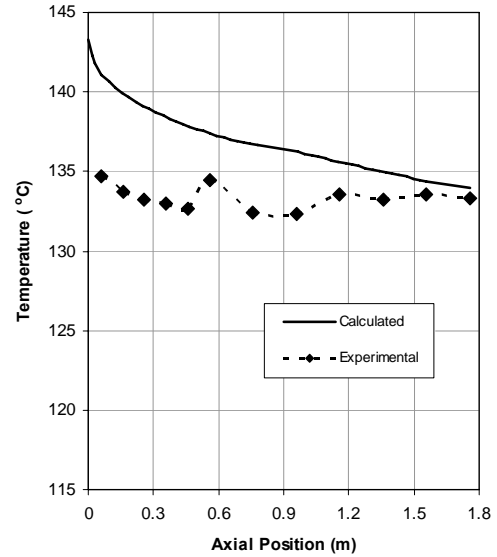


Figure 6.49 Inner surface temperature variation of the condenser tube wall for Run 1.4.1

In Figures 6.50 and 6.51, the calculated and experimental local heat transfer coefficients are presented for each case. There are significant deviations (more than $\pm 100\%$) between the experimental data and calculated values. In METU experiments, it is reported that the maximum uncertainty for the condensation heat transfer coefficient is $\pm 24\%$ [Tanrikut (1998)].

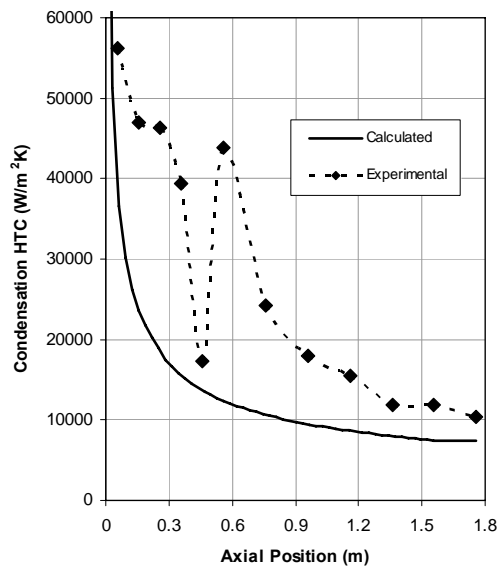


Figure 6.50 Local condensation heat transfer coefficients for Run 1.3.1

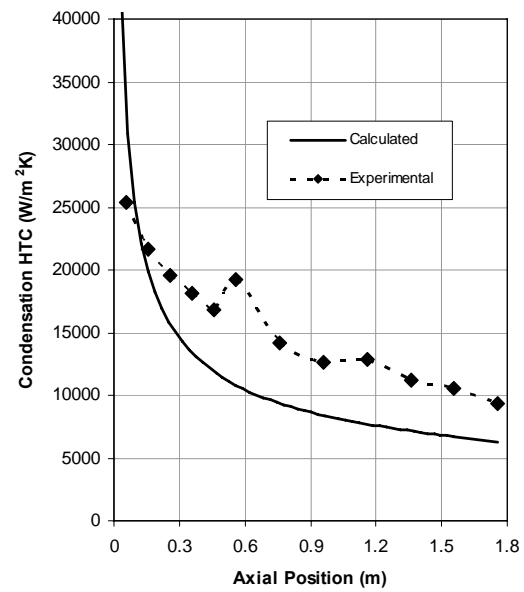


Figure 6.51 Local condensation heat transfer coefficients for Run 1.4.1

6.3.4 Concluding comments

After the comparisons between the results of developed computer code, ZEC, and the experimental results of 3 different databases (UCB, NASA and METU), the numerical results are found to reasonably agree with the experimental results of UCB and NASA. But, there are serious deviations between the calculated results and METU experimental results.

The maximum uncertainties for the condensation heat transfer coefficients of UCB and METU experiments are $\pm 18.7\%$ and $\pm 24\%$, respectively [Kuhn (1994), Tanrikut (1998)]. It should be noted that such kind of error analysis is not available for NASA experiments [Goodykontz (1966)]. Regarding the uncertainties in the experiments and also the assumptions given in Section 6.1 for the numerical calculations, it can be stated that the results of code ZEC are in agreement with the experimental data of UCB and NASA. Therefore, the numerical results reflect the general trend of experimental data reasonably well.

CHAPTER 7

EFFECTS OF PARAMETERS ON THE CONDENSATION

The predictions of the ZEC code are found to be in good agreement with the experimental results over a wide range of conditions. Therefore, this developed code, ZEC, may be used for the preliminary design of in-tube condensers and for the performance evaluation of such condensers.

In this respect, the effect of some parameters such as inlet pressure and mass flow rate of vapor, inlet temperature and mass flow rate of the coolant on the condensation process can be analyzed by using ZEC code. In order to perform such kind of analyses, a reference case, Run 1.3-2 of UCB data, from Table 6.1 is chosen arbitrarily and following results are obtained to show the effects of parameters on the condensation process.

7.1 The effect of steam inlet pressure

In order to investigate the effect of inlet steam pressure, calculations for three cases are conducted at different pressure levels which are 110 kPa, 199.2 kPa (reference case, Run 1.3-2 of UCB data) and 300 kPa. The basic principle employed in this analysis is to keep all parameters fixed while the inlet steam pressure is varied.

For three cases used in this analysis, the inlet saturation temperatures (T_{sat}) of the steam are 102.3 °C, 120.1 °C and 133.5 °C for the pressures 110.0 KPa,

199.2 KPa and 300.0 KPa, respectively. The increase of T_{sat} leads to a higher temperature difference between the steam and inner surface of the condenser tube wall along the axial direction. Variation of temperature difference, $\Delta T (=T_{sat} - T_i)$, along the condenser tube for different inlet pressures are shown in Figure 7.1. Local values of ΔT increases as steam inlet pressure increases.

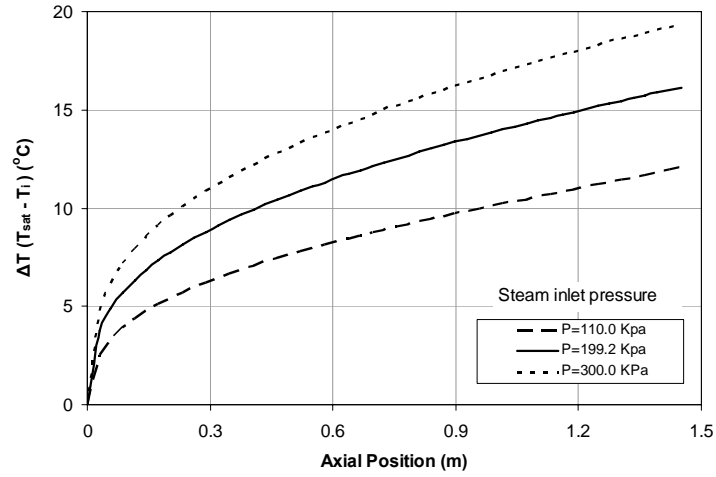


Figure 7.1 Variation of temperature difference between the steam and inner surface of condenser tube wall along the condenser tube

The condensate liquid film Reynolds number, Re_L , given in Eq.(4.13a) is a linear function of the condensation mass flow rate per unit length (Γ). The variations of the local Re_L are given in Figure 7.2 for three different inlet steam pressures. Local Γ and also local Re_L increase as the inlet pressure increases. Figure 7.3 depicts the variation of local liquid film thickness (δ) along the axial locations for different inlet steam pressures. As the inlet pressure increases, the local liquid film thickness also increases.

The condensation heat transfer coefficient (h_L) is a reciprocal function of the liquid film thickness (Eq. (4.36)). Therefore, as the local value of δ increases with increasing inlet pressure, h_L and liquid film Nusselt number (Eq. (4.38)) decrease (Figure 7.4).

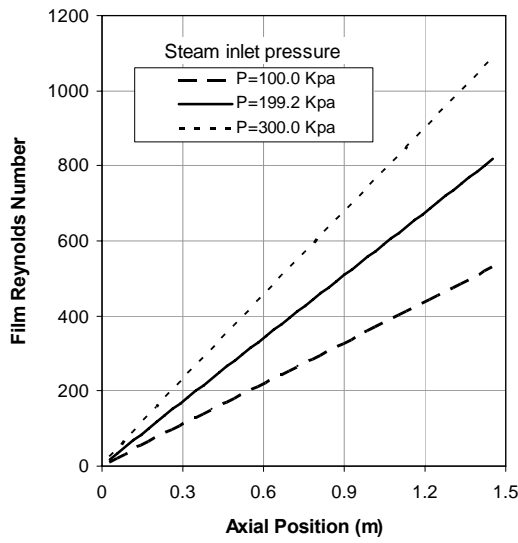


Figure 7.2 Local liquid film Reynolds number variation along the condenser tube

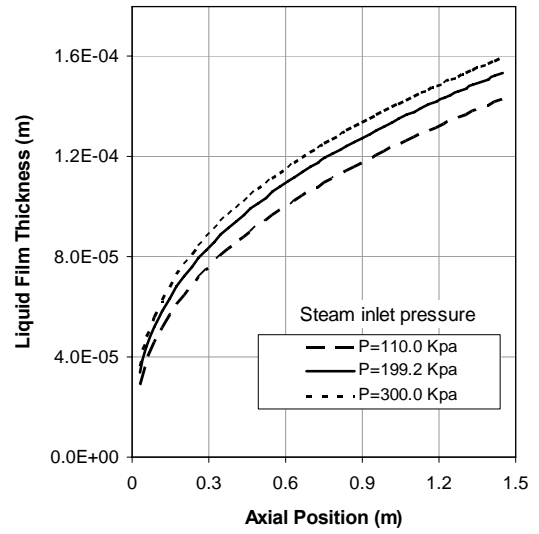


Figure 7.3 Local liquid film thickness variation along the condenser tube

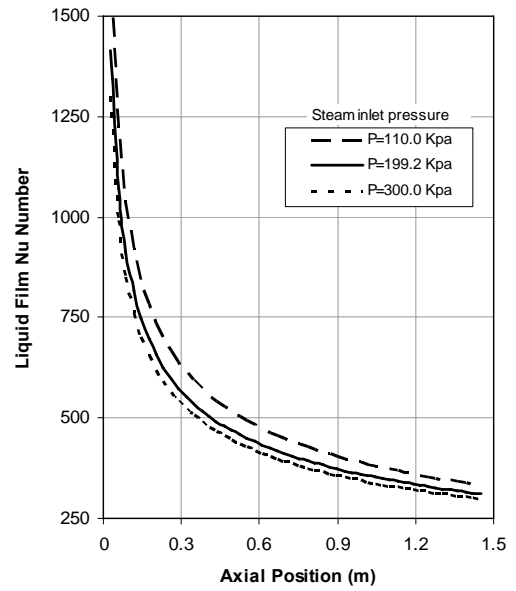
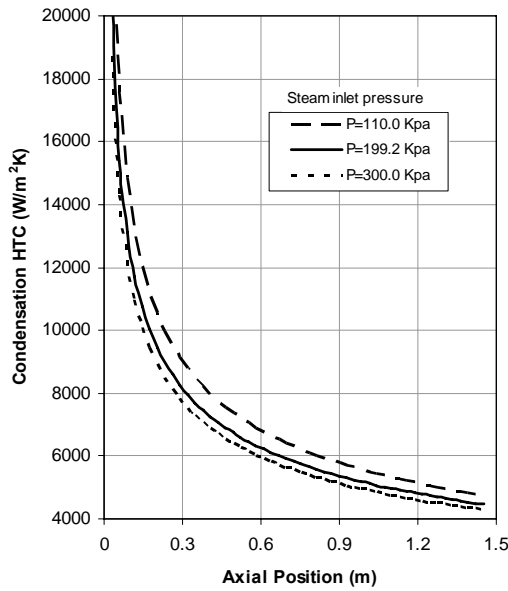


Figure 7.4 Local condensation heat transfer coefficient and liquid film Nusselt number variation along the condenser tube for different steam inlet pressures

In Figure 7.4, it is also noted that the local film Nusselt number given in Eq. (4.38) is not only the function of local condensation heat transfer coefficient and also the function of local thermal conductivity values of the liquid film (k_L) which is a function of local liquid temperature. Therefore, these two parameters are graphed separately although the behaviors are almost same. From this figure, one can see that if the steam inlet pressure is increased by 50% (referred to 199.2 KPa and 300.0 KPa cases), the condensation heat transfer coefficient decreases about 5%.

7.2 The effect of steam inlet mass flow rate

A similar analysis is performed for the effect of steam inlet mass flow rate. Three different mass flow rates; 30 kg/h, 40.4 kg/h as the reference case (Run 1.3-2 of UCB data) and 50 kg/h are considered, with the corresponding steam inlet Reynolds numbers 17237, 23213 and 28729, respectively.

The variations of the local condensate liquid film Reynolds number, Re_L , are given in Figure 7.5 for three different steam inlet mass flow rates. The local Re_L and also local Γ increases (Eq.(4.13a)) as the steam inlet mass flow rates increases. Figure 7.6 shows the variation of local liquid film thickness along the axial locations for different steam inlet mass flow rates. Higher steam inlet mass flow rates yield lower local liquid film thickness, although the local Re_L increases with the increase of the steam inlet mass flow rate.

Figure 7.7 shows the local variation of the condensation heat transfer coefficient (h_L) and the local condensation Nusselt number. h_L is a reciprocal function of the liquid film thickness (Eq. (4.36)). It is obvious that as the local δ decreases with the increase of the steam inlet mass flow rate, h_L and also Nusselt number (Eq. (4.36)) increases. Therefore, as the steam inlet mass flow rate increases, the local values of h_L and also local Nusselt number increase. For instance, if the inlet mass flow rate is increased with a factor 23.4% (referred to

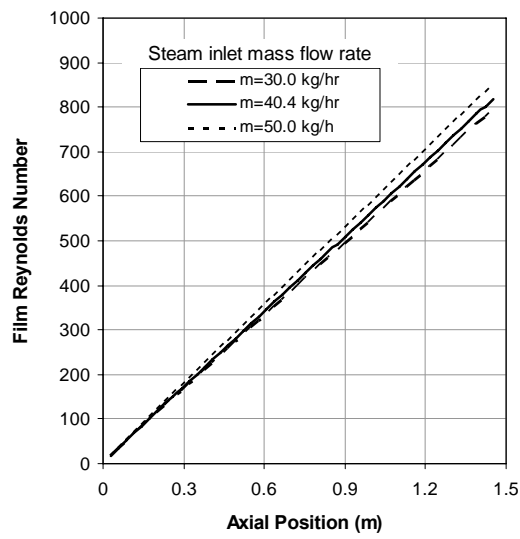


Figure 7.5 Local liquid film Reynolds number variation along the condenser tube

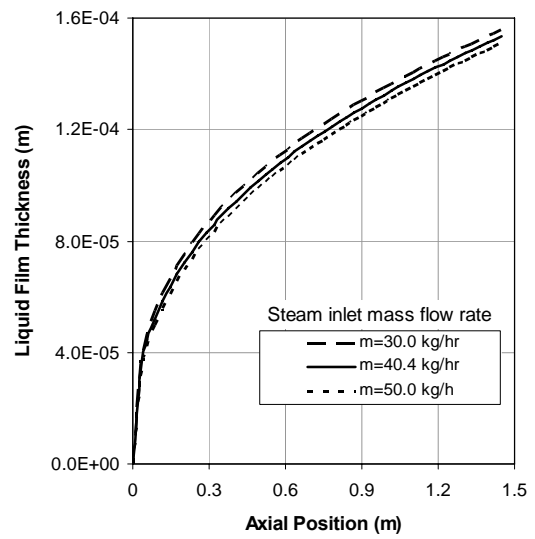


Figure 7.6 Local liquid film thickness variation along the condenser tube

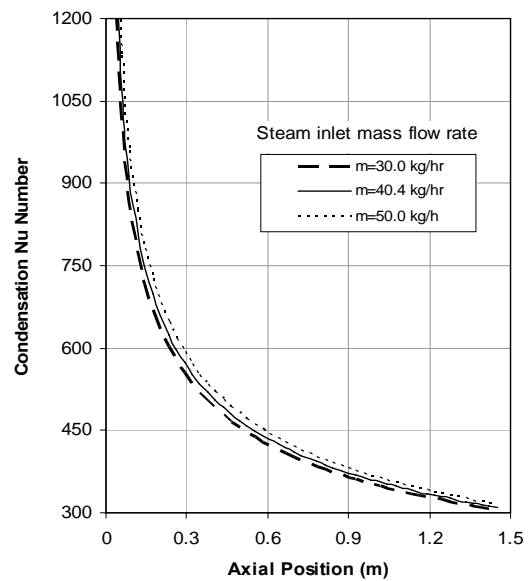
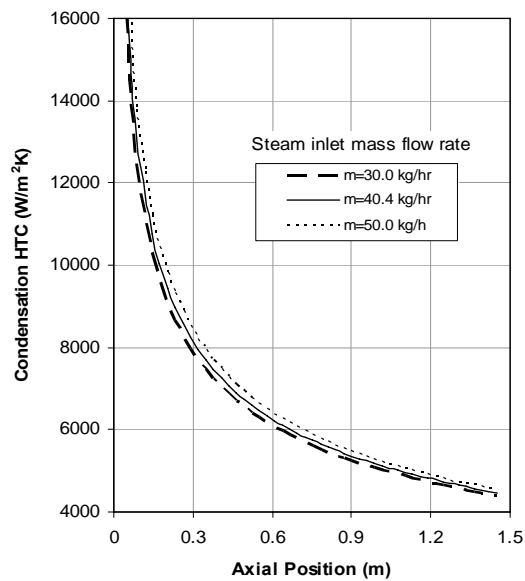


Figure 7.7 Local condensation heat transfer coefficient and liquid film Nusselt number variation along the condenser tube

40.4 kg/h and 50 kg/h cases), the condensation heat transfer coefficient increases about less than 2.5%.

7.3 The effect of cooling water inlet temperature

In order to analyze the effect of the cooling water inlet temperature, ZEC code runs are performed for different coolant inlet temperatures which are 20.0 °C, 38.2 °C (Run 1.3-2 of UCB data as reference case) and 60.0 °C. During this analysis, all other inlet conditions for steam and coolant in Run 1.3-2 of UCB data set are fixed.

The results given in Figure 7.8 show the increase of cooling water mean temperature along the jacket annulus as the inlet temperature increases. Also, the increase of the inlet temperature of the cooling water ($\bar{T}_{j,inlet}$) leads to an increase of the outer surface temperature of the condenser tube wall (T_{iw}) along the axial direction (Figure 7.9). Since the inner surface temperature of the condenser tube wall (T_i) is a linear function of the outer surface temperature of the condenser tube wall (Eq. (6.2)), T_i also increases as the inlet temperature of the coolant increases (Figure 7.10). It is also noticed that T_i reaches to 120.1 °C at the condenser tube inlet for all cases, which is the inlet steam temperature of the reference case.

As the inner surface temperature of the condenser tube wall (T_i) increases, the temperature difference between the steam and the inner surface of the condenser tube wall, $\Delta T (=T_{sat} - T_i)$, along the axial direction decreases where T_{sat} is constant (120.1 °C). Therefore, ΔT at any location decreases as the coolant inlet temperature increases. The variations of the local condensate liquid film Reynolds number, Re_L , are given in Figure 7.11 for three different coolant inlet temperatures. Local Re_L decreases with the decrease of local ΔT values, i.e., with the increase of the coolant inlet temperature.

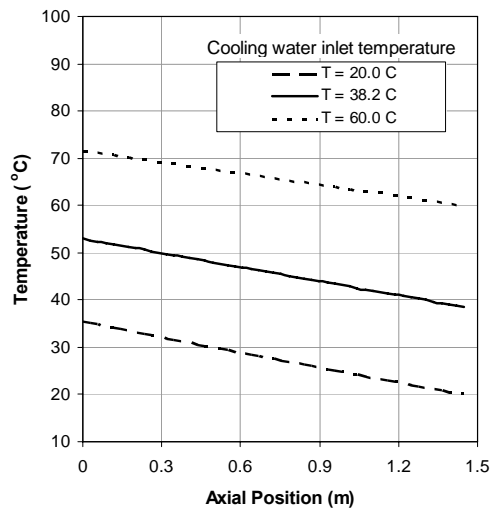


Figure 7.8 Variation of cooling water mean temperature inside the jacket annulus for different coolant inlet temperatures

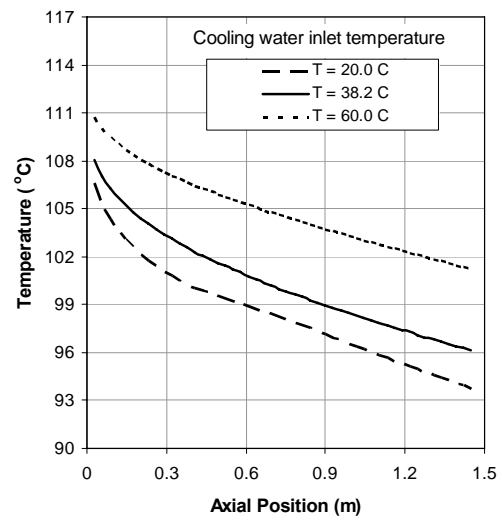


Figure 7.9 Variation of the outer surface temperature of the condenser tube wall for different coolant inlet temperatures

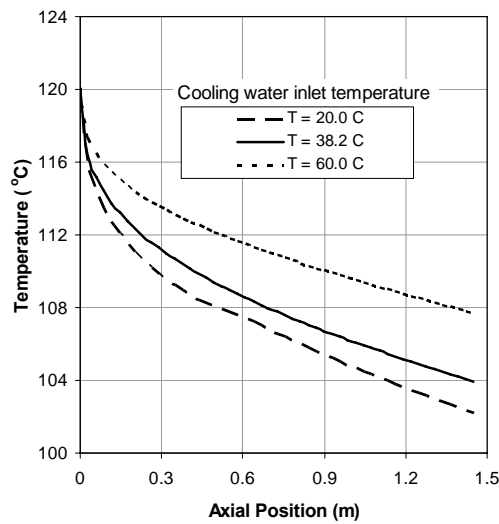


Figure 7.10 Variation of the inner surface temperature of the condenser tube wall for different coolant inlet temperatures

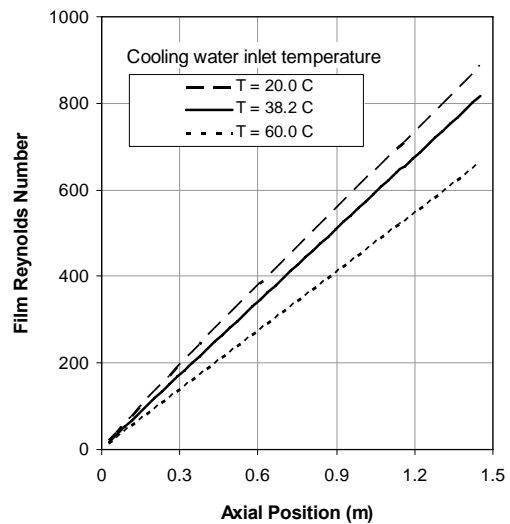


Figure 7.11 Local liquid film Reynolds number variation along the condenser tube for different coolant inlet temperatures

Figure 7.12 shows the variation of local liquid film thickness along the axial locations for different coolant inlet temperatures. As the coolant inlet temperature increases, the local liquid film thickness decreases.

Since the condensation heat transfer coefficient (h_L) is inversely proportional to the liquid film thickness (Eq. (4.36)), local h_L and also local condensation Nusselt number (Eq. (4.38)) increase, as the local values of δ decreases with the increase of the coolant inlet temperature (Figure 7.13). For example, if the coolant inlet temperature is increased by 57% (referred to 38.2 °C and 60.0 °C cases), the condensation heat transfer coefficient increases about 8%.

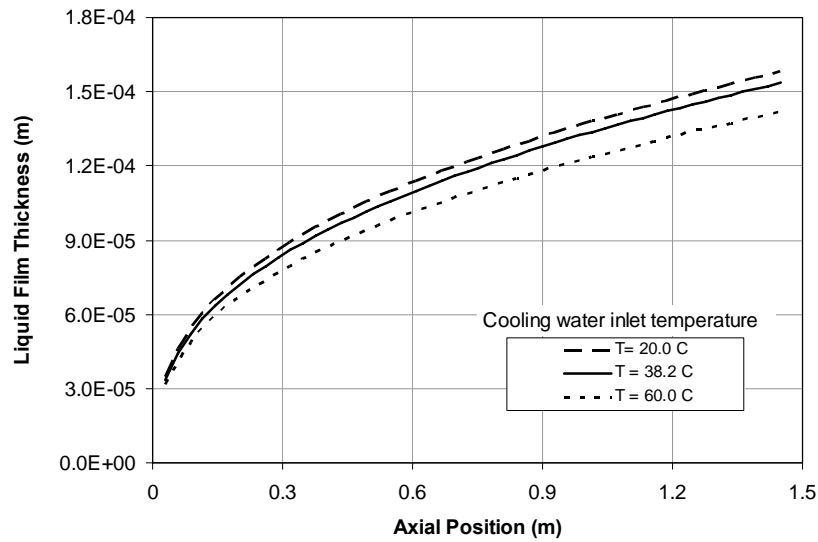


Figure 7.12 Local liquid film thickness variation along the condenser tube for different coolant inlet temperatures

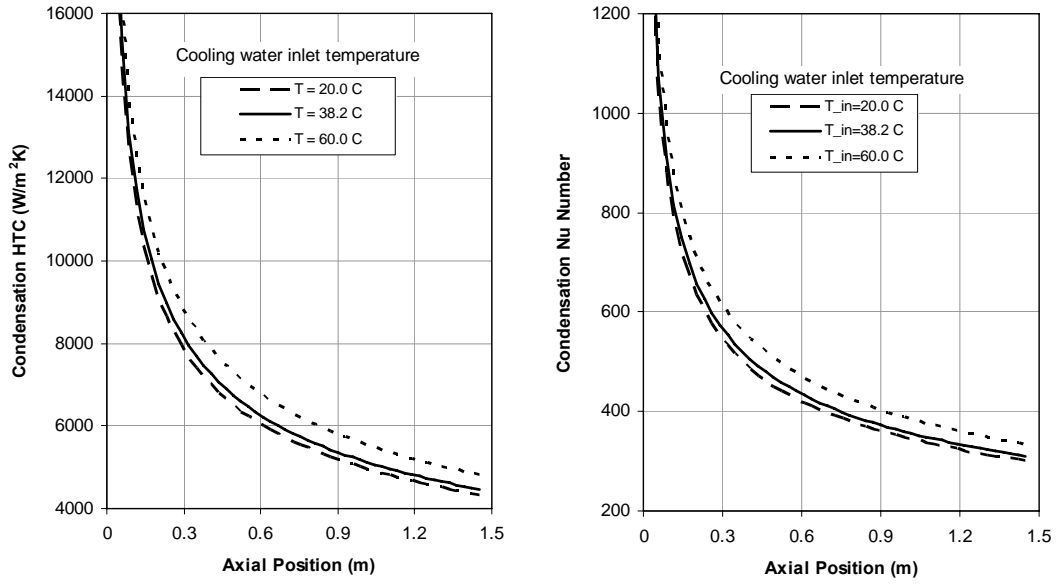


Figure 7.13 Local condensation heat transfer coefficient and liquid film Nusselt number variation along the condenser tube

7.4 The effect of cooling water inlet mass flow rate

Another analysis for the effect of the cooling water inlet mass flow rate is performed. Similarly, as in the previous analyses, all other inlet conditions for the steam and coolant in Run 1.3-2 of UCB data are set to be fixed whereas only the cooling water mass flow rate is varied. Three different inlet flow rates; 800.0 kg/h, 932.5 kg/h (reference case) and 1100.0 kg/h are considered, with the corresponding inlet water Reynolds numbers 3385.9, 3946.4 and 4657.7, respectively.

One can readily perceive that if the coolant water inlet mass flow rate or inlet water Reynolds number increases, local heat transfer coefficient (Eq. (5.52)) and also local Nusselt number (Eq. (5.53)) at the jacket side increase (Figure 7.14). This increase leads to the decrease of local temperature differences ($T_{iw} - \bar{T}_j$) between the outer surface of the condenser tube wall and the mean temperature of the cooling water (Figure 7.15). Therefore, higher coolant inlet mass flow rates yield lower outer surface temperatures of the condenser tube wall

as given in Figure 7.16. Since the inner surface temperature of the condenser tube wall (T_i) is a linear function of the outer surface temperature of the condenser tube wall (Eq. (6.2)), local T_i values also decrease as the cooling water inlet mass flow rate increases (Figure 7.17).

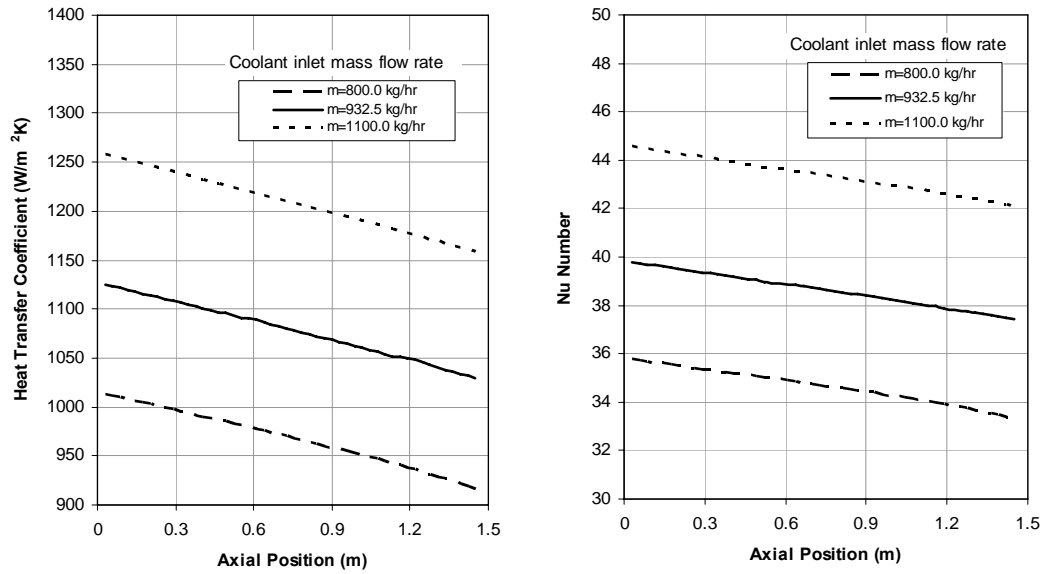


Figure 7.14 Variation of local heat transfer coefficient and local Nusselt number inside the jacket for different coolant inlet mass flow rates

In case of the decrease of the T_i , temperature difference between the steam and inner surface of the condenser tube wall, ΔT ($=T_{sat} - T_i$), along the axial direction increases where T_{sat} is constant (120.1°C). Therefore, ΔT at any location increases, as the coolant inlet mass flow rate increases. The variation of ΔT directly affects the condensation process. Figure 7.18 shows the variations of the local condensate liquid film Reynolds number, Re_L , for three different coolant inlet mass flow rates. Local Re_L and also local Γ Eq.(4.13a) increase with the increase of local ΔT values. Figure 7.19 depicts the variation of local liquid film thickness along the axial locations for different coolant inlet mass flow rates. As the coolant inlet temperature increases, the local liquid film thickness also increases.

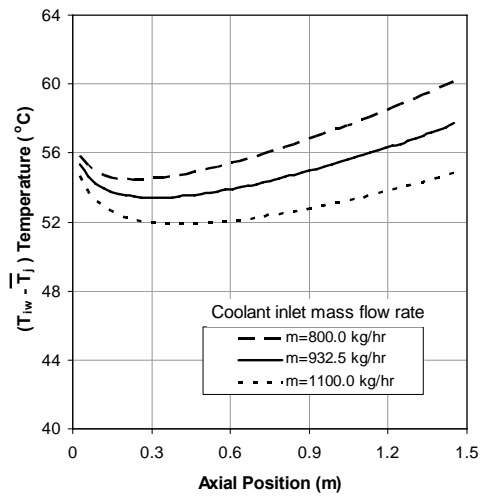


Figure 7.15 Temperature difference between outer surface of the condenser tube wall and the mean temperature of the cooling water

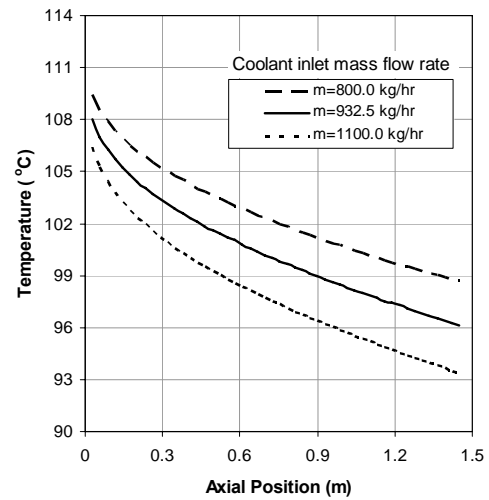


Figure 7.16 Condenser tube outer surface temperature variation for different coolant inlet mass flow rates

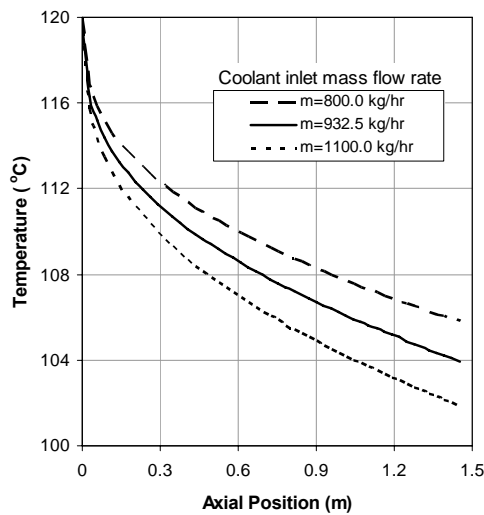


Figure 7.17 Condenser tube inner surface temperature variation for different coolant inlet mass flow rates

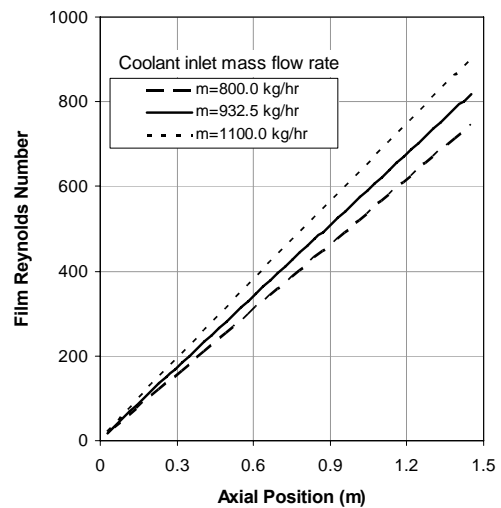


Figure 7.18 Local liquid film Reynolds number variation along the condenser tube for different coolant inlet mass flow rates

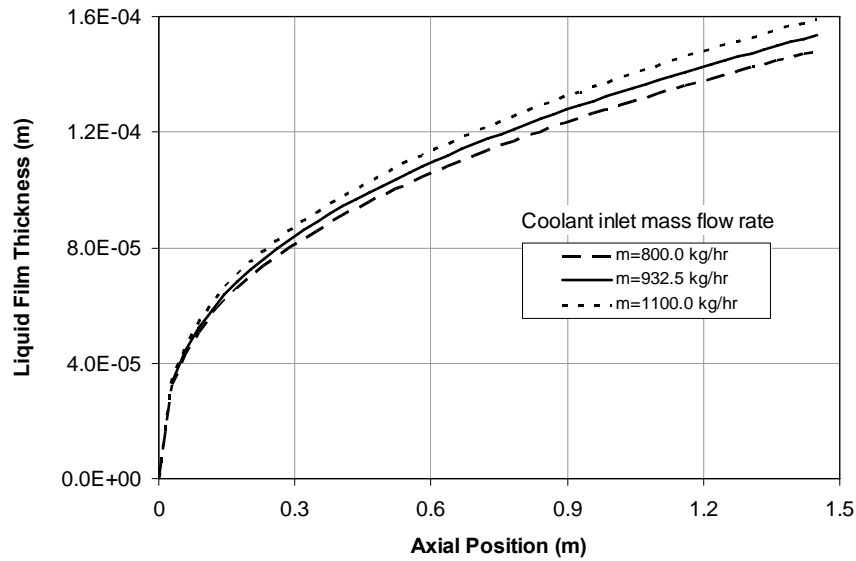


Figure 7.19 Local liquid film thickness variation along the condenser tube for different coolant inlet mass flow rates

The condensation heat transfer coefficient (h_L) is inversely proportional to the liquid film thickness (Eq. (4.36)). Therefore, as local values of δ increases for higher coolant mass flow rates, the condensation heat transfer coefficient and the condensation Nusselt number decrease along downward direction as well as the coolant inlet mass flow rate at the jacket side increases (Figure 7.20).

All of these facts show that the coolant inlet temperature and inlet mass flow rate affect the condensation process and they should be taken into account if any meaningful comparisons between the experimental works, correlations and analytical studies on condensation are to be made.

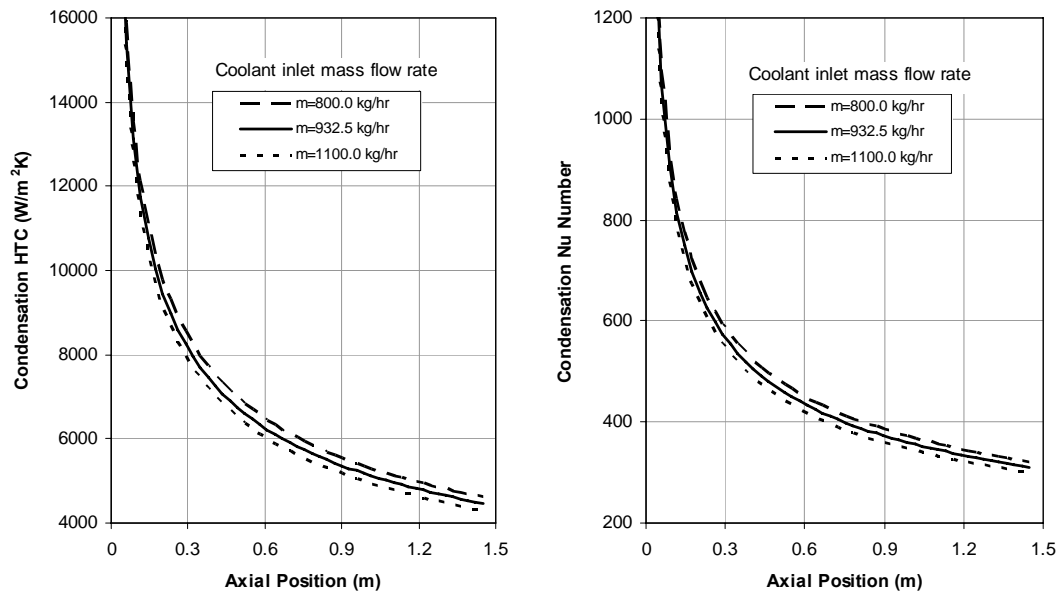


Figure 7.20 Local condensation heat transfer coefficient and Nusselt number variation along the condenser tube for different coolant inlet mass flow rates

CHAPTER 8

CONCLUSIONS

8.1 General comments

In this thesis, a comprehensive analytical and numerical study is conducted to simulate the conjugate condensation heat transfer in vertical tubes cooled by counter-currently forced liquid flow.

At the first step of the study, two phase heat transfer is modeled and analyzed inside the condenser tube by using an annular flow pattern with a liquid film at the tube wall and a turbulent vapor core. The momentum balance at the liquid and steam interface is established on the correlative interfacial shear stress expressions. The liquid phase heat transfer is modeled as heat conduction across a falling film. Surface temperature profile of the tube wall ($T_i(z)$) is used as a boundary condition. This developed model is compared to various experimental data from the point of view of the vapor Reynolds number, the condensate liquid film thickness and the condensation heat transfer coefficient. The agreement between the calculated and experimental results is quite satisfactory.

At the second step of the study, the cooling water flow and the heat transfer mechanism is modeled at the outside of the condenser tube. Inside the annular passages, the velocity and temperature distributions for the turbulent water flow are solved with a given variable heat flux ($q''(z)$) from the outer surface of the condenser tube as boundary condition while water is flowing inside

the annular passage. This model is compared with the experimental results in the literature. The analytical model predicts the general trend of the experimental data reasonably well.

At the final step, these two separate problems are combined by an energy balance and by the conduction equation for the condenser tube wall. They are coupled via temperature and heat flux predictions at the inner and outer surfaces of the condenser tube wall respectively. In order to solve this identified conjugate problem involving condensation-conduction-convection phenomena, a computer code named ZEC is developed in Fortran-90 language. The results of code ZEC and the available experimental data are compared. The results of ZEC are found to be in reasonable agreement with the experimental data over a wide range of conditions.

As an important outcome of this study, the effect of some parameters such as inlet pressure and mass flow rate of vapor, inlet temperature and mass flow rate of the coolant on the condensation process are analyzed. The parametric analysis show that the boundary conditions at the outside of the condenser tube such as coolant inlet temperature and mass flow rate affect the condensation process and might be taken into account if any meaningful comparisons between the experimental works, correlations and analytical studies on condensation are to be made. As a result of this study, it reveals that these parameters directly govern the condensation heat transfer processes and this mutual dependency might be coupled by means of a conjugate model implemented in code ZEC.

Although specifically, this work is aimed to predict the steam condensation process in the passive cooling systems of nuclear reactors during the LOCA, it is also applicable in other industrial areas, where in-tube condensation is employed such as distillation, evaporation etc. processes. Therefore, this developed code, ZEC, may be used for the preliminary design of in-tube condensers and for the performance evaluation of such condensers.

8.2 Recommendations for future work

During the condensation process, in case of the operational mode of the passive containment cooling systems of AP1000 reactors and ice condenser of SBWR, the steam contains some amount of non-condensable gasses such as air. The existing experimental studies in the literature show that the presence of non-condensable gas in the vapor can greatly reduce the performance of condensers even though it contains very small amount of non-condensable gas. Therefore, a condensation model taking the presence of non-condensable gas into account can be developed and this model can be incorporated with the computer code ZEC.

The ice condenser of SBWR is located in a liquid water pool. Hence, the performance of the condensation process inside the ice condenser tubes is directly influenced by the natural circulation mode in the pool. But, the present computer code, ZEC does not contain natural convection model at the jacket side (outside of the condenser tube). For this purpose, a natural circulation model may be added into ZEC with some modifications.

REFERENCES

- Abdelmeguid A.M., Spalding D.B., (1979), “Turbulent flow and heat transfer in pipes with buoyancy effects”, J. Fluid Mech., Vol. 94, pp. 383-400
- Arici M.E., Aydın O., (2009), “Conjugate heat transfer in thermally developing laminar flow with viscous dissipation effects”, Heat Mass Transfer, Vol. 45, pp. 1199–1203
- Assael M.J., Gialou K., Kakosimos K., Metaxa I., (2004), “Thermal Conductivity of Reference Solid Materials”, International Journal of Thermophysics, Vol. 25, No 2, pp. 397-408
- Azous I., Shirazi S.A., Pilehvari A., Azar J.J., (1993), “Numerical simulation of turbulent flow in concentric and eccentric annuli”, AIAA Paper 93-3106
- Barford N.C., (1985), “Experimental measurements: Precision, error and truth”, Second edition, John Wiley and Sons, New York, 1985
- Barletta A., Schio E.R., Comini G., D’Agaro P., (2008), “Conjugate forced convection heat transfer in a plane channel: Longitudinally periodic regime”, International Journal of Thermal Sciences, Vol. 47, pp. 43-51
- Bautista O., Mendez F, (2006), “Internal heat generation in a discrete heat source: Conjugate heat transfer analysis”, Applied Thermal Engineering, Vol. 26, pp. 2201–2208

- Bellinghausen R., Renz U., (1992), “Heat transfer and film thickness during condensation of steam flowing at high velocity in a vertical pipe”, *International Journal of Heat and Mass Transfer*, Vol. 35, pp.683–689
- Bilgen E., (2009), “Conjugate heat transfer by conduction and natural convection on a heated vertical wall”, *Applied Thermal Engineering*, Vol. 29, pp. 334–339
- Blangetti F., Krebs R., Schlunder E.U, (1982), “Condensation in vertical tubes; experimental results and modeling”, *Chemical Engineering Fundamentals*, Vol. 1, pp. 20–63
- Ball H.D., Azer N.Z., (1972), “Experimental investigation of Eddy diffusivities of air in turbulent annular flow”, *Proc. 1972 Heat Transfer and Fluid Mechanics Institute*, pp. 19-38
- Brouwers H.J.H., (1989), “Film condensation on non-isothermal vertical plates”, *International Journal of Heat and Mass Transfer*, Vol. 32, pp. 655-663
- Carpenter F.G., Colburn A.P., Schoenborn E.M., Wurster A., (1946), “Heat transfer and friction of water in an annular space”, *Trans. Am. Inst. Chem. Eng.*, Vol. 41, pp. 165–187
- Carpenter F.S, Colburn A.P., (1951), “The effect of vapour velocity on condensation inside tubes”, In: *Proc Gen Discussion of Heat Transfer*, Inst Mech Engrs and Am Soc Mech Engrs, pp. 20–26
- Char M.I., Lin J.D., (2001), “Conjugate film condensation and natural convection between two porous media separated by a vertical plate”, *Acta Mechanica*, Vol. 148, pp.1-15

- Chen S.L., Ke M.T., (1993), “Forced convective film condensation inside vertical tubes”, *International Journal of Multiphase Flow*, Vol. 19, pp.1045-1060
- Chen C., Wu L., Yang Y., (2005), “Estimation of unknown outer-wall heat flux in turbulent circular pipe flow with conduction in the pipe wall”, *International Journal of Heat and Mass Transfer*, Vol. 48, pp. 3971–3981
- Cheney W., Kincaid D., (1999), “Numerical Mathematics and Computing”, 4th ed., Brooks-Cole Publishing Co., Pacific Grove
- Churchill S.W., Chan C., (1995), “Turbulent flow in channels in terms of local turbulent shear and normal stresses”, *AIChE J.*, Vol. 41 (12), pp 2513–2521
- Churchill S.W., (1997), “New wine in new bottles: unexpected findings in heat transfer. Part II. A critical examination of turbulent flow and heat transfer in circular annuli”, *Thermal Sci. Engng.*, Vol. 5 (3), pp. 1–12
- Cess RD., (1960), “Laminar film condensation on a flat plate in the absence of a body force”, *Z Angew Math Phys*, Vol.11, pp. 426–433
- Chiu W.K.S., Richards C.J., Jaluria Y., (2001), “Experimental and numerical study of conjugate heat transfer in a horizontal channel heated from below”, *ASME J. Heat Transfer* Vol.123, pp. 688–697
- Chou G., Chen J., (1997), “Linear stability study of waviness effect on film condensation with non uniform surface tension”, *International Journal of Heat and Mass Transfer* Vol. 40, pp.2477–2482
- Collier J.G., Thome J.R., 2001, “Convective Boiling and Condensation”, 3rd Edition, Oxford University Press, Oxford

- Cotton M.A., Jackson J.D., (1990), “Vertical tube air flows in the turbulent mixed convection regime calculated using a k - ϵ model”, International Journal of Heat and Mass Transfer, Vol. 33, pp. 275-286
- Dobran F., Thorsen R.S., (1979), “Forced flow laminar filmwise condensation of a pure saturated vapor in a vertical pipe”, International Journal of Heat and Mass Transfer, Vol. 23, pp. 161-177
- Dobson M.K., Chato J.C., (1998), “Condensation in smooth tubes”, Trans ASME J Heat Transfer, Vol. 120, pp.193–213
- Dufinescz M., Marcus P., (1938), “Heat transfer coefficients in annular spaces”, M.S. Thesis, Carnegie Institute of Technology, Pittsburgh, PA
- EasyMED -project, (2007), www.easymed-eu.com
- Fujii T., Uehara H., (1972), “Laminar filmwise condensation on a vertical surface”, International Journal of Heat and Mass Transfer, Vol.15, pp.217–233
- Garg V.K., Velusamy K., (1986), “Heat transfer characteristics for a plate fin”, ASME J. Heat Transfer, Vol. 108, pp. 224–226
- Goodykoontz J.H, Dorsch R.G, (1966), “Local heat transfer coefficients for condensation of steam in vertical downflow within a 5/8 inch-diameter tube”, NASA-TN-D-3326
- Goodykoontz J.H, Dorsch R.G, (1967), “Local heat transfer coefficients and static pressures for condensation of high velocity steam with in a tube”, NASA-TN-D-3953

- Hanjalic K., (1974), "Prediction of turbulent flow in annular ducts with differential transport model of turbulence", *Warme Stoffübertragung*, Vol. 7, pp. 72-78
- Hasan A., Roy R.P., Kalra S.P., (1992), "Velocity and temperature fields in turbulent liquid flow through a vertical concentric annular channel", *International Journal of Heat and Mass Transfer*, Vol. 35, pp. 1455-1467
- Heikal M.R.F., Walklate P.J., Hatton A.P., (1976), "The effect of free stream turbulence level on the flow and heat transfer in the entrance region of an annulus", *International Journal of Heat and Mass Transfer*, Vol. 20, pp. 763-771
- Honda H., Fujii T., (1984), "Condensation of flowing vapor on a horizontal tube—numerical analysis as a conjugate problem", *Trans ASME J Heat Transfer*; Vol.106, pp. 841–848
- Huang S., Chun C.H., (2003), "A numerical study of turbulent flow and conjugate heat transfer in concentric annuli with moving inner rod", *International Journal of Heat and Mass Transfer*, Vol. 46, pp. 3707–3716
- Hung C., Chen C., Tsai J., (1996), "Weakly nonlinear stability analysis of condensate film flow down a vertical cylinder", *International Journal of Heat and Mass Transfer*, Vol. 39, pp. 2821–2829
- IAEA-TECDOC-1149, (1998), "Experimental Test and Qualification of Analytical Methods to Address Thermal-hydraulic Phenomena in Advanced Water Cooled Reactors", IAEA, Vienna, Austria

- IAEA-TECDOC-872, (2001), “Progress in Design, Research and Development and Testing of Safety Systems for Advanced Water Cooled Reactors” , IAEA, Vienna, Austria
- IAPWS, (1998), “Revised Release on the IAPS Formulation 1985 for Ordinary Water substance”, International Association for the Properties of Water and Steam”, London, 23
- Incropera F.P., Dewitt D.P., (1985), “Fundamentals of Heat and Mass Transfer”, John Wiley & Sons, New York
- Jacobs H.R., (1966), “An integral treatment of combined body force and forced convection in laminar film condensation”, International Journal of Heat and Mass Transfer Vol. 9, pp.637–648
- Jahangeer S., Ramis M.K, Jilani G., (2007), “Conjugate heat transfer analysis of a heat generating vertical plate”, International Journal of Heat and Mass Transfer, Vol. 50, pp. 85–93
- Jayanti S., Hewitt G.F., (1997), “Hydrodynamics and heat transfer of wavy thin film flow”, International Journal of Heat and Mass Transfer, Vol.40, pp. 179–190
- Jilani G., Jayaraj S., Ahmad M.A., (2002) “Conjugate forced convection-conduction heat transfer analysis of a heat generating vertical cylinder”, International Journal of Heat and Mass Transfer, Vol. 45, pp. 331–341
- Jischa M., Rieke H.B., (1979), “About the prediction of turbulent Prandtl and Schmidt numbers from modified transport equations”, International Journal of Heat and Mass Transfer, Vol. 22, pp. 1547–1555

- Juncu Gh., (2004), “Unsteady conjugate heat/mass transfer from a circular cylinder in laminar crossflow at low Reynolds numbers”, *International Journal of Heat and Mass Transfer*, Vol. 47, pp. 2469–2480
- Kaneda M., Yu B., Ozoe H., Churchill S.W., (2003), “The Characteristics of Turbulent Flow and Convection in Concentric Circular Annuli. Part I: Flow”, *Int. J. Heat Mass Transfer*, Vol. 46 (26), pp. 5045–5057
- Kang S., Patil B., Zarate J.A., Roy R.P., (2001), “Isothermal and heated turbulent upflow in a vertical annular channel - Part I. Experimental measurements”, *Int. J. Heat Mass Transfer*, Vol. 44, pp 1171-1184
- Kanna P.R., Das M.K., (2006), “Conjugate heat transfer study of backward-facing step flow – A benchmark problem”, *International Journal of Heat and Mass Transfer*, Vol. 49, pp. 3929–3941
- Karvinen R., (1978), “Some new results for conjugated heat transfer in a flat plate”, *International Journal of Heat and Mass Transfer*, Vol. 21, pp. 1261–1264
- Kays W.M., Leung E.Y., (1963), “Heat transfer in annular passages; hydrodynamically developed turbulent flow with arbitrarily prescribed heat flux”, *International Journal of Heat and Mass Transfer*, Vol. 6, pp.537-557
- Kays W.M., Leung E.Y., (1963), “Heat transfer in annular passages- hydrodynamically developed turbulent flow with arbitrarily prescribed heat flux”, NASA-NSG-52-60
- Kays W.M., Crawford M.E., (1993), “Convective Heat and Mass Transfer”, 3rd ed., McGraw-Hill, New York

- Kjellstrom B, Hedberg S., (1966), "On shear stress distributions for flow in smooth or partially rough annuli", Aktiebolaget Atomenergi, Report AE-243, Stockholm
- Kuhn S.Z., Schrock V.E., Peterson P.F., (1994), "Final Report on UCB Single Tube Condensation Studies", Department of Nuclear Engineering, UCB-NE-4201
- Kuhn S.Z., Schrock V.E., Peterson P.F., (1997), "An investigation of condensation from steam–gas mixtures flowing downward inside a vertical tube", Nuclear Engineering and Design 177, pp 53–69
- Kuzay T.M., (1973), "Turbulent heat and momentum transfer studies in an annulus with rotating inner cylinder", Ph.D. Thesis, University of Minnesota, Minneapolis
- Kuzay T.M., Scott C.J., (1977), "Turbulent heat transfer studies in annulus with inner cylinder rotation", ASME J. Heat Transfer Vol. 99, pp. 12-19
- Lawn C.J., Elliott C.J., (1972), "Fully developed turbulent flow through concentric annuli", Journal of Mech. Engng. Sci., Vol. 14 (3), pp. 195–204
- Leung E.Y., Kays W.M., Reynolds W.C., (1962), "Heat transfer with turbulent flow in concentric and eccentric annuli with constant and variable heat flux", Rept. AHT-4, Thermal Sciences Division, Department of Mechanical Engineering, Stanford University, Palo Alto, CA
- Lin J. F., Chiu S. Y., Ho C. J., (2008), "Conjugate heat transfer simulation of a rectangular natural circulation loop", Heat Mass Transfer, Vol. 45, pp.167–175

- Louahlia H., Panday P.K., (1996), “Transfert thermique pour la condensation du R123, du R134a et de leurs melanges en ecoulement force entre deux plaques planes horizontales: etude numerique”, Rev. Gen. Therm., Vol. 35, pp. 615–624
- Lorenz F.R., (1937), “Über turbulente stromung durch rohre mit kreisformigen querschnitt”, Mitt. Inst. Stromungs., T.H. Karlsruhe, Vol 2, pp. 26–66.
- Luikov A.V., Aleksashenko V.A., (1971), “Analytical methods of solution of conjugated problems in convective heat transfer”, International Journal of Heat and Mass Transfer, Vol. 14, pp. 1047–1056
- Luikov A.V., (1974), “Conjugate convective heat transfer problems”, International Journal of Heat and Mass Transfer, Vol.17, pp. 257–265
- Malik M.J., Pletcher R.H., (1981), “A study of some turbulence models for flow and heat transfer in ducts of annular cross section”, ASME J. Heat Transfer, Vol. 103, pp 146-152
- Mathews R.N., Balaji C., (2006), “Numerical simulation of conjugate, turbulent mixed convection heat transfer in a vertical channel with discrete heat sources”, International Communications in Heat and Mass Transfer, Vol. 33, pp. 908–916
- Mc.Adams W.H., (1974), “Heat Transmission”, McGraw Hill, New York
- McMillan E.L., Larson R.E., (1946), “Annular heat transfer coefficients for turbulent flow”, Trans. Am. Inst. Chem. Eng., Vol. 41, pp 177–202
- Mendez F., Trevino C., (1996), “Film condensation generated by a forced cooling fluid”, Journal of European Mechanics/Fluids, Vol. 15, pp. 217-240

- Mendez F., Trevino C., (1997), "Film condensation induced by a natural convective flow: steady-state analysis", *International Journal of Heat and Mass Transfer*, Vol. 40, pp. 1279-1289
- Mendez F., Lizardi J.J., Trevino C., (2000), "Laminar film condensation along a vertical fin", *International Journal of Heat and Mass Transfer*, Vol. 43, pp. 2859-2868
- Miller P., Byrnes J.J., Benforado D.M., (1955), "Heat transfer to water in an annulus", *AIChE J.*, Vol. 1 (4), pp 501–504
- Mobedi M., Sunden B., (2006), "Natural convection heat transfer from a thermal heat source located in a vertical plate fin", *International Communications in Heat and Mass Transfer*, Vol. 33, pp. 943–950
- Monrad C.C., Pelton J.F., (1942), "Heat transfer by convection in annular spaces", *Trans. Am. Inst. Chem. Eng.*, Vol. 38, pp 593–611
- Munoz-Cobo J.L., Herranz L, Sancho J., Tkachenko I., Verdu G., (1996), "Turbulent vapor condensation with non-condensable gases in vertical tubes", *International Journal of Heat and Mass Transfer*, Vol. 39, pp 3249–3260
- Narain A., Yu G., Liu Q., (1997), "Interfacial shear models and their required asymptotic form for annular/stratified film condensation flows in inclined channels and vertical pipe", *International Journal of Heat and Mass Transfer*, Vol. 40, pp.3559–3575

NECS 0525/01, (1971), “ORTHIS, ORTHAT – Two Computer Programs for Solving Two-dimensional Steady-state and Transient Heat Conduction Problems”, OECD/NEA Data bank

Nusselt, W., (1916), “Die Oberflächenkondensation des Wasserdampfes”, Zeit. Ver. Deut. Ing., Vol. 60, pp. 541-545, 569-575

Oh S., (2004), “Experimental and analytical study of the effects of non-condensable gas in a passive condenser system”, Ph.D. Thesis, Purdue University

Oh S., Revankar S.T., (2005a), “Complete condensation in a vertical tube passive condenser”, International Communications in Heat and Mass Transfer, Vol. 32, pp. 593–602

Oh S., Revankar S.T., (2005b), “Analysis of the complete condensation in a vertical tube passive condenser”, International Communications in Heat and Mass Transfer, Vol. 32, pp. 716–727

Oh S., Revankar S.T., (2005c), “Effect of non-condensable gas in a vertical tube condenser”, Nuclear Engineering and Design, Vol. 235, pp. 1699–1712

Oh S., Revankar S.T., (2006), “Experimental and theoretical investigation of film condensation with non-condensable gas”, International Journal of Heat and Mass Transfer, Vol. 49, pp. 2523–2534

Panday P.K., (2003), “Two-dimensional turbulent film condensation of vapors flowing inside a vertical tube and between parallel plates: a numerical approach”, International Journal of Refrigeration, Vol. 26, pp. 492–503

- Patankar S.V., (1980), "Numerical Heat Transfer and Fluid Flow", Hemisphere Publishing Corp., New York
- Patankar S.V., Sparrow E.M., (1979), "Condensation on an extended surface", Journal of Heat Transfer, Vol. 101, pp. 434-449
- Perelman T.L., (1961), "On conjugated problems of heat transfer", International Journal of Heat and Mass Transfer, Vol. 3, pp. 293-303
- Pietrzyk J.R., Crawford M.E., (1985), "A numerical investigation of turbulent mixed convection in vertical annular channels", ASME HTD, Vol. 42, pp. 149-158
- Petukhov B.S., Roizen L.I., (1963), "An experimental investigation of heat transfer in a turbulent flow of gas in tubes of annular section", High Temp., Vol. 1 (3), pp. 373-380
- Raach H., Mitrovic J., (2005), "Seawater falling film evaporation on vertical plates with turbulence wires", Desalination, Vol. 183, pp. 307-316
- Raach H., Mitrovic J., (2007), "Simulation of heat and mass transfer in a multi-effect distillation plant for seawater desalination", Desalination, Vol. 204, pp. 416-422
- Ramis M.K., Jilani G., Jahangeer S., (2008), "Conjugate conduction-forced convection heat transfer analysis of a rectangular nuclear fuel element with non-uniform volumetric energy generation", International Journal of Heat and Mass Transfer, Vol. 51, pp. 517-525
- Ramis M.K., Jilani G., (2010), "Heat and fluid flow characteristics of liquid sodium flowing past a nuclear fuel element with non-uniform energy

- generation”, International Journal of Heat and Mass Transfer, Vol. 53, pp. 1682–1690
- Rohsenow WM., (1956), “Heat transfer and temperature distribution in laminar film condensation”, Trans ASME, Vol. 78, pp. 1645–1648
- Rehme K., (1974), “Turbulent flow in smooth concentric annuli with small radius ratios”, J. Fluid Mech., Vol. 64, pp. 263–287
- Roberts A., Barrow H., (1968), “Turbulent heat transfer to air in the vicinity of the entry to an internally heated annulus”, Proc. Inst. Mech. Eng., Vol. 182 (3H), pp 268–276
- Quarmby A., (1967), “Some measurements of turbulent heat transfer in the thermal entrance region of concentric annuli”, Int. J. Heat Mass Transfer, Vol. 10, pp 267–276
- Quarmby A., (1968), “An analysis of turbulent flow in concentric annuli”, Appl. Sci. Res., Vol. 19, pp 250–271
- Sarma P.K., Chary S.P., Dharma R.V., (1988) “Condensation on a vertical plate fin of variable thickness”, International Journal of Heat and Mass Transfer, Vol. 31, pp. 1941- 1944
- Sato T., Kojima Y., (2007), “Variations of a passive safety containment for a BWR with active and passive safety systems”, Nuclear Engineering and Design, Vol. 237, pp. 74–86
- Seul K.W, Bang Y.S., Kim H.J., (1999), “Plant Behavior Following Loss-of-Residual Heat Removal Event under a Shutdown Condition”, Nuclear Technology, Vol. 126, pp. 265-278

- Shekriladze I.J., Gomelauro V.I., (1966), "Theoretical study of laminar film condensation of flowing vapor", International Journal of Heat and Mass Transfer., Vol.9, pp.581–589
- Silver R.S., (1964), "An approach to a general theory of surface condensers", Proc. Inst. Mech. Engrs, 178, pp 339-376
- Spalding D.P., (1963), "Convective Mass Transfer", McGraw-Hill, New York
- Sparrow E.M., Gregg J.L., (1959), "A boundary layer treatment of film condensation", Trans ASME J Heat Transfer, Vol. 81, pp. 13–18
- Sparrow E.M., Chyu M.K., (1982), "Conjugate forced convection-conduction analysis of heat transfer in plate fin", International Journal of Heat and Mass Transfer, Vol. 104, pp. 204–206
- Srzic V., Soliman H.M., Ormiston S.J., (1999), "Analysis of laminar mixed convection condensation on isothermal plates using the full boundary layer equations: mixtures of a vapor and a lighter gas", International Journal of Heat and Mass Transfer, Vol.42, pp.685–695
- Ueda T., Akiyoshi K., Matsui T., Inoue M., (1972), "Heat transfer and pressure drop for flow condensation inside a vertical tube", Bull JSME, Vol. 15, pp.1267–1277
- Unsal M., (1988a), "Non linear stability of forced vapour flow condensation", International Journal of Heat and Mass Transfer; Vol.31, pp.1619–1626
- Unsal M., (1988b), "Effect of waves on Nusselt condensation", International Journal of Heat and Mass Transfer, Vol. 31, pp.1944–1947

- Tanrikut A., (1998), “In-Tube Condensation in the Presence of Air”, Ph.D. Thesis, Mechanical Engineering Department, Middle East Technical University, Ankara
- Tanrikut A., Yeşin O, (2005), “Experimental Research on In-Tube Condensation under Steady State and Transient Conditions”, *Nuclear Technology*, Vol. 149, p. 88
- Trefethen L.M., (1951), “Liquid Metal Heat Transfer in Circular Tubes and Annuli in General Discussion on Heat Transfer”, Inst. Mech. Eng. and ASME, pp. 436–438
- Trevino C., Mendez F., (1996), “Transient conjugate condensation process on a vertical plate with finite thermal inertia”, *International Journal of Heat and Mass Transfer*, Vol. 39, pp. 2221-2230
- Velidandla V., Putta S., Roy R.P., (1996), “Turbulent velocity field in isothermal and heated liquid flow through a vertical annular channel”, *International Journal of Heat and Mass Transfer*, Vol. 39, pp. 3333-3346
- Vilemas J., Cesna B., Zukauskas A., Karni J., (1987), “Heat Transfer in Gas-cooled Annular Channels”, Hemisphere Publ. Corp., Washington, DC
- Vynnycky M., Kimura S., Kanev K., Pop I., (1998), “Forced convection heat transfer from a flat plate: the conjugate problem”, *International Journal of Heat and Mass Transfer*, Vol. 41, pp. 45–59
- Wallis G.B., (1969), “One-Dimensional Two Phase Flow”, McGraw-Hill, New York

- Wilkins J.E., (1980), "Condensation on an extended surface", *Journal of Heat Transfer*, Vol. 102, pp. 186-187
- Wilson N.W., Medwell J.O., (1968), "An analysis of heat transfer for fully developed turbulent flow in concentric annuli", *ASME J. Heat Transfer*, Vol. 90C, pp. 43–50
- Yu W.S., Lin H.T., Hwang T.Y., (1991), "Conjugate heat transfer of conduction and forced convection along wedges and a rotating cone", *International Journal of Heat and Mass Transfer*, Vol. 34, pp. 2497–2507
- Yu B., Ozoe H., Churchill S.W., (2001), "The characteristics of fully developed turbulent convection in a round tube", *Chem. Eng. Sci.*, Vol. 56, pp. 1781–1800
- Yu B., Kawaguchi Y., Kaneda M., Ozoe H., Churchill S.W., (2005a), "The characteristics of turbulent flow and convection in concentric circular annuli, Part II: Uniform heating on the inner surface", *Int. J. Heat Mass Transfer*, Vol. 48, pp. 621–634
- Yu B., Kawaguchi Y., Kaneda M., Ozoe H., Churchill S.W., (2005b), "The characteristics of turbulent flow and convection in concentric circular annuli, Part III: Alternative thermal boundary conditions", *Int. J. Heat Mass Transfer*, Vol 48, pp. 635–946
- Yu B., Kawaguchi Y., Kaneda M., Ozoe H., Churchill S.W., (2005c), "The characteristics of turbulent flow and convection in concentric circular annuli, Part IV: Generalizations", *Int. J. Heat Mass Transfer*, Vol. 48, pp.3057–3072

Zagarola M.V., (1996), “Mean-Flow Scaling of Turbulent Pipe Flow”, Ph.D.
Thesis, Princeton University, Princeton, NJ

APPENDIX A

OH-MODEL FOR IN-TUBE CONDENSATION

Liquid Film Model

For the liquid film, the force balance in the control volume depicted in Figure A.1 can be described in wall coordinate system as follows;

$$\tau_l P_l dz + A_1 p + \rho_L g [A_2 (z + dz) - A_1 z] = \tau_L P_L dz + A_2 \left[p + \left(\frac{\partial p}{\partial z} \right) dz \right] \quad (\text{A.1})$$

where

$$P_l = P_L = t \text{ (depth of the film thickness)}$$

$$A_1 = A_2 = A = (\delta - y)t$$

Inserting above expressions into Eq. (A.1);

$$\begin{aligned} \tau_l t dz + (\delta - y)t p + \rho_L g (\delta - y)t dz \\ = \tau_L t dz + (\delta - y)t p + (\delta - y)t \left[\left(\frac{\partial p}{\partial z} \right) dz \right] \end{aligned} \quad (\text{A.2})$$

Eq. (A.2) becomes:

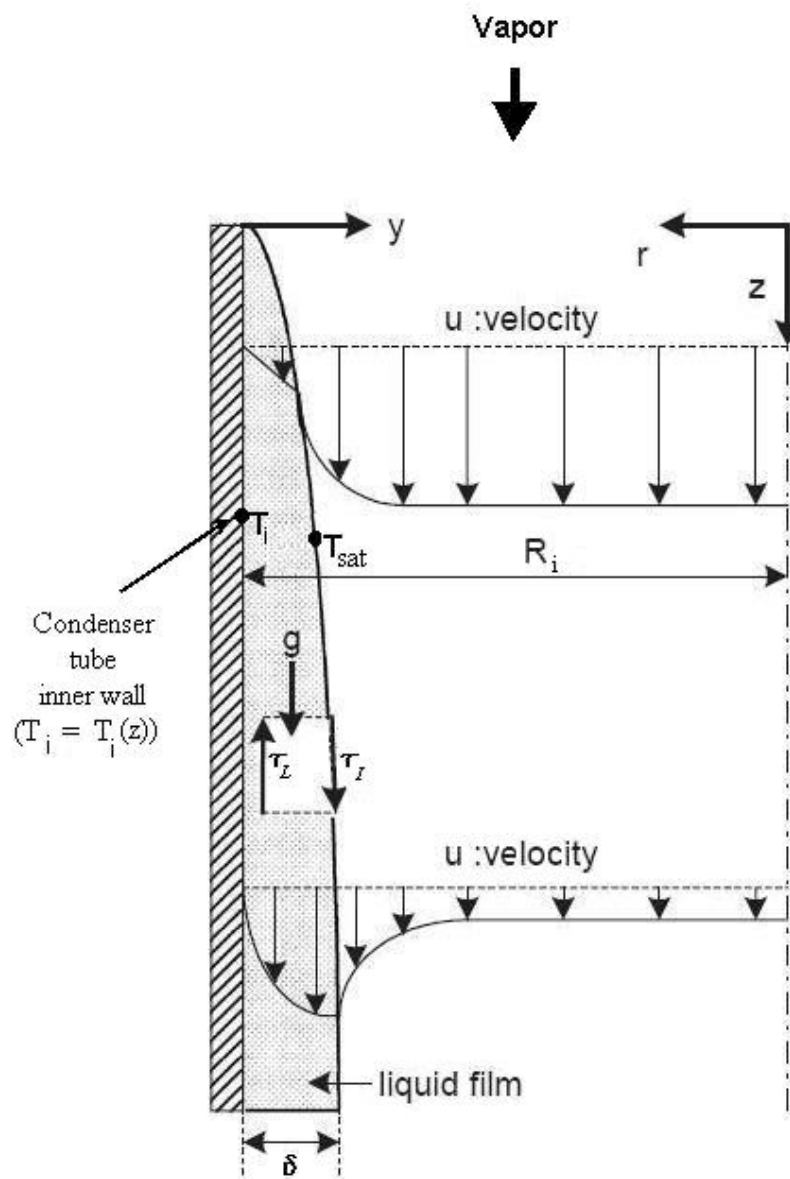


Figure A.1 Physical model of the in-tube condensation used by OH-model

$$\tau_I + (\delta - y) \rho_L g = \tau_L + (\delta - y) \left(\frac{\partial p}{\partial z} \right) \quad (\text{A.3})$$

$$\tau_L(y) = \left[\rho_L g - \left(\frac{\partial p}{\partial z} \right) \right] (\delta - y) + \tau_I \quad (\text{A.4})$$

If the pressure gradient is assumed due to the vapor head, then we can write it in terms of the vapor density as in Nusselt (1916) solution;

$$\left(\frac{dp}{dz} \right) = \rho_v g \quad (\text{A.5})$$

Defining the shear stress in the liquid layer as;

$$\tau_L(y) = \mu_L \left(\frac{du_L}{dr} \right) \quad (\text{A.6})$$

Inserting Eq. (A.5) and (A.6) into (A.4);

$$\left(\frac{du_L}{dr} \right) = \frac{[r^2 - (R - \delta)^2]}{2r} \frac{(\rho_L - \rho_v)g}{\mu_L} + \frac{(R - \delta)}{r} \frac{\tau_{IL}}{\mu_L} \quad (\text{A.7})$$

Hence for laminar film, the velocity profile in the liquid film can be obtained from the integration of Eq. (A.7);

$$u_L(r) = \frac{(\rho_L - \rho_v)g}{\mu_L} \left[\delta y - \frac{y^2}{2} \right] - \frac{\tau_I}{\mu_L} y \quad (\text{A.8})$$

The first term in the right hand side of above equation is the parabolic velocity distribution, as in case of Nusselt analysis with no interfacial shear. The second term is the linear velocity distribution due to the interfacial shear. For high

interfacial shear, the second term is dominant. So the velocity distribution is almost linear. The liquid flow rate can be calculated using the velocity profile;

$$\dot{m}_L = 2\pi \int_0^{\delta} \rho_L u_L(y)(R_i - y) dy \quad (\text{A.9})$$

From Eq. (A.8) and (A.9), the mass flow rate per unit width in liquid film can be expressed as follows:

$$\Gamma = \frac{\dot{m}_L}{2\pi R_i} = \frac{(\rho_L - \rho_v)}{\nu_L} g \left[\frac{\delta^3}{3} - \frac{5\delta^4}{24R_i} \right] + \frac{\tau_I}{\nu_L} \left[\frac{\delta^2}{2} - \frac{\delta^3}{3R_i} \right] \quad (\text{A.10})$$

In Eq. (A.10), it is assumed that $\frac{\delta}{R_i} \ll 1$. Then it becomes;

$$\Gamma = \frac{(\rho_L - \rho_v)g}{\nu_L} \delta^3 + \frac{\tau_I}{2\nu_L} \delta^2 \quad (\text{A.11})$$

Eq. (A.11) can be simplified by using of dimensionless parameters as;

$$\text{Re}_L = \left(\frac{4}{3} (\delta^*)^3 + 2\tau_I^* (\delta^*)^2 \right) \quad (\text{A.12})$$

where the dimensionless parameters are;

$$\text{Film Reynolds number : } \text{Re}_L \equiv \frac{4\Gamma}{\mu_L}$$

$$\text{Dimensionless film thickness : } \delta^* \equiv \frac{\delta}{L^*}$$

Characteristic length scale : $L^* \equiv \left(\frac{\mu_L^2}{\rho_L(\rho_L - \rho)g} \right)^{1/3}$

Dimensionless shear stress : $\tau_I^* \equiv \frac{\tau_I}{(\rho_L - \rho).g.L^*}$

By solving Eq. (A.12), film thickness can be calculated.

Energy Balance

The heat transfer rate at the vapor region and the film region is balanced at the interface as;

$$\left(\frac{d\Gamma}{dz} \right) h_{fg} = h_L (T_{SAT} - T_i) \quad (A.13)$$

For laminar film, the temperature distribution in the film region at wall coordinates of the Cartesian system is assumed to be linear. Therefore film heat transfer coefficient can be expressed as;

$$h_L = \frac{k_L}{\delta(z)} \quad (A.14)$$

Film Nusselt number is defined as follow;

$$Nu_L \equiv \frac{h_L.L^*}{k_L} \quad (A.15)$$

From Eq. (A.14) and (A.15), film Nusselt number for laminar film can written as;

$$Nu_L \equiv \frac{L^*}{\delta} = \frac{1}{\delta^*} \quad (\text{A.16})$$

Vapor Interfacial Shear

For the above analysis, the interfacial shear is an unknown parameter, which will be used at the film–vapor interface. One of the methods to calculate interfacial shear is to use appropriate correlation. The interfacial shear is correlated with interfacial friction factor defined as

$$f = \frac{\tau_i}{\rho_v (\bar{u}_v - \bar{u}_L)^2 / 2} \quad (\text{A.17})$$

Since the condensation can be regarded as a kind of wall suction, the results of the transpiration effect should be taken into account in the condensation problems. The effect of transpiration was formulated by the ratio of the dimensionless transport quantity with transpiration to one without transpiration as a function of blowing parameter. For the momentum transfer, the friction factor with the transpiration effect can be expressed as follows:

$$\frac{f}{f_0} = \frac{b_f}{\exp(b_f) - 1} \quad (\text{A.18})$$

Here, subscript 0 represents the quantity without transpiration and momentum transfer blowing parameter, b_f is defined as;

$$b_f = \frac{\left(\frac{d\Gamma}{dz} \right)}{\rho_v \bar{u}_v (f/2)_0} \quad (\text{A.19})$$

Here, the blowing parameter is negative for the suction. For turbulent friction factor without transpiration, the Blasius equation is used,

$$f_0 = 0.079 \text{ Re}_d^{-0.25} \quad (\text{A.20})$$

For laminar friction factor, the analytic solution is used,

$$f_0 = \frac{16}{\text{Re}_d} \quad (\text{A.21})$$

Concluding Comments

Although OH-model gives satisfactory (but not adequate) results compared to the experimental results, it contains some certain deficiencies which can be underlined as follows:

- Force balance is established for the cartesian geometry, disregarding the area differences in the radial direction for the shear forces,
- Energy balance and local heat transfer coefficient is also constructed in cartesian geometry assuming that the temperature profile in the liquid film is linear.
- Pressure gradient is assumed due to the only vapor head as in the solution of stagnant vapor. But, this is not a good approach if the vapor flow is highly turbulent and vapor interfacial shear is dominant.
- $\frac{\delta}{R_i}$ terms in velocity profile are neglected, assuming that $\frac{\delta}{R_i} \ll 1$.
- Shear stress from the liquid to vapor is assumed to be equal to shear stress from the vapor to liquid ($\tau_{ll} = \tau_{lv} = \tau_l$).

APPENDIX B

NUMERICAL ACCURACY FOR IN-TUBE CONDENSATION MODEL

For the numerical accuracy of the in-tube condensation model, an illustrative example is considered. In this case, a condenser tube with a inner diameter of 33.5 mm. is chosen. The steam inlet conditions entering into the tube are defined as $Re_v = 93400$ and $p_v = 5.45$ bar, where corresponding saturation temperature of the vapor (T_{sat}) is 155.2 °C. The inner surface temperature of the condenser tube (T_i) is assumed to be uniform and equal to 140.0 °C. Taking these inlet and boundary conditions, local condensate mass flow rate per unit length (Γ), used as the comparison parameter in the numerical calculations, are plotted for 20, 30, 50 and 100 nodes in Figure B.1.

From Figure B.1, it can be seen that the solution of $\Gamma(z)$ varies with the number of nodes up to a value of 50. However, $\Gamma(z)$ does not change significantly upon 50 nodes. Therefore, the number of nodes for in-tube condensation model is chosen 50 for numerical accuracy.

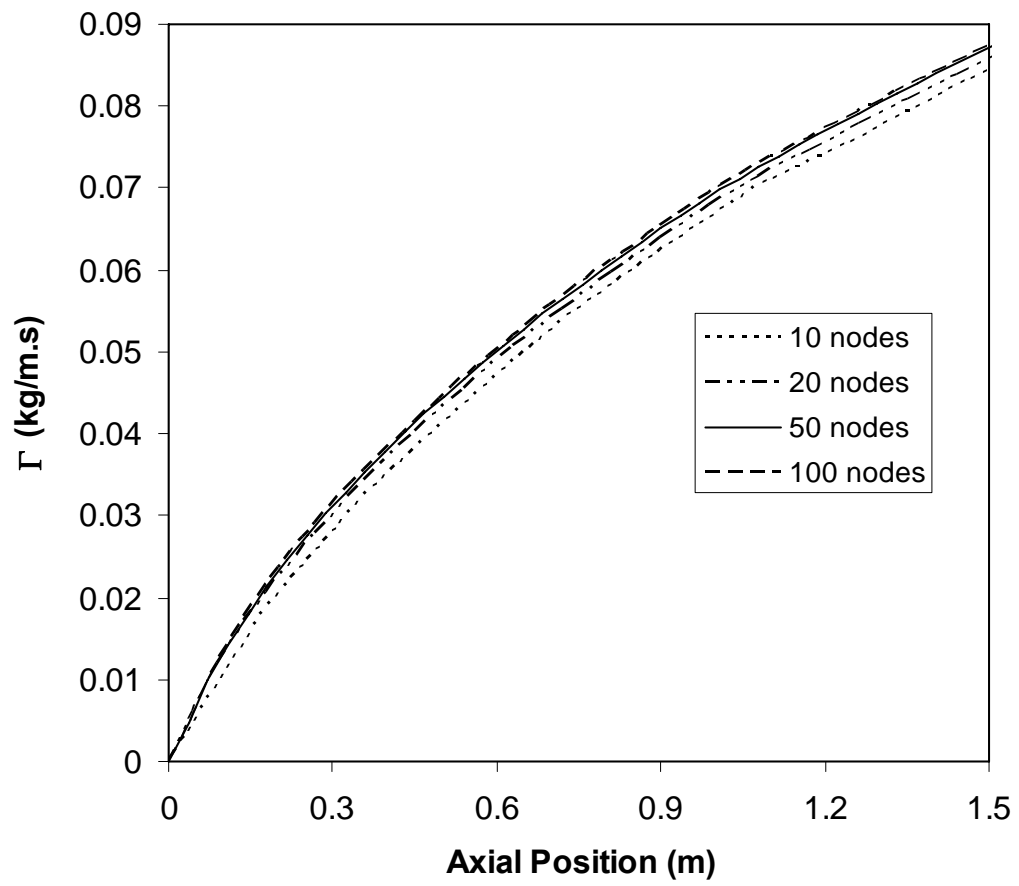


Figure B.1 P Calculated local Γ values for different number of nodes

APPENDIX C

THERMODYNAMIC PROPERTIES OF WATER

Thermodynamic properties of liquid water and saturated water vapor should be calculated accurately. Therefore, polynomial functions are generated by the author based on the reference data of IAPWS (1998) for the density, specific enthalpy, specific heat, latent heat of evaporation, viscosity and thermal conductivity of the liquid and vapor separately. The temperatures (T) and pressures (p) as the variables of polynomial functions are in °C and bar respectively. The functions can be given as follows:

LIQUID:

For $10\text{ }^{\circ}\text{C} < T < 160\text{ }^{\circ}\text{C}$ and $0.012282\text{ bar} < p < 6.1823\text{ bar}$

Density (kg/m³):

$$\begin{aligned}\rho_L = & (9.9983787916129\text{e}+02) + (5.8058967389981\text{e}-02)*T \\ & - (8.2565642525968\text{e}-03)*T^2 + (6.7539935426860\text{e}-05)*T^3 \\ & - (5.2668976816741\text{e}-07)*T^4 + (2.7971099514142\text{e}-09)*T^5 \\ & - (8.7577313496460\text{e}-12)*T^6 + (1.1865119914629\text{e}-14)*T^7\end{aligned}\tag{C.1}$$

Specific heat (kJ/kg.K):

$$\begin{aligned} c_{p,L} = & (4.2181343648751) - (3.0708559730143\text{e-}03)*T \\ & + (9.4186019724207\text{e-}05)*T^2 - (1.5238751829861\text{e-}06)*T^3 \\ & + (1.5295470564867\text{e-}08)*T^4 - (8.8692324825506\text{e-}11)*T^5 \\ & + (2.8162179783441\text{e-}13)*T^6 - (3.7611775384704\text{e-}16)*T^7 \end{aligned} \quad (\text{C.2})$$

Viscosity (Pa*s x10⁶):

For $10^\circ\text{C} < T < 97^\circ\text{C}$

$$\begin{aligned} \mu_L = & (1.7915554327740\text{e+}03) - (6.2163507473114\text{e+}01)*T \\ & + (1.6829344018615\text{e+}00)*T^2 - (3.8400144168028\text{e-}02)*T^3 \\ & + (7.1188983512218\text{e-}04)*T^4 - (1.0078431100307\text{e-}05)*T^5 \\ & + (1.0222306506924\text{e-}07)*T^6 - (6.8950998887318\text{e-}10)*T^7 \\ & + (2.7461798323833\text{e-}12)*T^8 - (4.8612593243955\text{e-}15)*T^9 \end{aligned} \quad (\text{C.3})$$

For $97^\circ\text{C} \leq T < 160^\circ\text{C}$

$$\begin{aligned} \mu_L = & (1.2764020925091\text{e+}03) - (2.3268599626198\text{e+}01)*T \\ & + (2.1549612399498\text{e-}01)*T^2 - (9.3377353595445\text{e-}04)*T^3 \\ & - (3.4111616102061\text{e-}07)*T^4 + (2.2498240643136\text{e-}08)*T^5 \\ & - (9.2681770547603\text{e-}11)*T^6 + (1.2823757849057\text{e-}13)*T^7 \end{aligned} \quad (\text{C.4})$$

Thermal conductivity (W /m.K):

$$\begin{aligned} k_L = & (5.6126785572601\text{e-}01) + (1.8416150716531\text{e-}03)*T \\ & + (6.2563532972956\text{e-}06)*T^2 - (3.3449666434981\text{e-}07)*T^3 \\ & + (3.3722807205271\text{e-}09)*T^4 - (1.7183110924796\text{e-}11)*T^5 \\ & + (4.5037880446942\text{e-}14)*T^6 - (4.8398822286715\text{e-}17)*T^7 \end{aligned} \quad (\text{C.5})$$

VAPOR:

For $97^\circ\text{C} < T < 160^\circ\text{C}$ and $0.9103 \text{ bar} < p < 6.1823 \text{ bar}$

Density (kg/m³):

$$\begin{aligned} \rho_{vap} = & (3.1988265967439) - (1.8664521411958\text{e-}01)*T \\ & + (4.6727995592512\text{e-}03)*T^2 - (6.4011191046976\text{e-}05)*T^3 \\ & + (5.2829106789094\text{e-}07)*T^4 - (2.5608235480252\text{e-}09)*T^5 \\ & + (6.9198504672038\text{e-}12)*T^6 - (7.9366040203236\text{e-}15)*T^7 \end{aligned} \quad (\text{C.6})$$

Specific heat (kJ/kg.K):

$$\begin{aligned} c_{p,vap} = & (8.5936439645380) - (3.7201763423003\text{e-}01)*T \\ & + (8.8370524502143\text{e-}03)*T^2 - (1.1551137194773\text{e-}04)*T^3 \\ & + (9.0149167963064\text{e-}07)*T^4 - (4.1904030885193\text{e-}09)*T^5 \\ & + (1.0763302143065\text{e-}11)*T^6 - (1.1794539489510\text{e-}14)*T^7 \end{aligned} \quad (\text{C.7})$$

Viscosity (Pa*s x10⁶):

$$\begin{aligned} \mu_{vap} = & (9.1559727427739) + (2.5703234961848\text{e-}02)*T \\ & + (8.3129421653614\text{e-}05)*T^2 - (3.3789071207916\text{e-}07)*T^3 \\ & + (4.9472169118131\text{e-}10)*T^4 \end{aligned} \quad (\text{C.8})$$

Thermal conductivity (W /m.K):

$$\begin{aligned} k_{vap} = & (4.3489484412211e-02) - (1.4373254247784e-03)*T \\ & + (3.6193305025181e-05)*T^2 - (4.8025505077748e-07)*T^3 \\ & + (3.8411016793502e-09)*T^4 - (1.8347942914227e-11)*T^5 \\ & + (4.8506805301235e-14)*T^6 - (5.4762823430520e-17)*T^7 \end{aligned} \quad (C.9)$$

Latent heat of vaporization (kJ/kg):

$$\begin{aligned} h_{fg} = & (2.2034116342447e+03) + (1.4109197368505e+01)*T \\ & - (3.8625984171934e-01)*T^2 + (4.9679482070573e-03)*T^3 \\ & - (3.7996504881038e-05)*T^4 + (1.7181588198110e-07)*T^5 \\ & - (4.2659788319882e-10)*T^6 + (4.4812018155219e-13)*T^7 \end{aligned} \quad (C.10)$$

Saturation temperature for a known pressure:

For $0.9103 \text{ bar} < p < 6.1823 \text{ bar}$

$$\begin{aligned} T_{sat} = & (5.0142626496345e+01) + (8.7088982376435e+01)*p \\ & - (6.1670818220560e+01)*p^2 + (3.4504290676744e+01)*p^3 \\ & - (1.3489900098263e+01)*p^4 + (3.6034252763654e+00)*p^5 \\ & - (6.4260811100028e-01)*p^6 + (7.3006309391489e-02)*p^7 \\ & - (4.7711513110239e-03)*p^8 + (1.3635842511078e-04)*p^9 \end{aligned} \quad (C.11)$$

The properties for vapor and liquid obtained from polynomial functions are compared to a tabulated source [IAPWS(1998)]. The errors for the saturated water vapor and the liquid properties are summarized in Table C.1 and Table C.2 respectively.

Table C.1 Error percentages of thermodynamic properties of saturated water vapor estimated by polynomial functions

Pressure (bar)	Error for saturation temperature calculation (%)	Error for density calculation (%)	Error for latent heat calculation (%)	Error for specific heat calculation (%)	Error for viscosity calculation (%)	Error for conductivity calculation (%)
0.9103	0.00314614	0.0005622	0.0008194	0.00024208	0.00193604	0.000271
1.0142	0.00119781	0.0009067	0.0011793	0.00096284	0.00140104	0.000883
1.1277	0.0005777	0.0016242	0.0009229	0.00076339	0.00173489	0.000212
1.2515	0.00100045	0.0006630	0.0014820	0.00027174	0.00335364	0.002197
1.3863	0.00152587	0.0009149	0.0014436	0.00112482	0.00364434	0.001483
1.5328	0.00039509	6.7714E-05	0.0007464	0.00050271	0.00281863	0.000127
1.6918	0.000776208	9.8785E-05	0.00117883	0.001685878	0.001031576	0.000840
1.8641	0.001066822	0.00081194	0.00043129	0.001376106	0.001545583	0.000835
2.0505	0.000472896	0.00323888	0.00102126	0.000775540	0.002961406	0.000101
2.2518	0.000129208	0.00274001	0.00071318	0.002177685	0.000791831	0.001158
2.4689	0.00043854	0.00102281	0.00077192	0.001783332	0.002673768	0.000795
2.7028	0.000845102	0.00035038	0.00083113	0.001565391	0.001743637	0.000991
2.9543	2.29455E-05	0.00271796	0.00104873	0.000612033	0.001166976	0.000670
3.2245	0.000347811	0.00217984	0.00003397	0.001892045	0.003480965	0.000976
3.5143	0.000252484	0.00202936	0.00208071	0.001946021	0.000734972	0.001024
3.8247	0.000214913	0.00057492	0.00050238	0.001711334	0.002022426	0.000110
4.1568	0.000536688	0.00175441	0.00017200	0.000649034	0.002369333	0.000211
4.5118	0.00044333	0.00074813	0.00048369	6.01966E-05	0.000666297	0.000179
4.8907	0.000121262	0.00226283	0.00123771	0.000238141	0.003222721	0.001338
5.2946	0.00058459	0.00052493	0.00249806	0.002079859	0.000302521	0.000150
5.7247	0.001049649	0.00095956	0.00098046	0.001696964	0.002926639	0.000354
6.1823	0.001716614	0.00095087	0.00083259	0.000795272	0.001230676	0.000495

Table C.2 Error percentages of thermodynamic properties of liquid water estimated by polynomial functions

Temperature (°C)	Error for density calculation (%)	Error for specific heat calculation (%)	Error for viscosity calculation (%)	Error for conductivity calculation (%)
10.00	0.000537297	0.000829677	0.001551016	0.001243476
22.00	0.000171287	0.000193785	0.000774508	0.000643615
34.00	0.000220980	0.001540172	0.000467946	0.000134210
46.00	0.000185002	0.000809823	0.000139148	0.000345329
58.00	0.000353493	0.000193730	0.000835291	0.000703531
70.00	0.000380795	0.000261736	0.000785480	0.000539335
82.00	0.000157224	0.000533807	0.001052473	0.000905846
97.00	0.000158866	0.000407524	0.000800435	0.000360399
100.00	0.000101900	0.000769147	0.000898713	0.000175543
103.00	0.000453209	0.000497270	0.001150939	0.000482104
106.00	0.000191943	0.000372617	0.000329564	0.000271412
109.00	0.000198810	0.000857337	0.000769494	0.000034985
112.00	0.000495013	0.000788868	0.000034946	0.000262164
115.00	0.000199781	0.000011258	0.000862726	0.000340563
118.00	0.000000000	0.000663476	0.001613595	0.000061091
121.00	0.000077727	0.000269577	0.000733955	0.000392549
124.00	0.000025977	0.000953585	0.001338197	0.000427299
127.00	0.000175808	0.000190475	0.000199962	0.000854434
130.00	0.000535379	0.000123084	0.001968507	0.000130769
133.00	0.000013094	0.000547511	0.001134898	0.000601565
136.00	0.000393915	0.001249608	0.002253329	0.001011490
139.00	0.000454297	0.000323068	0.000991825	0.000122109
142.00	0.000396186	0.000266936	0.000270649	0.000427542
145.00	0.000490072	0.000510770	0.001860800	0.000480134
148.00	0.000352048	0.000166265	0.001320615	0.000131026
151.00	0.000039976	0.000918335	0.001140634	0.000061190
154.00	0.000507936	0.000596336	0.000049226	0.000568655
157.00	0.000187726	0.000991918	0.001457453	0.000175135
160.00	0.000053808	0.001440828	0.000675283	0.000096425

APPENDIX D

EFFECT OF AXIAL HEAT CONDUCTION INSIDE THE CONDENSER TUBE WALL

Since the computer code ZEC assumes that the heat transfer occurs in radial direction through the condenser tube wall, i.e., it neglects the axial conduction, it is necessary to analyze the effect of axial heat conduction inside the condenser tube wall.

In order to analyze the effect of axial conduction on the temperature distribution and also to the solution of the heat conduction equation through the condenser tube wall, a computer code ORTHIS [NECS 0525/01, (1971)] is used to solve the two dimensional heat conduction equation in a hollow cylindrical geometry. The results of the computer program ZEC for a reference case, Run 1.3-2 of UCB data, are prepared as input to code ORTHIS. Code ORTHIS requires local heat flux values at the inner surface of the condenser tube wall, local heat transfer coefficients of the cooling water at the jacket side, inlet temperature of the cooling water, condenser tube wall thickness and the temperature dependent thermal conductivity of the tube material.

The radial and the axial heat conduction rates are obtained from the code ORTHIS are shown in Figure D.1 and D.2, respectively. Since the ratio of axial to radial heat transfer rates (q_{axial} / q_{radial}) is in the range 0.01%-0.05%, the axial heat conduction can be neglected in the analyses.

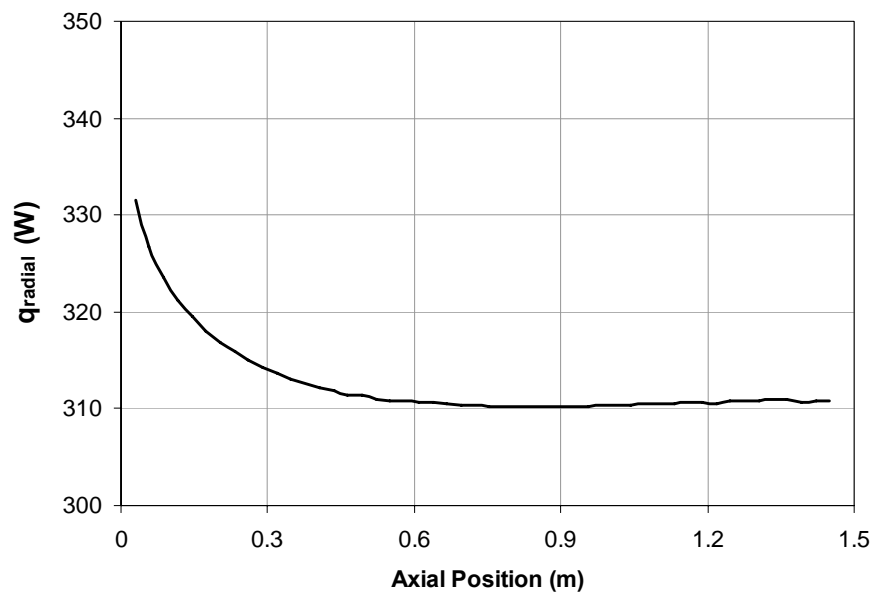


Figure D.1 Local radial heat transfer rate from the outer surface of the condenser tube wall

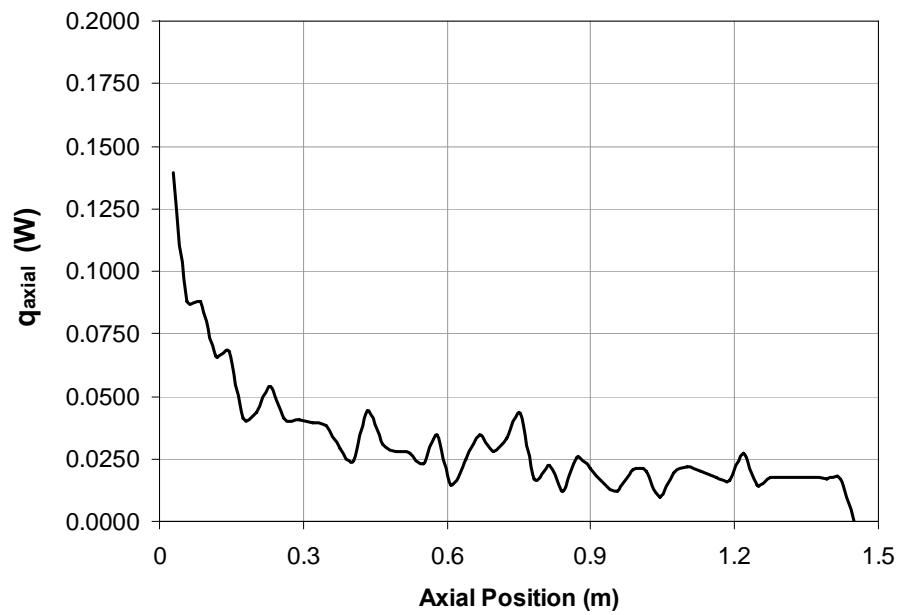


Figure D.2 Local axial heat transfer rate along the condenser tube

VITA

PERSONAL INFORMATION

Surname, Name: Köse, Serhat
Nationality: Turkish (TC)
Date and Place of Birth: 4 February 1969, Fethiye
Marital Status: Married
Phone: +90 312 295 87 91
Fax: +90 312 285 92 56
email: serhat.kose@taek.gov.tr

EDUCATION

<u>Degree</u>	<u>Institution</u>	<u>Year of Graduation</u>
MS	Hacettepe Un., Nuclear Engineering	1995
BS	Hacettepe Un., Nuclear Engineering	1992
High School	Gündoğdu High School, Konya	1986

WORK EXPERIENCE

<u>Year</u>	<u>Place</u>	<u>Enrollment</u>
2009- Present	Technology Dept., Turkish Atomic Energy Authority	Engineer
2004 -2009	Nuclear Energy Project Office, Turkish Atomic Energy Authority	Engineer
2001- 2004	Technology Dept., Turkish Atomic Energy Authority	Engineer
2000- 2001	Nuclear Regulatory Commission, USA	Engineer
1993- 2000	Nuclear Safety Dept., Turkish Atomic Energy Authority	Engineer
1992-1993	Nuclear Engineering, Hacettepe Un.	Research Assistant